

---

# Differences in brain connectivity between Essential tremor and Parkinson's disease: an EEG study

---

JULIA BERKHOUT

August 14, 2015

UNIVERSITY OF TWENTE.

*Supervisors:*

Dr.ir. G. Meinsma

Ir. F. Luft

Dr.ir. T. Heida

# Preface

This thesis is the result of my final project for obtaining the degree Master of Science in Applied Mathematics at the University of Twente in Enschede. For about 32 weeks I studied the EEG signals of patients with Essential tremor and Parkinson's disease. It gave me the opportunity to use mathematics in real life and to learn more about EEG and the brain. Although the project was quite hard sometimes, I really enjoyed working on this project and I am very pleased with the result. I hope you, as a reader, are too.

I want to thank Frauke Luft for all her help. Because EEG was new to me, she received a lot of questions. Really, a lot! Thank you for answering them and for all your input and advice. I also want to thank Gjerrit Meinsma for his supervision and help with this project. I wrote him countless e-mails and he answered every single one of them. Thank you for everything. Further, I want to thank Ciska Heida for her supervision and her input and comments on my thesis.

Lastly, I want to thank Olaf van Orizande for his love and support during these 32 weeks. Olaf, thank you for your confidence in me.

Julia Berkhout  
August 14, 2015

# List of abbreviations

AUC	Area under the ROC curve
BSS	Blind source separation
BAO1	Both arms outstretched (first time)
BAO2	Both arms outstretched (second time)
EEG	Electroencephalography
EOG	Electro-oculogram
ET	Essential tremor
FN	False negative fraction
FNR	False negative rate
FP	False positive fraction
HC	Healthy control
HT	Hilbert transform
IC	Independent component
ICA	Independent component analysis
IQR	Interquartile range
MSC	Magnitude squared coherence
PD	Parkinson's disease
PLV	Phase locking value
PS	Phase synchronization
PSD	Power spectral density
PCA	Principal component analysis
ROC	Receiver Operating Characteristic
REST	Rest task
RAO1	Right arm outstretched (first time)
RAO2	Right arm outstretched (second time)
TN	True negative fraction
TNR	True negative rate
TP	True positive fraction
TPR	True positive rate
WSS	Wide sense stationary

# Contents

<b>Preface</b>	<b>1</b>
<b>List of abbreviations</b>	<b>2</b>
<b>1 Introduction</b>	<b>5</b>
<b>2 EEG: recording and preprocessing</b>	<b>7</b>
<b>3 Coherence</b>	<b>11</b>
3.1 Mathematical method . . . . .	11
3.2 EEG analysis . . . . .	12
3.3 Statistics . . . . .	13
3.4 Results . . . . .	16
3.4.1 REST . . . . .	16
3.4.2 RAO1 . . . . .	19
3.4.3 RAO2 . . . . .	21
3.4.4 BAO1 . . . . .	25
3.4.5 BAO2 . . . . .	29
3.4.6 Overview . . . . .	33
3.5 Discussion . . . . .	33
<b>4 Phase Synchronization</b>	<b>34</b>
4.1 Mathematical method . . . . .	34
4.2 EEG analysis . . . . .	34
4.3 Statistics . . . . .	35
4.4 Results . . . . .	37
4.4.1 REST . . . . .	37
4.4.2 RAO1 . . . . .	40
4.4.3 RAO2 . . . . .	42
4.4.4 BAO1 . . . . .	46
4.4.5 BAO2 . . . . .	48
4.4.6 Overview . . . . .	52
4.5 Discussion . . . . .	52
<b>5 Global Field Synchronization</b>	<b>53</b>
5.1 Mathematical method . . . . .	53
5.2 EEG analysis . . . . .	55
5.3 Statistics . . . . .	55
5.4 Results . . . . .	56
5.4.1 REST . . . . .	56
5.4.2 RAO1 . . . . .	57
5.4.3 RAO2 . . . . .	58
5.4.4 BAO1 . . . . .	59
5.4.5 BAO2 . . . . .	60
5.4.6 Overview . . . . .	61
5.5 Discussion . . . . .	61

<b>6 Discussion</b>	<b>62</b>
<b>7 Conclusions and recommendations</b>	<b>65</b>
<b>Appendix A Examples</b>	<b>66</b>
<b>Bibliography</b>	<b>75</b>

# Chapter 1

## Introduction

A neurological disorder is any disorder of the nervous system. There are more than 600 neurological disorders and they are affecting more than a billion people worldwide. This thesis is about two of the most common neurological movement disorders: Parkinson's disease and Essential tremor.

Parkinson's disease (PD) is a chronic and progressive disorder. The primary motor symptoms of the disease are tremor at rest, rigidity and bradykinesia (slow movement). Bradykinesia and rigidity are caused by degeneration of dopamine generating neurons in the basal ganglia, which is involved in motor actions. Rest tremor is most easily recognized and is usually asymmetric. The cause of the rest tremor is not known. Besides motor symptoms, patients can have non-motor symptoms, like cognitive impairment, depression and sleep disorders.

The main motor symptoms of the disease are called parkinsonism. PD is sometimes called idiopathic PD, which means that the cause (of the degeneration) is unknown. Other forms of parkinsonism are due to known causes like treatment with particular medication.

In clinical practice, diagnosis is typically based on the presence of a combination of the motor features and response to medication. Differentiating PD from other forms of parkinsonism can be challenging early in the course of the disease, because symptoms overlap with that of other disorders.

Essential tremor (ET) is a neurological disorder that causes a tremor. ET is associated with degeneration of neurons in the cerebellum. The cerebellum is, like the basal ganglia, also involved in motor actions. ET can affect almost any part of the body, but the trembling occurs most often in the hands. ET usually affects both sides of the body and is primarily seen during action and goal directed movement.

Although there are many differences between PD and ET, tremor is a primary symptom for both disorders and the two are often mistaken for each other. A study showed that one-third of the patients who were diagnosed as ET were misdiagnosed, with PD being the most common true diagnosis (Jain et al., 2006). In a study of patients presumed to have PD and who were taking antiparkinsonian medication, ET was one of the most common causes of misdiagnoses (Meara et al., 1999).

In many neurological disorders, neural oscillations play an important role. Neural oscillations are rhythmic neural activities in the central nervous system. There are different frequency ranges of the oscillations, which are associated with different mental states. Delta waves ( $\delta$ , 0 – 4 Hz) are associated with deep, dreamless sleep. Theta waves ( $\theta$ , 4 – 7 Hz) are associated with light sleep or extreme relaxation. The alpha band ( $\alpha$ , 7 – 13 Hz) corresponds to an awake but relaxed mental state. Beta waves ( $\beta$ , 13 – 30 Hz) are associated with a wide awake state. The gamma waves ( $\gamma$ , > 30 Hz) are associated with the formation of ideas, language and memory processing and various types of learning.

Research has been done into the role of the different frequency bands in PD. Beta oscillations are increased in PD and there is evidence linking beta activity at rest and beta changes in response to treatment with bradykinesia and rigidity (Little and Brown, 2014). There are also findings that support a relationship between low gamma oscillations (30 - 45 Hz) and PD tremor (Beudel et al., 2015).

Because both disorders are associated with different parts of the brain, the question arises as to whether changes in brain activity can be used to differentiate between PD and ET. Changes in brain network activity are often described with connectivity, which describes the dependencies of several cortical areas on each other. The three types of connectivity are anatomical, functional, and effective connectivity.

Anatomical connectivity refers to a network of physical connections linking sets of neurons or neuronal elements. Functional connectivity is defined as the temporal correlation among different neural assemblies. Effective connectivity is defined as the direct or indirect influence that one neural system exerts over another. In this thesis, we use functional connectivity to investigate differences in connectivity between ET and PD.

Information about functional connectivity can be obtained by studying the features of the signals recorded from neurophysiological systems, including electroencephalographic signals. Electroencephalography is a medical imaging technique that reads scalp electrical activity generated by brain structures (Teplan, 2002). The electroencephalogram (EEG) is the electrical activity recorded from the scalp surface being picked up by metal electrodes. Because the electrodes are placed on the scalp surface, electroencephalography is a non-invasive procedure and can therefore be applied with virtually no risk.

While EEG has high temporal resolution, the main disadvantage is the fact that it has poor spatial resolution. Determining the exact location of the source of the activity might not be possible.

There are many mathematical methods for calculating connectivity and there is no consensus about the best method. In this work, connectivity is analyzed using *Magnitude Squared Coherence*, *Phase Locking Value* and *Global Field Synchronization*<sup>1</sup>. All measures have their own advantages and disadvantages, which are discussed in more detail later in this thesis.

Magnitude Squared Coherence (MSC), or simply coherence, gives the linear correlation between two signals as a function of frequency. High coherence between two signals means linear correlation and indicates a stronger functional relationship between the related brain regions.

Coherence has been applied to EEG signals in multiple studies. In the work of Murias et al. (2007a), coherence differences were found between attention-deficit hyperactivity disorder (ADHD) and control children. ADHD subjects showed elevated coherence in the lower alpha band and reduced coherence in the upper alpha band. Control coherence was elevated in the delta and theta bands.

Coherence differences were also found in subjects with autism spectrum disorder (ASD). Murias et al. (2007b) showed that reduced coherence was evident for the ASD group in the lower alpha range. In the theta range, elevated coherence for the ASD group was found within the left hemisphere frontal and temporal regions.

The Phase Locking Value (PLV) is an index to measure the degree of phase synchronization. Phase synchronization is defined as the locking of the phases of two oscillators, which means that the phase difference of the two oscillators is constant over time. If two signals are perfectly phase synchronized, the PLV will be 1. Otherwise, it will be smaller.

The PLV has successfully been applied to EEG signals from patients with epilepsy, where differences in the degree of synchronization were observed between seizure-free intervals and prior to seizure activity (Mormann et al., 2000).

Whereas coherence and the PLV are used for two signals, Global Field Synchronization (GFS) quantifies synchrony for multiple signals. When applied to all EEG signals at once, GFS quantifies the amount of common phase across all electrodes and hence is a measure of *zero-phase or instantaneous synchronization*. As noted in the work of Koenig et al. (2001), increased values can be interpreted as increased functional connectivity of brain processes. A value of zero indicates the absence of a dominating phase and therefore the absence of connectivity.

GFS has been applied to EEG signals from patients with schizophrenia and the conclusion was that patients had decreased GFS values in the theta band compared to controls (Koenig et al., 2001). Koenig et al. (2005) showed that patients with Alzheimer's disease had decreased GFS values in the alpha, beta and gamma bands and increased GFS values in the delta band.

This thesis reports our study of the functional connectivity in the brains of subjects with Essential tremor and Parkinson's disease. The aim was to investigate differences in connectivity between these two subject groups and to compare the results of different connectivity measures. Furthermore, if differences were found, the aim was to investigate if they could be used in clinical practice. We investigate if it is possible to construct a test that can correctly classify patients based on one of the connectivity measures.

---

<sup>1</sup>A review of other commonly used connectivity methods can be found in Pereda et al. (2005) and Sakkalis (2011).

## Chapter 2

# EEG: recording and preprocessing

Included in the study were 9 subjects with Parkinson’s disease (PD) and 15 subjects with Essential Tremor (ET) (see Table 2.1). All patients were off tremor medication and did not have other neurological disorders. Written informed consent was obtained and the study was approved by the METC.

While the EEG was recorded, the patients were sitting on a hospital bed, elevated to a sitting position. Three different tasks were performed:

- **Rest:** The subject had to sit with the hands resting comfortably on the legs with the palms turned upwards. This task is denoted as REST and lasted three minutes.
- **Right arm outstretched:** The subject had to lift the right arm up to shoulder height for one minute. After some rest, this task was performed again. These two one-minute tasks are denoted as RAO1 and RAO2.
- **Both arms outstretched:** The subject has to lift both arms up to shoulder height for one minute. This task was also repeated after some rest. These tasks are denoted as BAO1 and BAO2.

During the different tasks, the cortical activity was recorded using a 64-channel EEG measurement setup (standard 10-20 configuration). An example of an EEG signal is shown in Figure 2.1. The placement of the electrodes is shown in Figure 2.2. Electrodes M1 and M2 are placed behind the ears and were not included in the analysis.

The EEG records were band-pass filtered between 1 and 85 Hz and resampled at 512 samples/second. A notch filter was used to remove artifact caused by electrical power lines (50 Hz). De eye blink artifact removal is explained on page 9. ET patient 2 is excluded from the analysis because the signals contained to many eye movement artifacts.

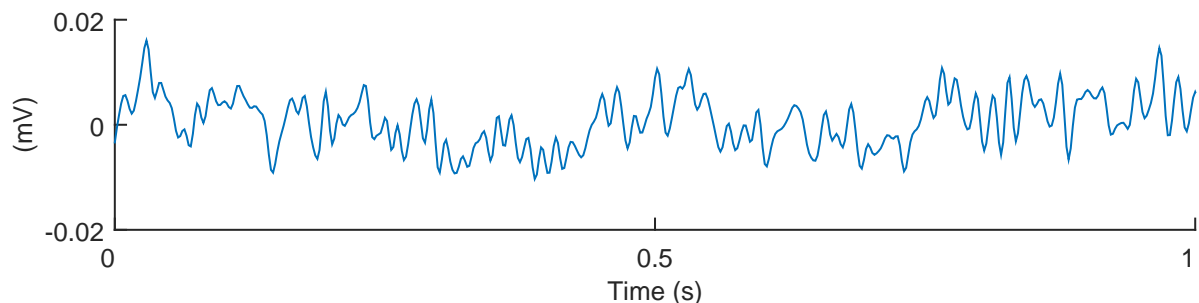


**Figure 2.1:** One second of an EEG signal.

After artifact removal a local average montage was used for re-referencing the signals, which means that a unique reference was constructed for each electrode. In our case, a small number of electrodes surrounding the target electrode were used to compute the reference. For example, for electrode Cz, the reference is computed as

$$\text{ref}_{Cz} = \frac{FCz + C2 + CPz + C1}{4}$$

and the signal  $s$  used in further analysis is given by

$$s = Cz - \text{ref}_{Cz}.$$

This montage is chosen to reduce reference effects. Reference effects occur when a common reference is used for all electrodes. When this common reference electrode responds to electrical activity or artifact, the EEG at all electrodes changes. This may lead to artificially high connectivity values. With the local montage there are no reference effects except at electrodes that are close to each other, because they might use a common electrode in their references.

Because GFS measures a common phase among the different electrodes, this local reference cannot be used when GFS values are determined. This is because with the local montage, phases at different electrodes are changed independently of each other. With GFS, one reference signal has to be used for all electrodes. Because this is the case during recording, no re-referencing was done on the EEG signals before the GFS analysis.

The frequency ( $f$ ) bands used in the analysis are given in Table 2.2. We did not consider the delta waves. An extra division was made in the alpha and beta band.

**Table 2.1:** Patient information

(a)				(b)			
Parkinson's Disease				Essential Tremor			
Patient	Gender	Age	Onset disease	Patient	Gender	Age	Onset disease
1	M	59	age 50	1	M	51	birth
2	M	70	age 64	2	M	55	age 50
3	M	68	age 63	3	M	86	unknown
4	F	82	age 76	4	M	66	high school
5	F	63	age 60	5	F	52	childhood
6	M	50	age 47	6	M	66	age 20
7	M	72	age 71	7	F	24	high school
8	F	55	age 44	8	M	50	age 40
9	F	44	age 40	9	M	55	age 16
				10	M	71	unknown
				11	M	65	unknown
				12	M	56	age 12
				13	M	73	age 60
				14	M	28	birth
				15	F	82	unknown

**Table 2.2:** Frequency bands

Name	$f$ (Hz)
$\theta$	4 - 7
$\alpha_1$	7 - 10
$\alpha_2$	10 - 13
$\beta_1$	13 - 20
$\beta_2$	20 - 30
$\gamma_1$	30 - 45

## Eye blink artifacts

Eye movement and blinks are sources of artifacts in EEG data. Figure 2.3 shows an example of electro-oculograms (EOG), that show horizontal (EOG<sub>H</sub>) and vertical (EOG<sub>V</sub>) eye movement, and an EEG signal with eye blink artifacts. These eye blink artifacts can give inaccurate results about connectivity. Rejecting parts of the EEG signal with an eye blink artifact can result in the loss of a large amount of data. Independent component analysis (ICA) can be used to correct the EEG at the time instances eye movement occurs. Information about ICA can be found in Infobox 1.

### Infobox 1: Independent Component Analysis

Independent component analysis (ICA) is an example of blind source separation (BSS). BSS is the separation of a set of source signals from a set of mixed signals, where blind stands for the fact that very little information is known about the sources or the mixing process. With ICA,  $M$  simultaneously recorded signals are split into  $M$  independent and nongaussian sources.

Given a set of  $M$  observations of random variables,  $\mathbf{x}(t) = [x_1(t), x_2(t), \dots, x_M(t)]^T$ , assume that they are generated as a mixture of independent components:

$$\mathbf{x}(t) = \mathbf{H} \cdot \mathbf{s}(t),$$

where  $\mathbf{H} \in \mathbb{R}^{M \times M}$  is called the mixing matrix and  $\mathbf{s}(t) = [s_1(t), s_2(t), \dots, s_M(t)]^T$  are the independent components (IC's). Only  $\mathbf{x}(t)$  is known, and ICA consist of estimating both  $\mathbf{H}$  and  $\mathbf{s}(t)$ .

Seperation into independent components is useful when a specific component is unwanted. When  $\mathbf{H}$  and  $\mathbf{s}(t)$  are found, the unwanted component can be removed by setting the corresponding signal  $s_i(t)$  in  $\mathbf{s}(t)$  to zero. Let  $\tilde{\mathbf{s}}(t)$  be  $\mathbf{s}(t)$  with the unwanted signal set to zero. The 'clean' signals can now be reconstructed by

$$\tilde{\mathbf{x}}(t) = \mathbf{H}\tilde{\mathbf{s}}(t).$$

Because of the large amount of signals to be inspected for eye blink artifacts, an automatic approach was used to remove them. The EEG signals where given as input to the ICA algorithm, together with the two EOG signals. The output is a set of independent components (IC), of which two are set to zero each time: the IC that has the highest (absolute) cross correlation with EOG<sub>V</sub> and the IC that has the highest (absolute) cross correlation with EOG<sub>H</sub>. An example can be found in Example 1 in Appendix A.

The procedure described above was performed on sets of 16 EEG-signals. This automatic removal failed occasionally if a subject blinked or moved his eyes very often. Therefore, the signal from electrode FP1 was checked afterwards to see if it still contained eye blink artifacts. If that was the case, ICA was performed again and unwanted IC's were removed manually.

In this thesis, ICA is performed with an algorithm called RobustICA. More information about this algorithm can be found in the work of Zarzoso (2010).

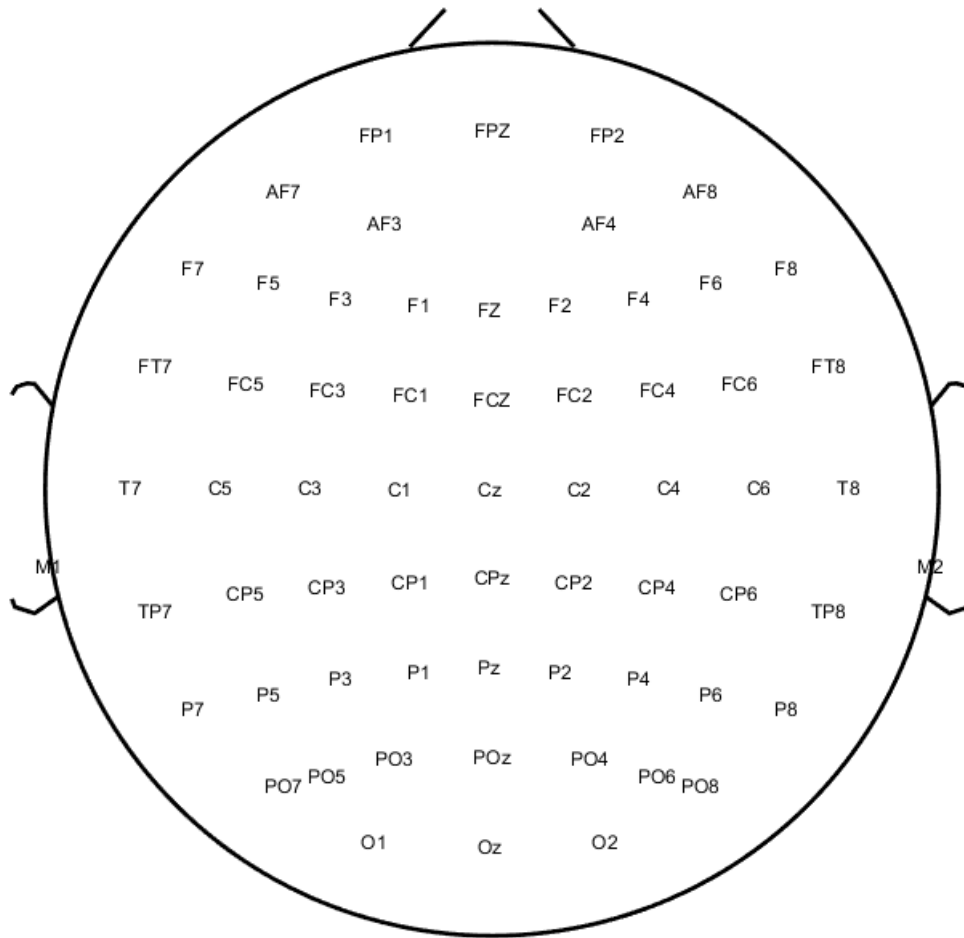


**Figure 2.2:** Electrode placement.

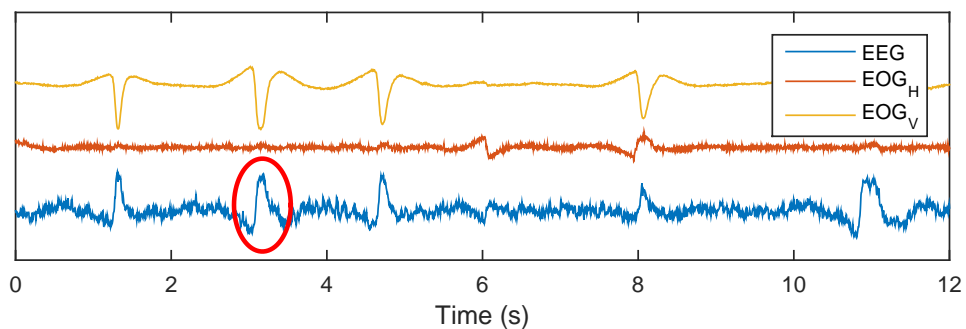


**Figure 2.3:** Example of EEG signal together with the (scaled) EOG signals that show horizontal ( $EOG_H$ ) and vertical ( $EOG_V$ ) eye movement. The red ellipse encircles one of the eye blink artifacts.

# Chapter 3

## Coherence

*Magnitude Squared Coherence* (MSC), or simply coherence, quantifies linear correlations in the frequency domain. It is a measure of the coupling between two signals at any given frequency. This chapter is about coherence analysis. In Section 3.1, some background mathematics is introduced and the definition for coherence is given. How this method is applied to the EEG signals is demonstrated in Section 3.2. Section 3.3 explains the statistics used to determine statistical differences between groups and Section 3.4 shows the results. The discussion of the results can be found in Section 3.5. The discussion of the used methods is given in Chapter 6.

### 3.1 Mathematical method

Let  $X_n$ ,  $n \in \mathbb{Z}$ , be a random process. The *autocorrelation function* is defined as

$$r_x(t, s) = \mathbb{E}[(X_t - m_X(t))(X_s - m_X(s))], \quad (3.1)$$

where  $t$  and  $s$  are two time indices and  $m_X(t)$  is the mean of  $X_n$ . The autocorrelation function describes the correlation between values of the process at different times.

A random process is called wide-sense stationary (WSS) if the mean is constant over time and the autocorrelation function only depends on the time lag  $k = s - t$ . Assume  $X_n$  is a WSS process with zero mean. Then, the autocorrelation function is redefined as

$$r_x(k) = \mathbb{E}(X_t X_{t+k}), \quad (3.2)$$

where  $k$  is the lag.

Information about a random process cannot only be found in the time domain. The *power spectral density* (PSD) decomposes the process into its different frequencies. For a WSS process  $X_n$ , the PSD is defined as the Fourier transform of its autocorrelation function  $r_x(k)$ :

$$S_{xx}(f) = \sum_{k=-\infty}^{\infty} r_x(k) e^{-i2\pi f k}. \quad (3.3)$$

Let  $Y_n$  be another WSS process with zero mean. The *cross-correlation function* of  $X_n$  and  $Y_n$  is defined as

$$r_{xy}(t, s) = \mathbb{E}(X_t Y_s). \quad (3.4)$$

$X_n$  and  $Y_n$  are jointly WSS if their cross-correlation function depends on the lag  $k = s - t$  only. Then,

$$r_{xy}(k) = \mathbb{E}(X_t Y_{t+k}). \quad (3.5)$$

The *cross power spectral density* (cross PSD) for two joint WSS processes is the Fourier transform of the cross-correlation function  $r_{xy}(k)$ :

$$S_{xy}(f) = \sum_{k=-\infty}^{\infty} r_{xy}(k) e^{-i2\pi f k}. \quad (3.6)$$

Coherence is now given by the following equation:

$$\gamma_{xy}(f) = \frac{|S_{xy}(f)|^2}{|S_{xx}(f)||S_{yy}(f)|}. \quad (3.7)$$

The Cauchy-Schwarz inequality guarantees that coherence for a given frequency  $f$  ranges between 0 (no coupling) and 1 (maximum linear interdependence).

All definitions above are properties of a stochastic process and can be estimated for a finite realization. Suppose  $x_n$  and  $y_n$  are two realizations of two stochastic processes  $X_n$  and  $Y_n$  respectively, with  $N$  samples each. The PSD can be estimated by the periodogram:

$$P_{xx}(f) = \frac{1}{N} \left| \hat{X}(f) \right|^2 = \frac{1}{N} \left| \sum_{n=0}^{N-1} x_n e^{-i2\pi f n} \right|^2, \quad f \in \left[ -\frac{1}{2}, \frac{1}{2} \right]. \quad (3.8)$$

Here  $\hat{X}(f)$  is the Fourier transform of  $x_n$ .

The cross PSD can be estimated as:

$$P_{xy}(f) = \frac{1}{N} \hat{X}(f) \hat{Y}^*(f) = \frac{1}{N} \left[ \sum_{n=0}^{N-1} x_n e^{-i2\pi f n} \right] \left[ \sum_{n=0}^{N-1} y_n e^{-i2\pi f n} \right]^*, \quad f \in \left[ -\frac{1}{2}, \frac{1}{2} \right], \quad (3.9)$$

where  $()^*$  means complex conjugate.

If  $x_n$  is a sampled continuous-time signal with sampling frequency  $F_s$ , the periodogram is defined as

$$P_{xx}(f) = \frac{T_s}{N} \left| \hat{X}(f) \right|^2 = \frac{T_s}{N} \left| \sum_{n=0}^{N-1} x_n e^{-i2\pi f T_s n} \right|^2, \quad f \in \left[ -\frac{F_s}{2}, \frac{F_s}{2} \right], \quad (3.10)$$

where  $T_s = 1/F_s$  is the sampling period and  $F_s/2$  is the *Nyquist frequency*. The cross PSD for two sampled continuous-time signals can be estimated similarly.

Because the periodogram can be highly erratic (see Figure 3.1 for an example), in practice the PSD is often estimated using Welch's method: the signals are split into  $M$  overlapping time segments (usually 50% overlap) and these segments are windowed with a windowing function, for example a Hamming or Hann window. Periodograms are computed for every segment and then these periodograms are averaged.

So in practice, coherence is calculated as

$$\gamma_{xy}(f) = \frac{|\langle P_{xy}(f) \rangle|^2}{\langle P_{xx}(f) \rangle \langle P_{yy}(f) \rangle}. \quad (3.11)$$

Here  $\langle \cdot \rangle$  stands for the average computed over the  $M$  segments.

## 3.2 EEG analysis

For each subject, coherence was calculated for all electrode combinations. The signals were divided into epochs of 2 seconds (which gives a frequency resolution of 0.5) with 50% overlap. Epochs were windowed using a Hamming window.

Let  $X$  and  $Y$  be two EEG signals with both  $M$  epochs. Coherence was determined as

$$\gamma_{xy}(f) = \frac{\left| \frac{1}{M} \sum_{i=1}^M \hat{e}_{x_i}(f) \hat{e}_{y_i}^*(f) \right|^2}{\left( \frac{1}{M} \sum_{i=1}^M \hat{e}_{x_i}(f) \hat{e}_{x_i}^*(f) \right) \left( \frac{1}{M} \sum_{i=1}^M \hat{e}_{y_i}(f) \hat{e}_{y_i}^*(f) \right)}, \quad (3.12)$$

where  $\hat{e}_{x_i}$  is the discrete Fourier transform of the  $i$ th epoch of  $X$  and  $\hat{e}_{y_i}$  the discrete Fourier transform of the  $i$ th epoch of  $Y$ .

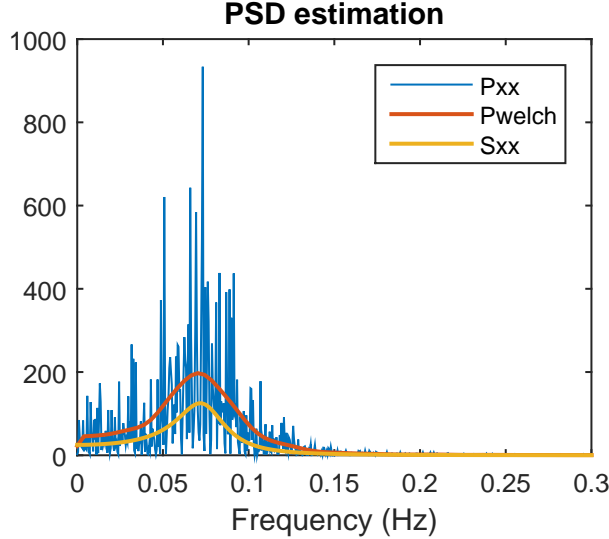


**Figure 3.1:** Estimation of the power spectral density.  $S_{xx}$  shows the true PSD and  $P_{xx}$  shows the (poor) estimation of  $S_{xx}$ .  $P_{welch}$  shows a possible PSD estimate using Welch’s method.

Coherence values were calculated for every pair of electrodes. With 62 electrodes included in the analysis, this results in 1891 pairs for each subject. For each pair, coherence values were averaged over the frequency bands given in Table 2.2. This results in 56730 coherence values per subject: one for every electrode pair, for every frequency band, for every task.

### 3.3 Statistics

For each electrode pair, group differences between PD and ET were tested using the Wilcoxon rank sum test, which is a nonparametric test of the null hypothesis that two samples come from the same population. If the null hypothesis is rejected, subjects from a certain group tend to have larger values than subjects from the other group. The null hypothesis was rejected with  $P < 0.05$ . If an electrode pair showed group differences, that electrode pair is said to be significant.

Before the Wilcoxon rank sum test was performed, outliers were removed. Let  $C = \{c_1, \dots, c_n\}$  be the set of coherence values of a specific group, where  $n$  is the number of subjects in the group. A value  $c_i$  was removed if

$$c_i > Q_3 + 1.5 \cdot IQR \quad \text{or} \quad c_i < Q_1 - 1.5 \cdot IQR.$$

Here,  $Q_1$  and  $Q_3$  are the first and third quartile of  $C$  and the interquartile range (IQR) is defined as the distance between  $Q_1$  and  $Q_3$ . If the data is normally distributed, the interval

$$[Q_1 - 1.5 \cdot IQR, \quad Q_3 + 1.5 \cdot IQR]$$

covers about 99.3 % of the data. An example of this statistical procedure can be found in Example 2 in Appendix A.

We visually inspected if the significant electrode pairs were located at a specific region, for example only in the frontal region or connections only between frontal and occipital regions. Furthermore, we checked the locations for asymmetry between the left and right hemisphere. This is done by comparing the percentage of significant electrode pair connections within the left hemisphere with connections within the right hemisphere.

Once the significant electrode pairs were determined, a test was developed to discriminate between the two groups. For every subject, the median of all coherence values (i.e. coherence at all possible electrode pairs) was used for testing, still separately for every task and frequency band. From now on this is simply called *the median*.

The diagnostic test has the following form: if the median of a patient is less than cut-off point  $c$ , the

patient gets the diagnosis ET. If the median is greater than  $c$ , the patients gets the diagnosis PD. Receiver Operating Characteristic (ROC) curves can be used to find the optimal cut-off point  $c$  and to evaluate the performance of the test (see Infobox 2).

### Infobox 2: ROC curve

When creating a diagnostic test, a cut-off point has to be chosen to separate one group (e.g. healthy) from the other (e.g. diseased). If the distributions of the two groups do not overlap, setting a cut-off point is easy. In practice, however, distribution often overlap and choosing a cut-off point becomes more difficult (see Figure 3.2). For every possible cut-off point, there will be

- cases with the disease correctly classified as positive: true positive fraction (TP);
- cases with the disease classified as negative: false negative fraction (FN);
- cases without the disease correctly classified as negative: true negative fraction (TN);
- cases without the disease classified as positive: false positive fraction (FP).

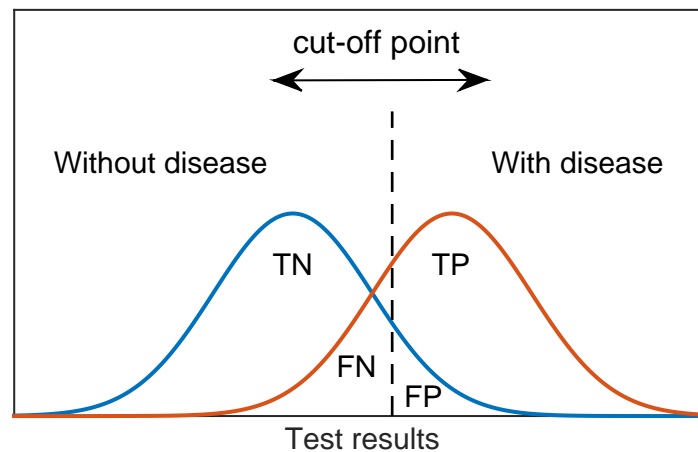


**Figure 3.2:** Distribution of people with and without the disease. Moving the cut-off point results in changes of sensitivity and specificity.

Choosing a cut-off point now becomes a trade off between *sensitivity* and *specificity*. Sensitivity is the probability the test result will be positive when the disease is present (also called the *true positive rate* (TPR)). It is calculated as

$$TPR = \frac{TP}{TP + FN}.$$

Specificity is the probability that the test will be negative when the disease is not present (also called *true negative rate* (TNR)). It is calculated as

$$TNR = \frac{TN}{FP + TN}.$$

The ROC curve plots the *false negative rate* (FNR, 100% - specificity) against the TPR (sensitivity). Ideal would be a 100% TPR and 0% FNR. The optimal point in a specific case depends on the distributions and if one of sensitivity/specificity is preferred over the other. An example of an ROC curve is shown in Figure 3.3.

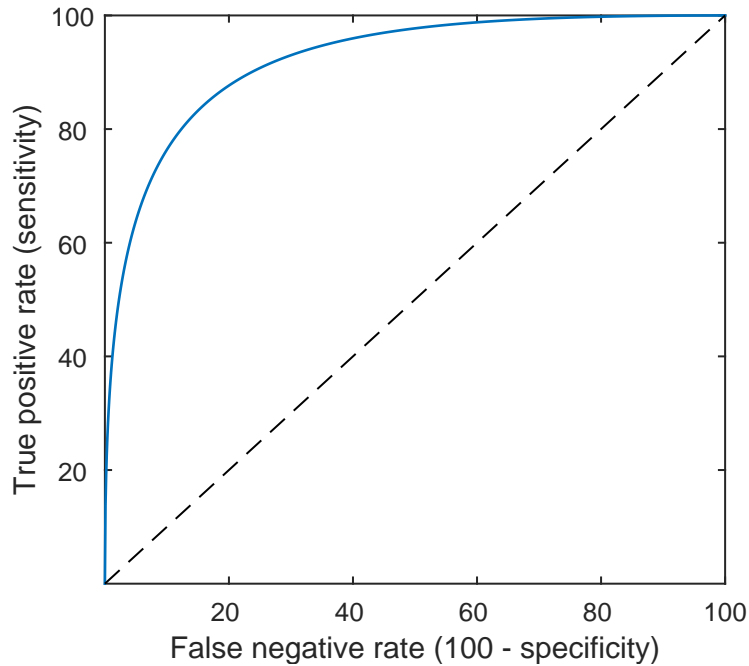


**Figure 3.3:** ROC curve (blue). The dotted line is the chance performance. If the optimal point lies on that line, the test does not do better than a random guess.

The area under a ROC curve (AUC) quantifies the overall ability of the test to discriminate between two groups. The area represents the probability that a randomly selected patient will have a higher test result than a randomly selected control (healthy subject). A useless test (one no better than a random guess) has an area of 0.5. A perfect test has an area of 1. So the greater the area, the better the test.

Sensitivity and specificity are in this case defined as the probability that the test results in ‘PD’ when the patient actually has PD (true PD rate) and as the probability that the test will result in ‘ET’ when a patient actually has ET (true ET rate). Because both are equally important, the ideal point would be (0% 1-specificity, 100% sensitivity). A way to determine the optimal cut-off point is to determine the point that has minimal distance to the ideal point.

A different test is determined for every frequency band - task combination. To compare the different tests, we use the area under the curve (AUC) (see Infobox 2). The higher the AUC, the better the test is able to distinguish between ET and PD. We use the classification in Table 3.1.

**Table 3.1:** AUC classification

AUC	Accuracy
0.50 - 0.75	Bad
0.75 - 0.80	Fair
0.80 - 0.90	Good
0.90 - 1.00	Excellent

Before the ROC curve was determined, outliers in the medians were removed the same way as outliers in the coherence values at an electrode pair.

## 3.4 Results

In this section, the results of the coherence analysis are given. The results are shown separately for each task. Only those frequency bands are discussed where more than 10% of all electrode pairs were significant electrode pairs or where  $AUC > 0.75$ . These bands will be called *significant frequency bands*.

### 3.4.1 REST

The coherence results at REST are summarized in Figure 3.4. The coherence values shown are the mean and standard deviation of the medians of all subjects. The frequency bands marked with an asterisk (\*) are the significant frequency bands. Significant at REST are the  $\alpha_1$  (7 - 10 Hz) and  $\alpha_2$  (10 - 13 Hz) frequency bands.

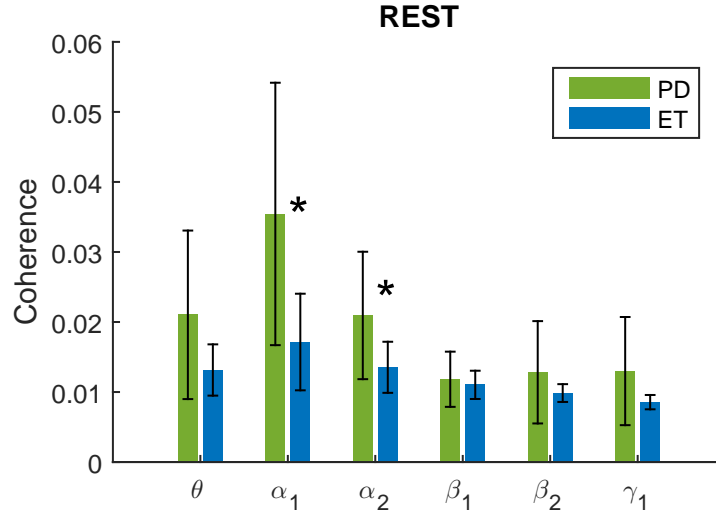
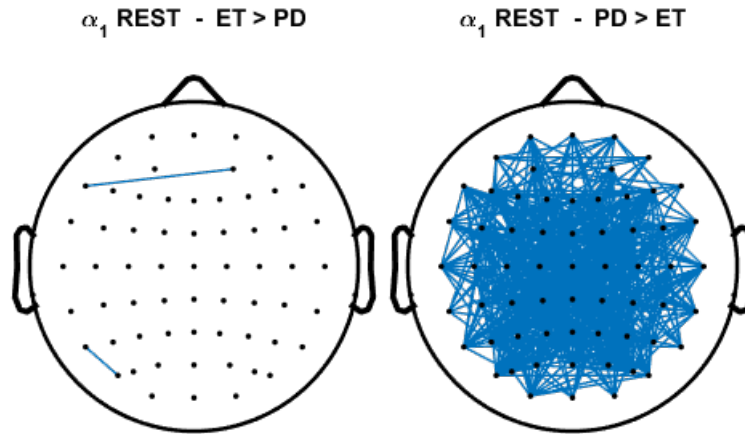


**Figure 3.4:** Coherence results at the task REST. For every subject, the median of the coherence values at all 1891 electrode pairs is taken. Shown are the average median (bars) and the standard deviation (black lines). Significant frequency bands are marked with an asterisk (\*). The following outliers were removed:  $\theta$ : ET 15,  $\beta_1$ : PD 8,  $\beta_2$ : ET 4,  $\gamma_1$ : ET 4.

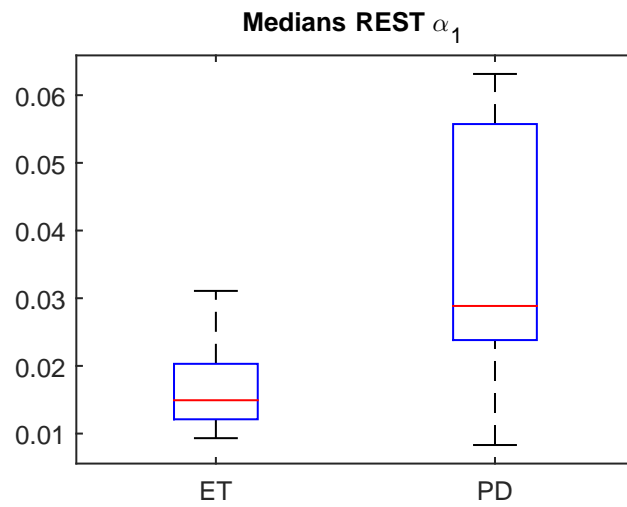
At the  $\alpha_1$  frequency band, PD coherence values exceeded ET at 30.0% of all electrode pairs, while ET exceeded PD at only 0.1 % of all pairs. The location of the significant electrode pairs are shown in Figure 3.5a. Of all significant electrode pairs, 28% were found within the right hemisphere, 34% in the left and 38% between hemispheres.

The medians are illustrated by the boxplots in Figure 3.5b. The ROC curve is shown in Figure 3.5c. The optimal cut-off point is 0.0210, which gives a true PD rate of 78% and a true ET rate of 79%. The AUC is equal to 0.81.

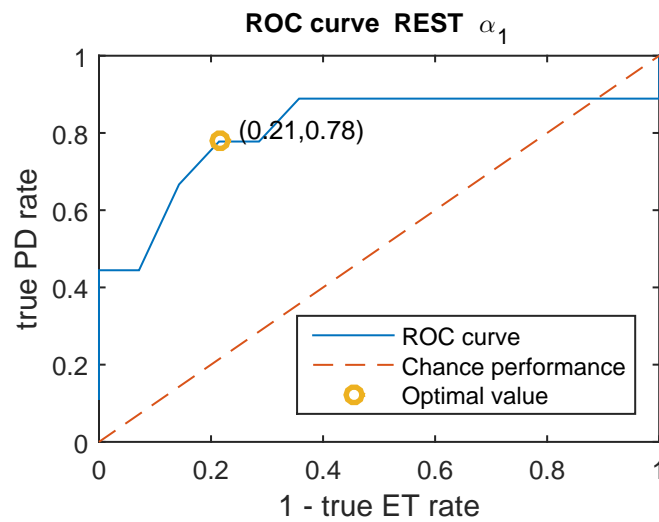
At  $\alpha_2$ , PD coherence exceeded ET at 14.8% of the electrode pairs (ET exceeded PD at 0.6% of all pairs). The locations of the significant electrode pairs are shown in Figure 3.6a. Of all significant electrode pairs, 28% were found within the right hemisphere, 30% in the left and 42% between hemispheres. Boxplots of the medians are shown in Figure 3.6b. The ROC curve for  $\alpha_2$  is shown in Figure 3.6c. The optimal cut-off point is 0.0180, which gives a true PD rate of 67% and a true ET rate of 93%. The AUC is equal to 0.75.



(a) Significant electrode pairs: electrode pairs that showed group differences at  $P < 0.05$ . Left: electrode pairs where ET coherence exceeded PD coherence. Right: electrode pairs where PD coherence exceeded ET coherence.

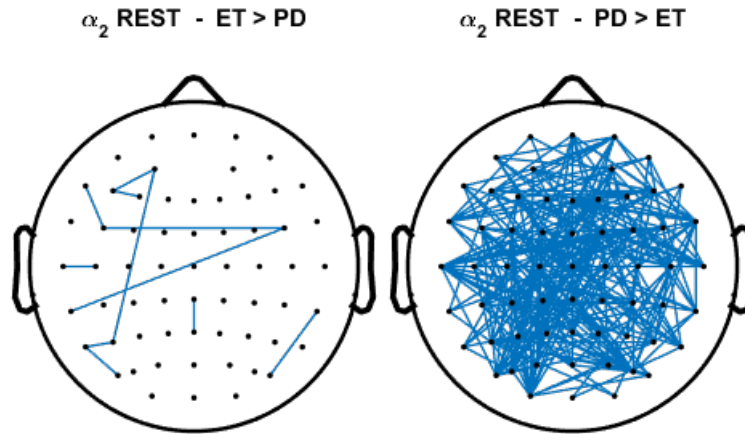


(b) Boxplot of the medians.

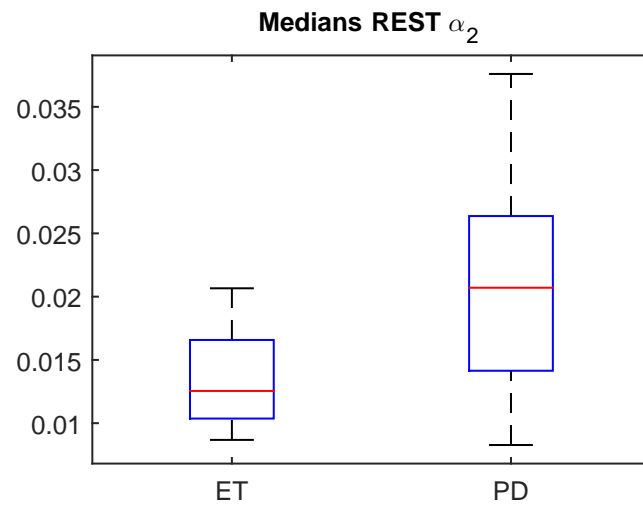


(c) ROC curve of the medians.

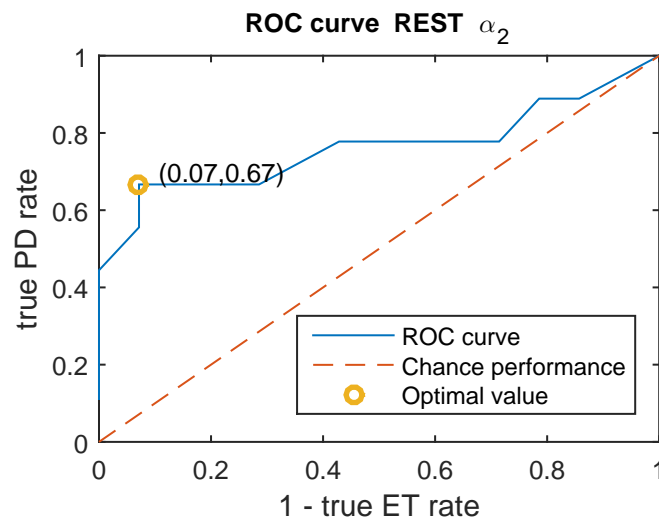
**Figure 3.5:** Results coherence analysis at the  $\alpha_1$  frequency band at the task REST.



(a) Significant electrode pairs: electrode pairs that showed group differences at  $P < 0.05$ . Left: electrode pairs where ET coherence exceeded PD coherence. Right: electrode pairs where PD coherence exceeded ET coherence.



(b) Boxplot of the medians.



(c) ROC curve of the medians.

**Figure 3.6:** Results coherence analysis at the  $\alpha_2$  frequency band at the task REST.

### 3.4.2 RAO1

The coherence results at RAO1 are summarized in Figure 3.7. The coherence values shown are the mean and standard deviation of the medians of all subjects. The frequency bands marked with an asterisk (\*) are the significant frequency bands. Significant at RAO1 is the  $\alpha_1$  frequency band.

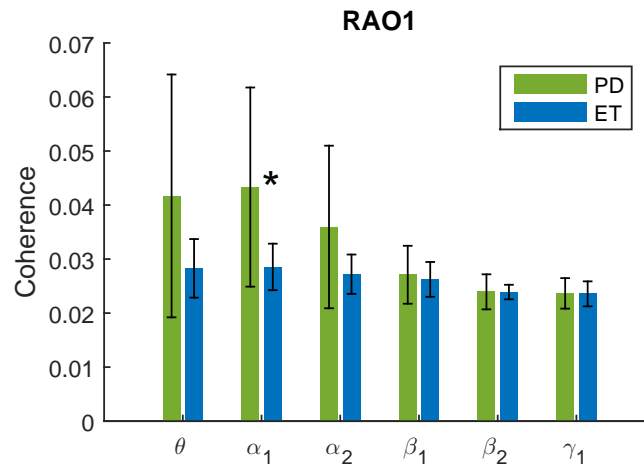
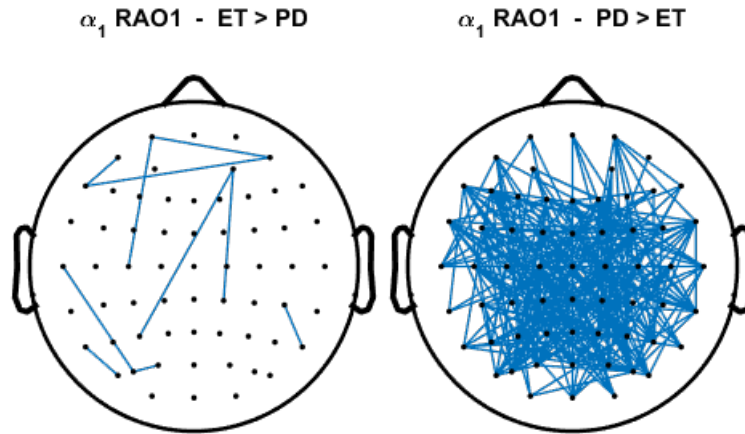
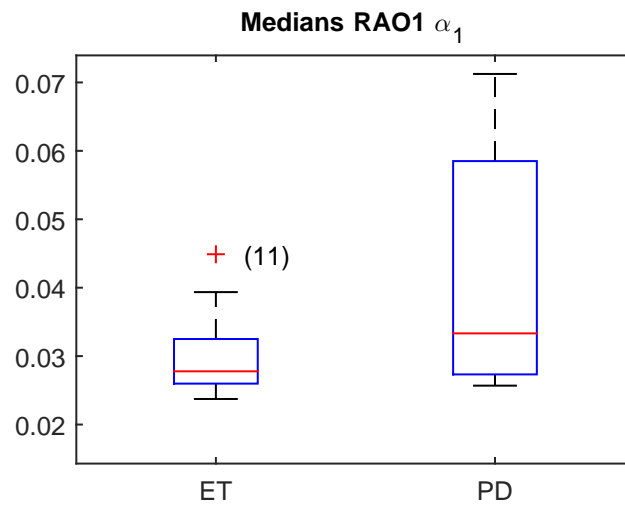


**Figure 3.7:** Coherence results at the task RAO1. For every subject, the median of the coherence values at all 1891 electrode pairs is taken. Shown are the average median (bars) and the standard deviation (black lines). Significant frequency bands are marked with an asterisk (\*). The following outliers were removed:  $\theta$ : ET 15,  $\alpha_1$ : ET 11,  $\beta_2$ : ET 4, 13, PD 5,  $\gamma_1$ : ET 4, PD 5.

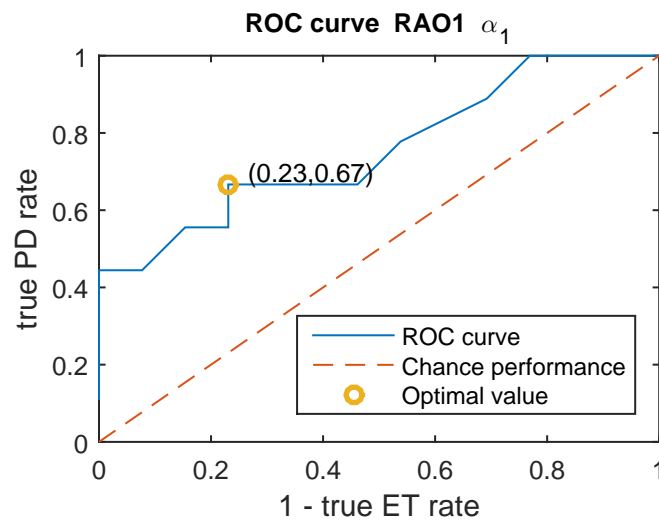
At  $\alpha_1$ , PD coherence values exceeded ET at 15.1% of all electrode pairs, while ET exceeded PD at 0.5% of all electrode pairs. The significant electrode pairs are shown in Figure 3.8a. Of all significant electrode pairs, 34% were found within the right hemisphere, 32% in the left and 34% between hemispheres. The medians are shown in the boxplots in Figure 3.8b. The ROC curve is shown in Figure 3.8c. The optimal cut-off point is 0.0290, which gives a true PD rate of 67% and a true ET rate of 77%. The AUC is equal to 0.74.



(a) Significant electrode pairs: electrode pairs that showed group differences at  $P < 0.05$ . Left: electrode pairs where ET coherence exceeded PD coherence. Right: electrode pairs where PD coherence exceeded ET coherence.



(b) Boxplot of the medians. Outliers are marked with a plus sign (+).



(c) ROC curve of the medians.

**Figure 3.8:** Results coherence analysis at the  $\alpha_1$  frequency band at the task RAO1.

### 3.4.3 RAO2

The coherence results at RAO2 are summarized in Figure 3.9. The coherence values shown are the mean and standard deviation of the medians of all subjects. The frequency bands marked with an asterisk (\*) are the significant frequency bands. Significant at RAO2 are the  $\alpha_1$  (7 - 10 Hz),  $\alpha_2$  (10 - 13 Hz) and  $\gamma_1$  (30 - 45 Hz) frequency bands (only  $\alpha_1$  was significant at RAO1).

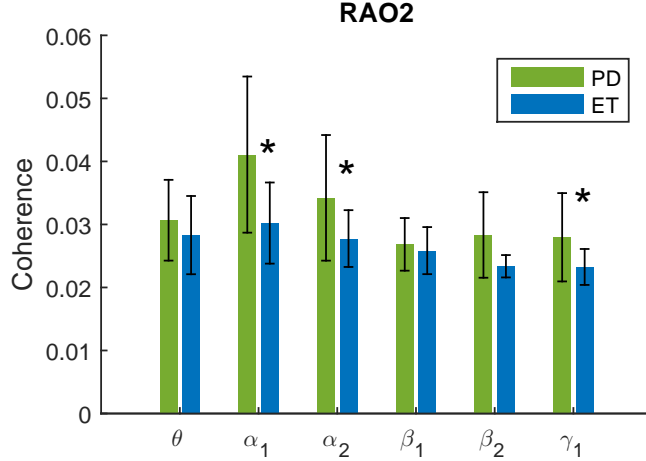
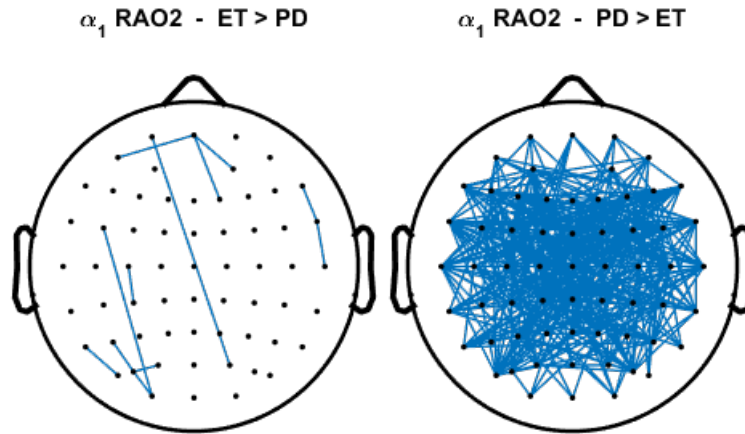


**Figure 3.9:** Coherence results at the task RAO2. For every subject, the median of the coherence values at all 1891 electrode pairs is taken. Shown are the average median (bars) and the standard deviation (black lines). Significant frequency bands are marked with an asterisk (\*). The following outliers were removed:  $\theta$ : ET 15, 5,  $\alpha_1$ : PD 6,  $\alpha_2$ : PD 9,  $\beta_1$ : PD 6,  $\beta_2$ : ET 13, 4,  $\gamma_1$ : ET 4.

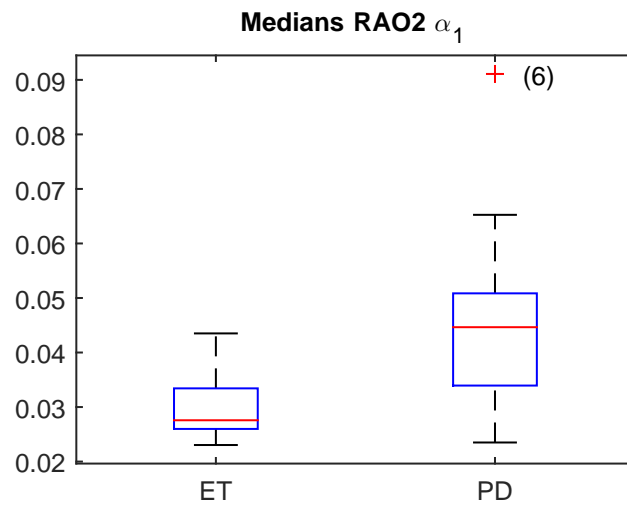
At the  $\alpha_1$  band, PD coherence values exceeded ET at 19.9% of all electrode pairs, while ET exceeded PD at 0.6% of all pairs. The significant electrode pairs are shown in Figure 3.10a. Of all significant electrode pairs, 24% were found within the right hemisphere, 31% in the left and 44% between hemispheres. Medians are shown in Figure 3.10b. The ROC curve is shown in Figure 3.10c. The optimal cut-off point is 0.0320, which gives a true PD rate of 88% and a true ET rate of 71% (67% and 77% at RAO1). The AUC is equal to 0.81 (0.74 at RAO1).

At  $\alpha_2$ , PD coherence values exceeded ET at 12.1% of all electrode pairs (ET exceeded PD at only 0.3% of all pairs). The significant electrode pairs are shown in Figure 3.11a. Of all significant electrode pairs, 25% were found within the right hemisphere, 36% in the left and 39% between hemispheres. Medians are shown in Figure 3.11b. The ROC curve is shown in Figure 3.11c. The optimal cut-off point is 0.0290, which gives a true PD rate of 75% and a true ET rate of 64%. The AUC is equal to 0.71.

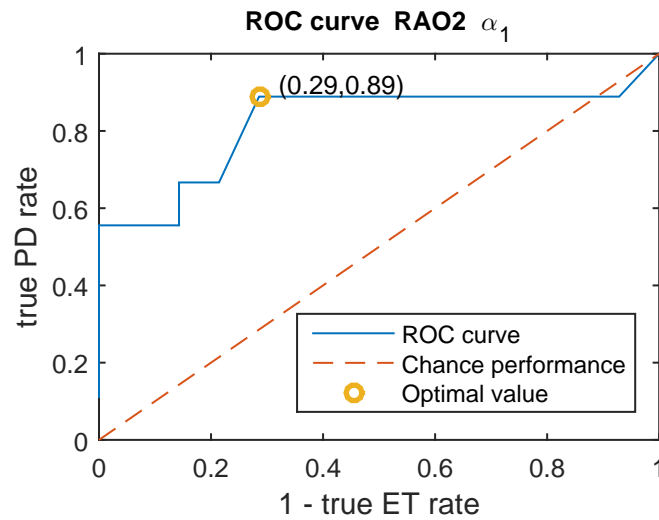
At  $\gamma_1$  band, PD coherence values exceeded ET at 11.2% of all electrode pairs (ET exceeded PD at 1.0% of all pairs). The significant electrode pairs are shown in Figure 3.12a. Of all significant electrode pairs, 25% were found within the right hemisphere, 30% in the left and 45% between hemispheres. Medians are shown in Figure 3.12b. The ROC curve is shown in Figure 3.12c. The optimal cut-off point is 0.0360, which gives a true PD rate of 89% and a true ET rate of 64%. The AUC is equal to 0.82.



(a) Significant electrode pairs: electrode pairs that showed group differences at  $P < 0.05$ . Left: electrode pairs where ET coherence exceeded PD coherence. Right: electrode pairs where PD coherence exceeded ET coherence.

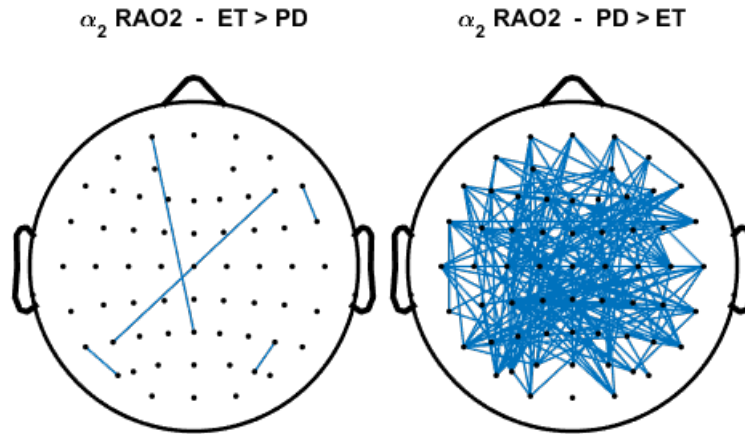


(b) Boxplot of the medians. Outliers are marked with a plus sign (+).

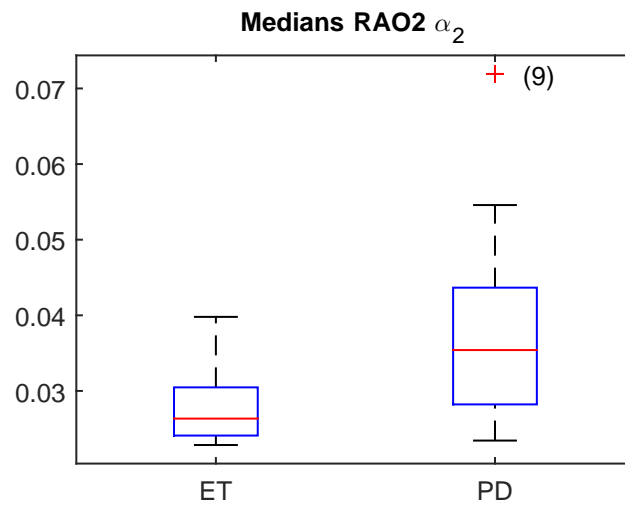


(c) ROC curve of the medians.

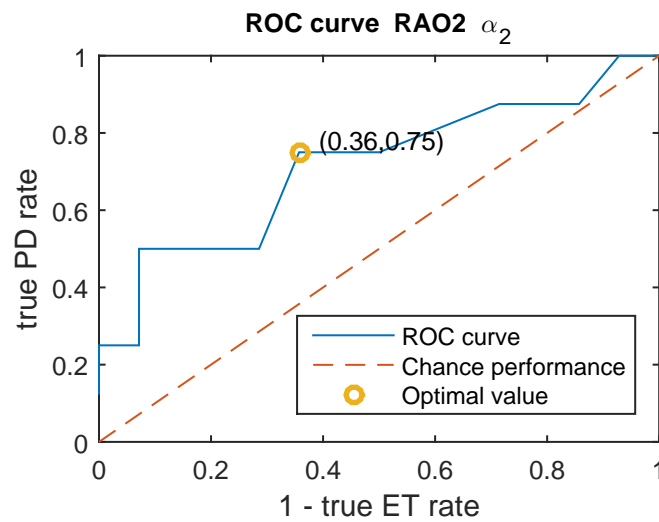
**Figure 3.10:** Results coherence analysis at the  $\alpha_1$  frequency band at the task RAO2.



(a) Significant electrode pairs: electrode pairs that showed group differences at  $P < 0.05$ . Left: electrode pairs where ET coherence exceeded PD coherence. Right: electrode pairs where PD coherence exceeded ET coherence.

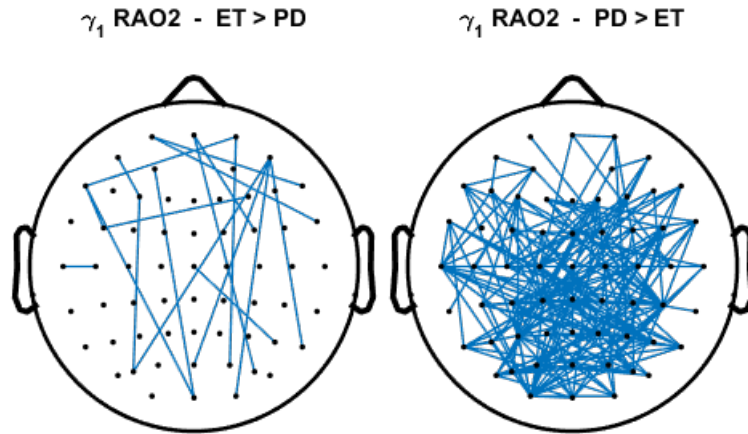


(b) Boxplot of the medians. Outliers are marked with a plus sign (+).

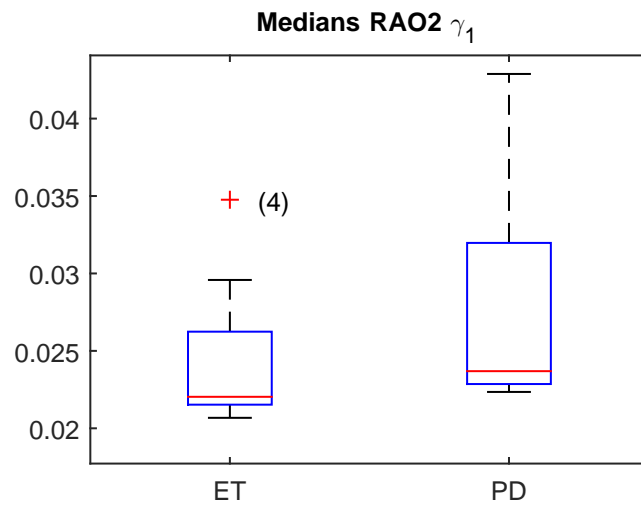


(c) ROC curve of the medians.

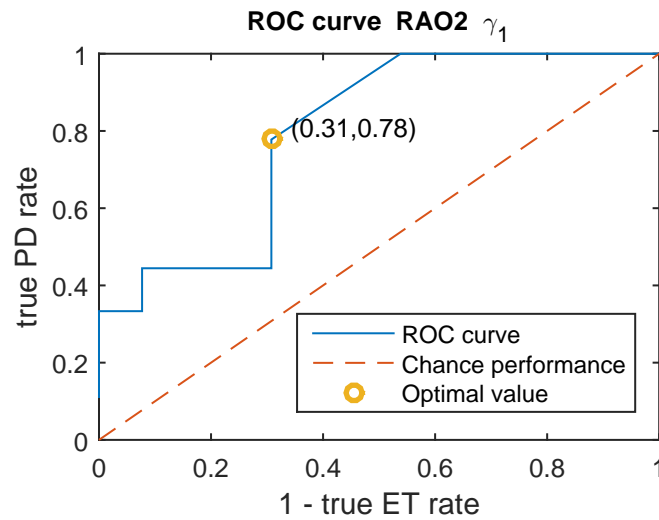
**Figure 3.11:** Results coherence analysis at the  $\alpha_2$  frequency band at the task RAO2.



(a) Significant electrode pairs: electrode pairs that showed group differences at  $P < 0.05$ . Left: electrode pairs where ET coherence exceeded PD coherence. Right: electrode pairs where PD coherence exceeded ET coherence.



(b) Boxplot of the medians. Outliers are marked with a plus sign (+).



(c) ROC curve of the medians.

**Figure 3.12:** Results coherence analysis at the  $\gamma_1$  frequency band at the task RAO2.

### 3.4.4 BAO1

The coherence results at BAO1 are summarized in Figure 3.13. The coherence values shown are the mean and standard deviation of the medians of all subjects. The frequency bands marked with an asterisk (\*) are the significant frequency bands. Significant at BAO1 are the  $\theta$  (4 - 7 Hz),  $\alpha_1$  (7 - 10 Hz) and  $\alpha_2$  (10 - 13 Hz) frequency bands.

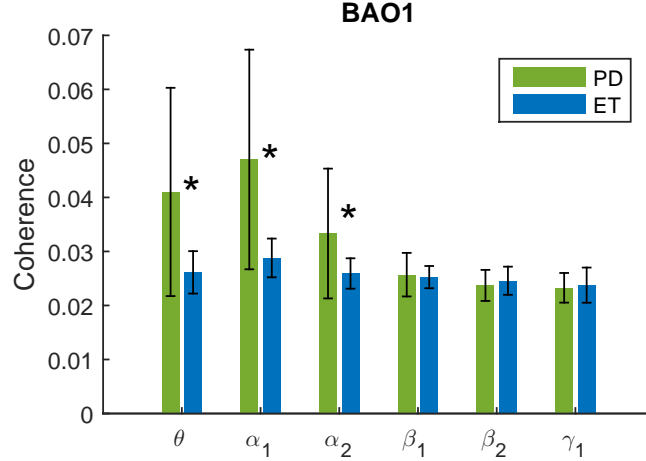


**Figure 3.13:** Coherence results at the task BAO1. For every subject, the median of the coherence values at all 1891 electrode pairs is taken. Shown are the average median (bars) and the standard deviation (black lines). Significant frequency bands are marked with an asterisk (\*). The following outliers were removed:  $\theta$ : ET 15, 3, 4,  $\alpha_1$ : ET 4,  $\alpha_2$ : ET 4,  $\beta_1$ : ET 4, 6,  $\beta_2$ : ET 4,  $\gamma_1$ : ET 4, PD 5, 9.

At the  $\theta$  frequency band, PD coherence values exceeded ET at 6.2% of all electrode pairs, while ET exceeded PD at 1.2% of all pairs. The locations of the significant electrode pairs are shown in Figure 3.14a. Of all significant electrode pairs, 29% were found within the right hemisphere, 28% in the left and 42% between hemispheres.

Boxplots of the medians are shown in Figure 3.14b. The ROC curve is shown in Figure 3.14c. The optimal cut-off point is 0.0270, which gives a true PD rate of 78% and a true ET rate of 82%.

The AUC is equal to 0.77.

At  $\alpha_1$ , PD coherence values exceeded ET at 14.9% of all electrode pairs, while ET exceeded PD at only 0.3% of all pairs. The locations of the significant electrode pairs are shown in Figure 3.15a. Of all significant electrode pairs, 26% were found within the right hemisphere, 35% in the left and 39% between hemispheres.

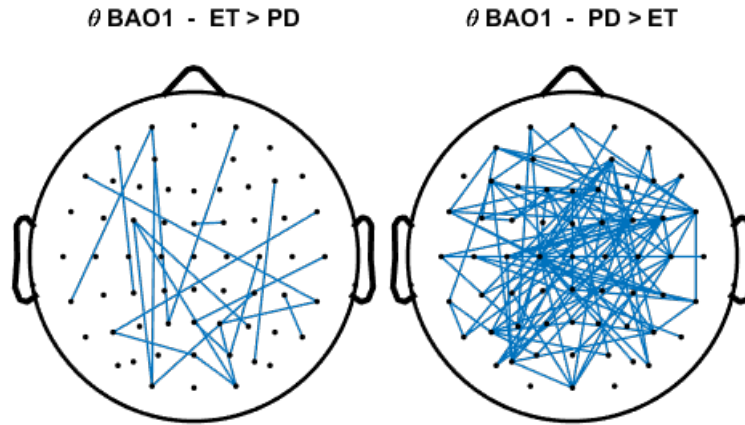
Medians are shown in Figure 3.15b. The ROC curve is shown in Figure 3.15c. The optimal cut-off point is 0.0320, which gives a true PD rate of 78% and a true ET rate of 77%.

The AUC is equal to 0.79.

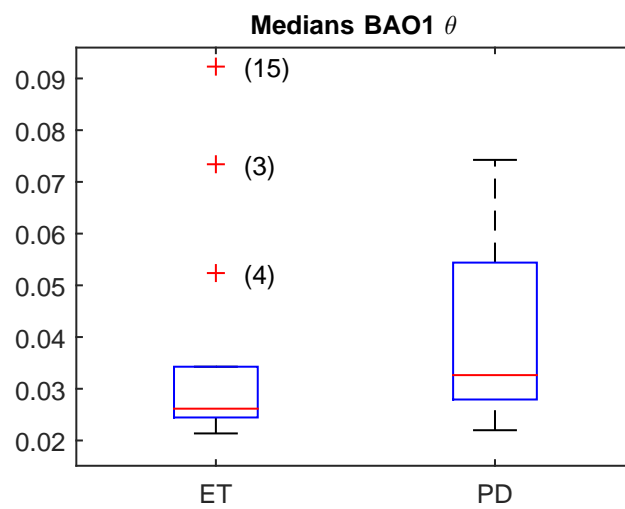
At  $\alpha_2$ , PD exceeded ET at 10.3% of all electrode pairs (ET exceeded PD at 0.6% of all pairs). The locations of the significant electrode pairs are shown in Figure 3.16a. Of all significant electrode pairs, 27% were found within the right hemisphere, 31% in the left and 42% between hemispheres.

Medians are shown in Figure 3.16b. The ROC curve is shown in Figure 3.16c. The optimal cut-off point is 0.0310, which gives a true PD rate of 50% and a true ET rate of 100%.

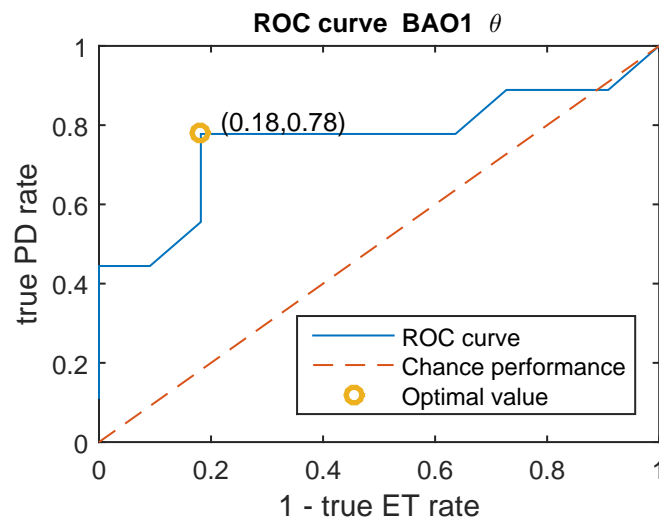
The AUC is equal to 0.71.



(a) Significant electrode pairs: electrode pairs that showed group differences at  $P < 0.05$ . Left: electrode pairs where ET coherence exceeded PD coherence. Right: electrode pairs where PD coherence exceeded ET coherence.

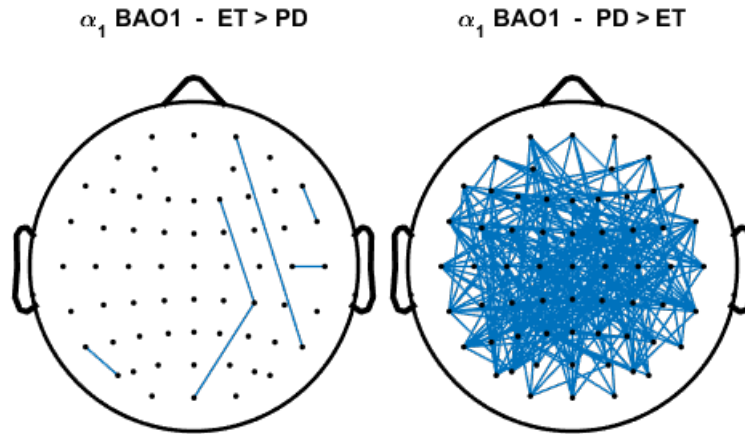


(b) Boxplot of the medians. Outliers are marked with a plus sign (+).

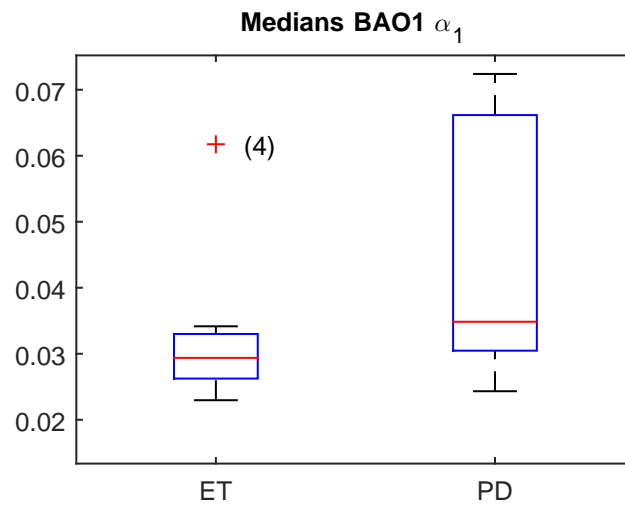


(c) ROC curve of medians.

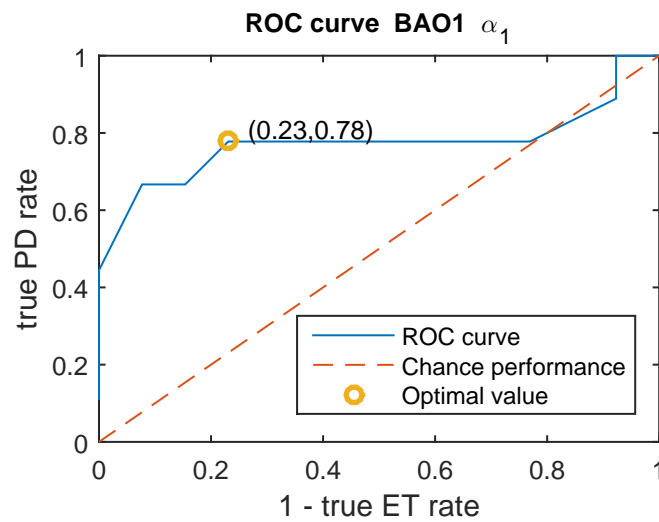
**Figure 3.14:** Results coherence analysis at the  $\theta$  frequency band at the task BAO1.



(a) Significant electrode pairs: electrode pairs that showed group differences at  $P < 0.05$ . Left: electrode pairs where ET coherence exceeded PD coherence. Right: electrode pairs where PD coherence exceeded ET coherence.

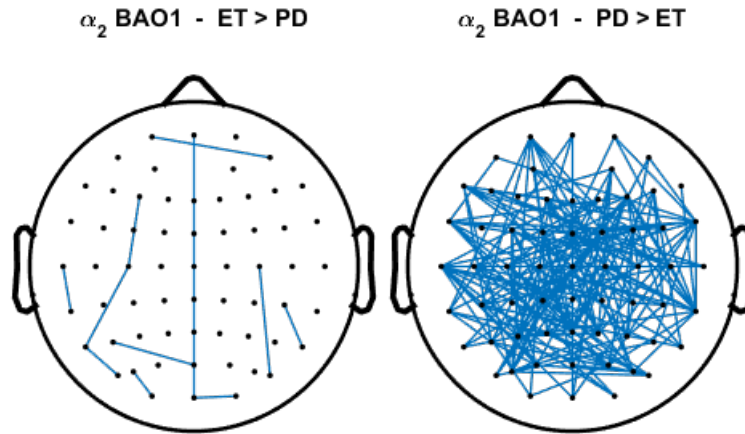


(b) Boxplot of the medians. Outliers are marked with a plus sign (+).

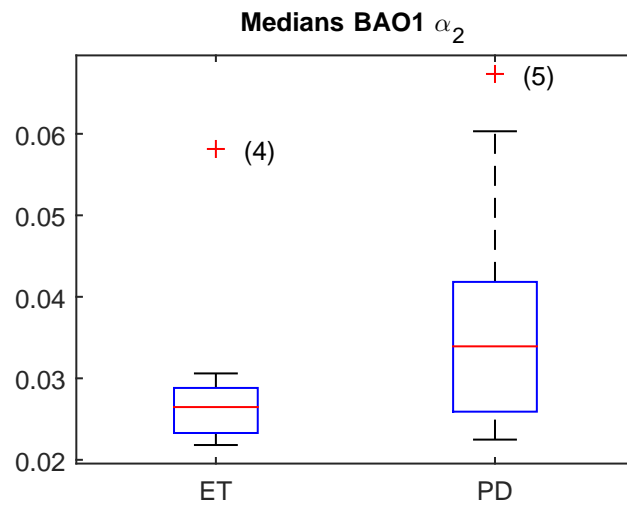


(c) ROC curve of the medians.

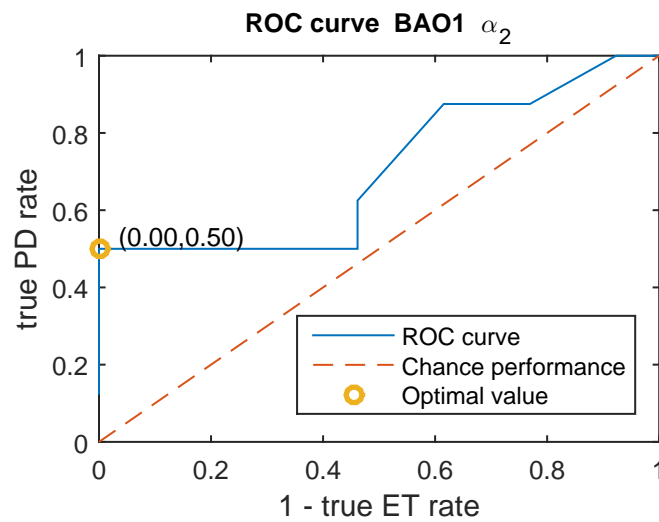
**Figure 3.15:** Results coherence analysis at the  $\alpha_1$  frequency band at the task BAO1.



(a) Significant electrode pairs: electrode pairs that showed group differences at  $P < 0.05$ . Left: electrode pairs where ET coherence exceeded PD coherence. Right: electrode pairs where PD coherence exceeded ET coherence.



(b) Boxplot of the medians. Outliers are marked with a plus sign (+).



(c) ROC curve of the medians.

**Figure 3.16:** Results coherence analysis at the  $\alpha_2$  frequency band at the task BAO1.

### 3.4.5 BAO2

The overall coherence at BAO2 is shown in Figure 3.17. The coherence values shown are the mean and standard deviation of the medians of all subjects. The frequency bands marked with a (\*) are the significant frequency bands. Significant at BAO2 are the  $\theta$  (4 - 7 Hz),  $\alpha_1$  (7 - 10 Hz) and  $\alpha_2$  (10 - 13 Hz) frequency bands (the same bands were significant at BAO1).

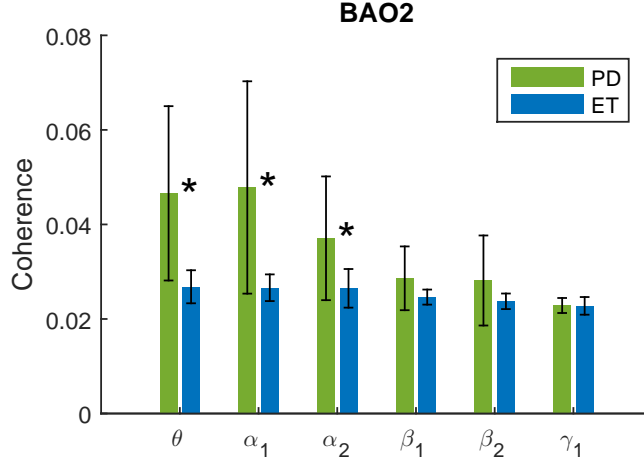


**Figure 3.17:** Coherence results at the task BAO2. For every subject, the median of the coherence values at all 1891 electrode pairs is taken. Shown are the average median (bars) and the standard deviation (black lines). Significant frequency bands are marked with an asterisk (\*). The following outliers were removed:  $\theta$ : ET 15, 3,  $\alpha_1$ : ET 4, 12,  $\alpha_2$ : ET 4  $\beta_1$ : ET 4, 6,  $\beta_2$ : ET 4,  $\gamma_1$ : ET 4, PD 5, 9.

At the  $\theta$  frequency band, PD coherence values exceeded ET at 17.4% of all electrode pairs, while ET exceeded PD at only 0.2% of all pairs. The locations of the significant electrode pairs are shown in Figure 3.18a. Of all significant electrode pairs, 21% were found within the right hemisphere, 32% in the left and 47% between hemispheres.

Boxplots of the medians are shown in Figure 3.18b. The ROC curve is shown in Figure 3.18c. The optimal cut-off point is 0.0290, which gives a true PD rate of 78% and a true ET rate of 83% (78% and 82% at BAO1).

The AUC is equal to 0.79 (0.77 at BAO1).

At  $\alpha_1$ , PD exceeded ET at 24.1% of all electrode pairs (ET exceeded PD at only 0.3% of all pairs). The locations of the significant electrode pairs are shown in Figure 3.19a. Of all significant electrode pairs, 22% were found within the right hemisphere, 39% in the left and 38% between hemispheres.

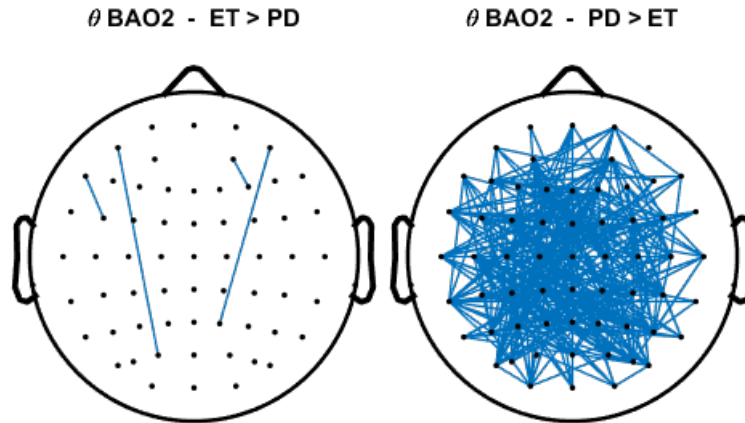
Boxplots of the medians are shown in Figure 3.19b. The ROC curve is shown in Figure 3.19c. The optimal cut-off point is 0.0290, which gives a true PD rate of 89% and a true ET rate of 83% (78% and 77% at BAO1).

The AUC is equal to 0.87 (0.79 at BAO1).

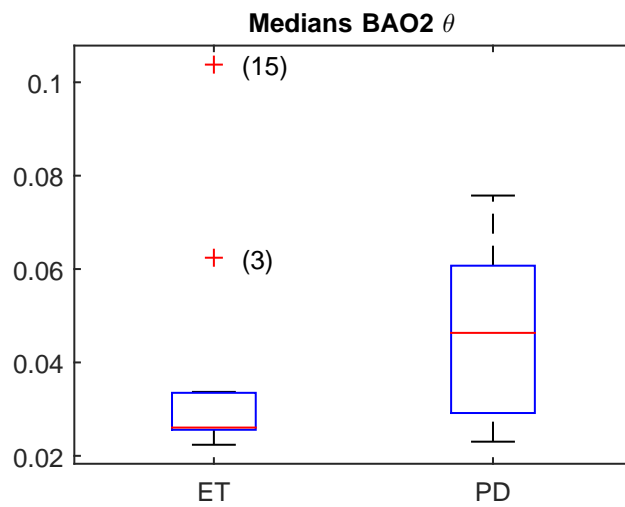
At  $\alpha_2$ , PD exceeded ET at 12.9% of all electrode pairs (ET exceeded PD at 0.9% of all pairs). The locations of the significant electrode pairs are shown in Figure 3.20a. Of all significant electrode pairs, 26% were found within the right hemisphere, 35% in the left and 39% between hemispheres.

Medians are illustrated by the boxplots in Figure 3.20b. The ROC curve is shown in Figure 3.20c. The optimal cut-off point is 0.0270, which gives a true PD rate of 78% and a true ET rate of 77% (50% and 100% at BAO1).

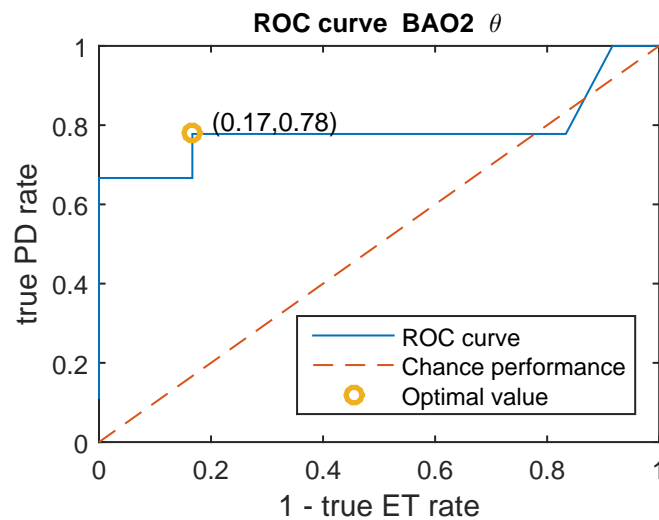
The AUC is equal to 0.79 (0.71 at BAO1).



(a) Significant electrode pairs: electrode pairs that showed group differences at  $P < 0.05$ . Left: electrode pairs where ET coherence exceeded PD coherence. Right: electrode pairs where PD coherence exceeded ET coherence.

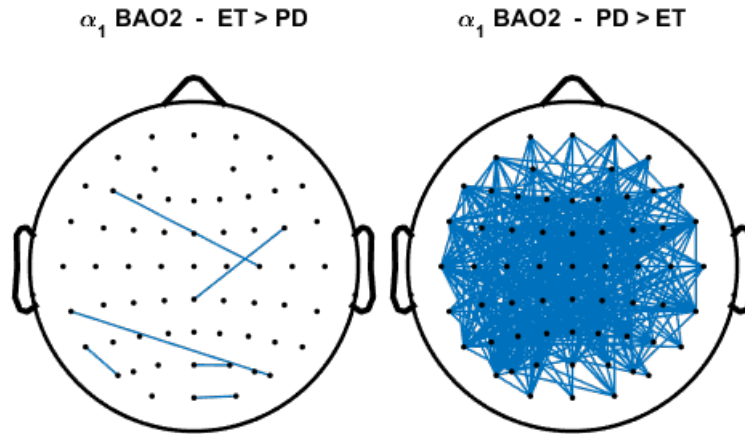


(b) Boxplot of the medians. Outliers are marked with a plus sign (+).

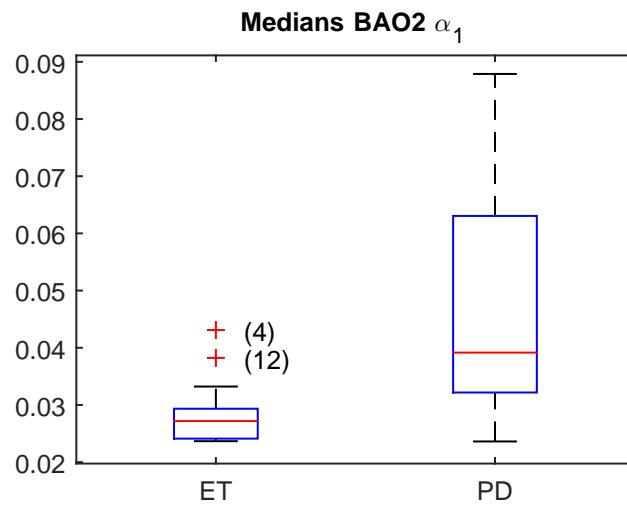


(c) ROC curve of the medians.

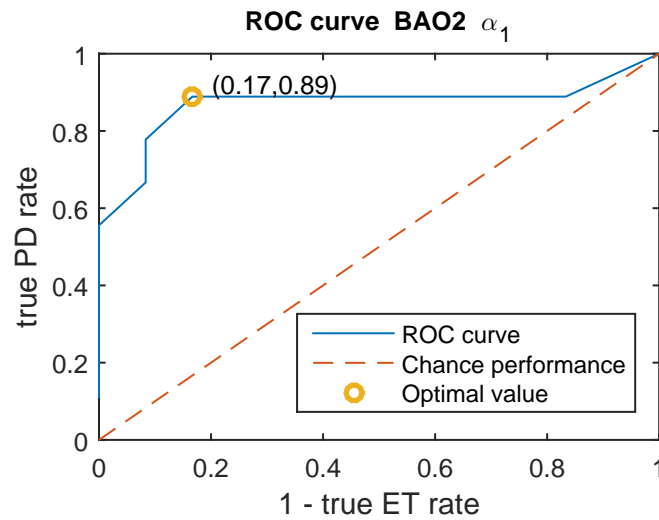
**Figure 3.18:** Results coherence analysis at the  $\theta$  frequency band at the task BAO2.



(a) Significant electrode pairs: electrode pairs that showed group differences at  $P < 0.05$ . Left: electrode pairs where ET coherence exceeded PD coherence. Right: electrode pairs where PD coherence exceeded ET coherence.

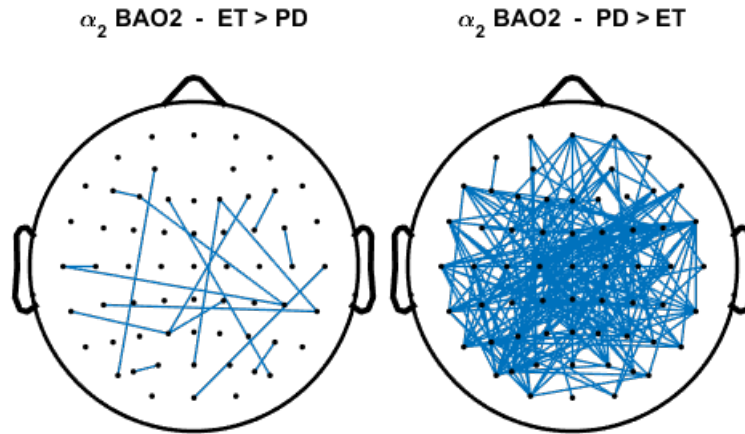


(b) Boxplot of the medians. Outliers are marked with a plus sign (+).

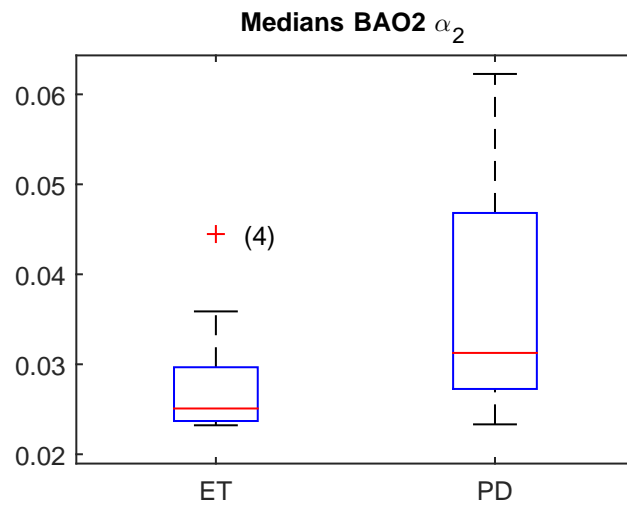


(c) ROC curve of the medians.

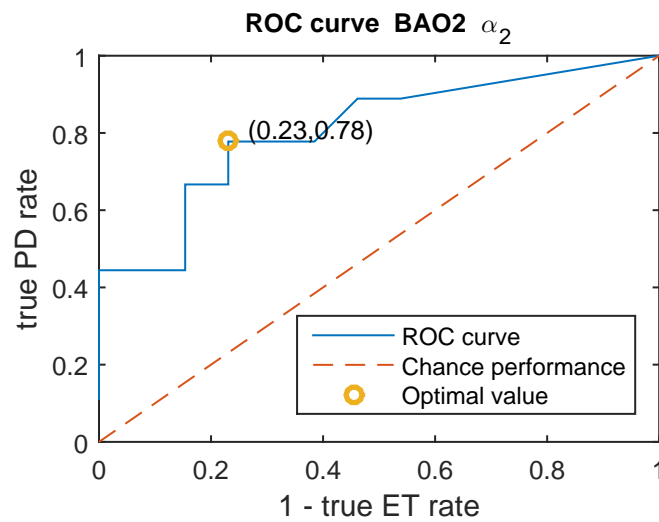
**Figure 3.19:** Results coherence analysis at the  $\alpha_1$  frequency band at the task BAO2.



(a) Significant electrode pairs: electrode pairs that showed group differences at  $P < 0.05$ . Left: electrode pairs where ET coherence exceeded PD coherence. Right: electrode pairs where PD coherence exceeded ET coherence.



(b) Boxplot of the medians. Outliers are marked with a plus sign (+).



(c) ROC curve of the medians.

**Figure 3.20:** Coherence: Results coherence analysis at the  $\alpha_2$  frequency band at the task BAO2.

### 3.4.6 Overview

An overview of the results of the coherence analysis is shown in Table 3.2. This table shows for every frequency band-task combination the AUC. For completeness, AUC values of the non-significant frequency bands are also included.

**Table 3.2:** Summary coherence ROC analysis.

	(a) AUC values.						(b) AUC color legend.		
	AUC						AUC legend		
	$\theta$	$\alpha_1$	$\alpha_2$	$\beta_1$	$\beta_2$	$\gamma_1$	Value	Accuracy	Color
REST	0.62	0.81	0.75	0.51	0.57	0.54	0.50 - 0.75	Bad	
RAO1	0.68	0.74	0.66	0.56	0.53	0.54	0.75 - 0.80	Fair	
RAO2	0.61	0.81	0.71	0.58	0.74	0.82	0.80 - 0.90	Good	
BAO1	0.77	0.79	0.71	0.52	0.61	0.52	0.90 - 1.00	Excellent	
BAO2	0.79	0.87	0.79	0.61	0.51	0.54			

## 3.5 Discussion

The previous section shows the results of the coherence analysis. The plots of the locations of the significant electrode pairs do not show that the significant electrode pairs are located in a specific region. There is, however, a slight asymmetry. At all tasks except RAO1 and the combination  $\theta$  - BAO1, the percentage of significant electrode pairs within the left hemisphere is larger than the percentage of significant electrode pairs within the right hemisphere, although less pronounced at REST. All patients in the group PD are right handed and have most tremor on the right side. More significant electrode pairs in the left hemisphere could indicate more abnormal behaviour in the hemisphere that controls the right side.

At almost all task-frequency band combinations, outliers were detected and removed before the ROC curve was determined. Because classification of the outliers depends on the set thresholds, it is important to note that all significant frequency bands, except  $\theta$  - BAO1, were also significant (AUC > 0.75) without outlier removal. Removing the outliers only improved the tests ability to distinguish between PD and ET. Furthermore, outliers were mostly the same patients. At the  $\theta$  frequency band, 5 of the 8 outliers were ET patient 15. At the other frequency bands, 16 of the 22 outliers were ET patient 4. For the PD group, 7 of the 13 outliers were PD patient 5.

There is a difference between the first and the second time the RAO and BAO tasks were performed. At RAO1, no frequency band had an AUC higher than 0.75. At RAO2,  $\alpha_1$  and  $\gamma_1$  had an AUC > 0.80. At BAO1, AUC values were above 0.75 at  $\theta$  (with outlier removal) and  $\alpha_1$ . At BAO2, these AUC values were higher, especially in the  $\alpha_1$  band. Furthermore,  $\alpha_2$  also had an AUC above 0.75.

We do not know what causes these differences, but it could be the case that abnormal brain activity increases when patients get tired or have to make more effort to perform the task. This could be further investigated by including another repetition (RAO3, BAO3) and determine the AUC values of those tasks. Another option could be to increase the duration of BAO1 and RAO1 and to evaluate coherence in time (see also Chapter 6).

Based on the AUC values, the best frequency band-task combinations to distinguish between PD and ET are  $\alpha_1$  - (REST, RAO2, BAO2) and  $\gamma_1$  - RAO2.

## Chapter 4

# Phase Synchronization

Phase synchronization can be used to measure connectivity between different brain regions. Section 4.1 introduces the definition of phase synchronization and the *Phase Locking Value* (PLV). The application of the method to the recorded EEG signals is explained in Section 4.2. The statistical methods used to test for significant differences are given in Section 4.3 and the results are shown in Section 4.4. The discussion about the results can be found in Section 4.5. The discussion about the used methods is given in Chapter 6.

### 4.1 Mathematical method

Phase synchronization is defined as the locking of the phases of two signals  $x(t)$  and  $y(t)$ , i.e.

$$\phi_{xy}(t) = \phi_x(t) - \phi_y(t) = \text{constant}, \quad (4.1)$$

where  $\phi_x$  and  $\phi_y$  are the instantaneous phases of two signals  $x(t)$  and  $y(t)$ .

To determine the instantaneous phase for signals that are not truly harmonic, the Hilbert transformation (HT) may be used. To this end, the signal  $x(t)$  is transformed into

$$z(t) = x(t) + i\tilde{x}(t) = A(t)e^{i\phi(t)}, \quad (4.2)$$

where  $\tilde{x}(t)$  is the HT of  $x(t)$  defined as

$$\tilde{x}(t) = \frac{1}{\pi} \text{PV} \int_{-\infty}^{\infty} \frac{x(\tau)}{t - \tau} d\tau. \quad (4.3)$$

Here PV denotes the Cauchy principal value. The signal  $z(t)$  is often called the analytic signal and  $A(t)$  is the ‘envelope’ or amplitude and  $\phi(t)$  the instantaneous phase.

One method capable to obtain the strength of phase synchronization is the PLV. For two signals  $x(t), y(t)$  with instantaneous phases  $\phi_x, \phi_y$ , the PLV is defined as

$$\text{PLV} = \left| \langle e^{i\phi_{xy}(t)} \rangle \right|, \quad (4.4)$$

where  $\langle \cdot \rangle$  denotes average over time. In words, the PLV measures how the relative phase  $\phi_{xy}$  is distributed over the unit circle. If two signals are phased synchronized, the relative phase will occupy a small portion of the unit circle and the PLV is high. Lack of synchronization gives rise to a relative phase that spreads out over the unit circle, resulting in a low PLV. PLV ranges between 0 and 1.

An example of high PLV and low PLV are shown in Example 3 and 4 in Appendix A.

### 4.2 EEG analysis

To determine the PLV, the phase difference between two EEG signals is needed. As explained in Section 4.1, this can be done using the HT. However,  $A(t)$  and  $\phi(t)$  only have a clear physical meaning if the

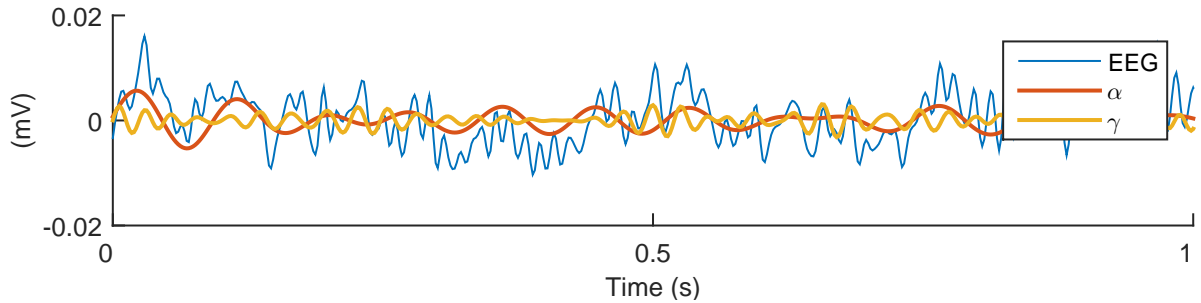


**Figure 4.1:** One second of an EEG signal (blue) and the  $\alpha$  waves (orange) and  $\gamma_1$  waves (yellow).

signal  $x(t)$  is a narrow-band signal (Boashash, 1992). Therefore, the EEG signals were filtered in the frequency bands in Table 2.2 before the HT was applied. An example of a filtered EEG signal is shown in Figure 4.1.

After both signals were filtered and phases were extracted, the PLV was determined according to Equation (4.4). This was done for all 1891 electrode pairs, which resulted in 56730 PLV's for each subject: one PLV for every electrode pair, for every task, for every frequency band.

### 4.3 Statistics

The statistical procedure described in this section is the same procedure used for the coherence analysis, given in Section 3.3. The procedure is, however, repeated here for convenience.

For each electrode pair, group differences between PD and ET were tested using the Wilcoxon rank sum test, which is a nonparametric test of the null hypothesis that two samples come from the same population. If the null hypothesis is rejected, subjects from a certain group tend to have larger values than subjects from the other group.

The null hypothesis was rejected with  $P < 0.05$ . If an electrode pair showed group differences, the electrode pair is said to be significant.

Before the Wilcoxon rank sum test was performed, outliers were removed. Let  $P = \{p_1, \dots, p_n\}$  be the set of PLV's of a specific group, where  $n$  is the number of subjects in the group. A value  $p_i$  was removed if

$$p_i > Q_3 + 1.5 \cdot IQR \quad \text{or} \quad p_i < Q_1 - 1.5 \cdot IQR.$$

Here,  $Q_1$  and  $Q_3$  are the first and third quartile of  $P$  and the interquartile range (IQR) is defined as the distance between  $Q_1$  and  $Q_3$ . If the data is normally distributed, the interval

$$[Q_1 - 1.5 \cdot IQR, \quad Q_3 + 1.5 \cdot IQR]$$

covers about 99.3 % of the data. An example of this statistical procedure can be found in Example 5 in Appendix A.

We visually inspected if the significant electrode pairs were located at a specific region. Furthermore, we checked the locations for asymmetry between the left and right hemisphere. This is done by comparing the percentage of significant electrode pair connections within the left hemisphere with connections within the right hemisphere.

Once the significant electrode pairs were determined, a test was developed to discriminate between the two groups. For every subject, the median of all PLV's (i.e. PLV's at all possible electrode pairs) is used for testing, still separately for every task and frequency band. From now on this is simply called *the median*.

The diagnostic test has the following form: if the median of a patient is less than cut-off point  $c$ , the patient gets the diagnosis ET. If the median is greater than  $c$ , the patients gets the diagnosis PD.

Receiver Operating Characteristic (ROC) curves can be used find the optimal cut-off point  $c$  and to evaluate the performance of such the test (see Infobox 2 on page 14).

Sensitivity and specificity are in this case defined as the probability that the test results in ‘PD’ when the patient actually has PD (true PD rate) and as the probability that the test will result in ‘ET’ when a patient actually has ET (true ET rate). Because both are equally important, the optimal cut-off point is the point that corresponds to the point on the ROC curve that has minimal distance to the ideal point (0% 1-specificity, 100% sensitivity).

A difference test is determined for every frequency band - task combination. To compare the different tests, we use the area under the curve (AUC) (see Infobox 2 on page 14). The higher the AUC, the better the test is able to distinguish between ET and PD. Before the ROC curve was determined, outliers in the medians were removed the same way as outliers in the PLV’s at an electrode pair.

## 4.4 Results

In this section, the results of the PLV analysis are given. The results are shown separately for each task. Only those frequency bands are discussed where more than 10% of all electrode pairs were significant electrode pairs or where  $AUC > 0.75$ . These bands will be called *significant frequency bands*.

### 4.4.1 REST

The PLV results at REST are summarized in Figure 3.4. The PLV's shown are the mean and standard deviation of the medians of all subjects. The frequency bands marked with an asterisk (\*) are the significant frequency bands. Significant at REST are the  $\alpha_1$  (7 - 10 Hz) and  $\alpha_2$  (10 - 13 Hz) frequency bands.

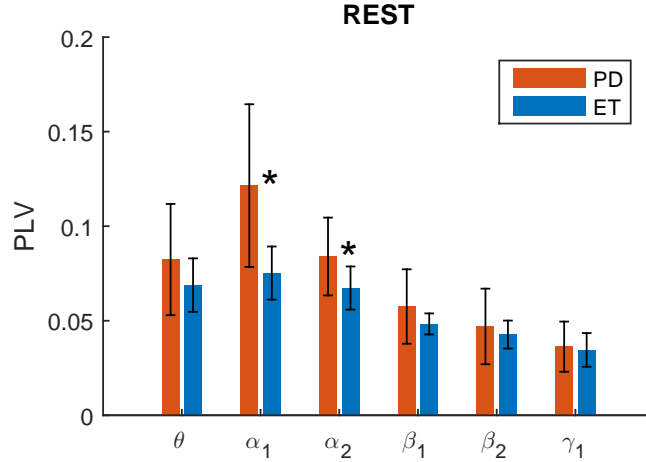


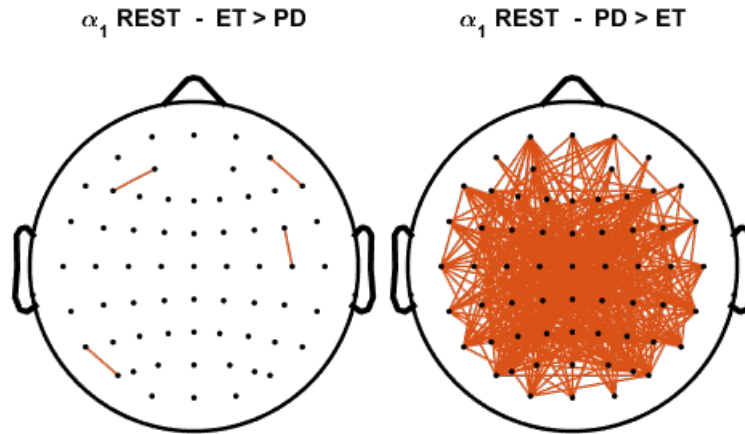
**Figure 4.2:** PLV results at the task REST. Shown are the mean (bars) and standard deviation (black lines) of the medians of all subjects. Significant frequency bands are marked with an asterisk (\*). The following outliers were removed:  $\theta$ : ET 15,  $\alpha_2$ : PD 9  $\beta_1$ : ET 6, 12,  $\gamma_1$ : PD 5.

At the  $\alpha_1$  frequency band, PD PLV exceeded ET at 24.5% of all electrode pairs, while ET exceeded PD at only 0.2 % of all pairs. The location of the significant electrode pairs are shown in Figure 4.3a. Of all significant electrode pairs, 26% were found within the right hemisphere, 35% in the left and 38% between hemispheres.

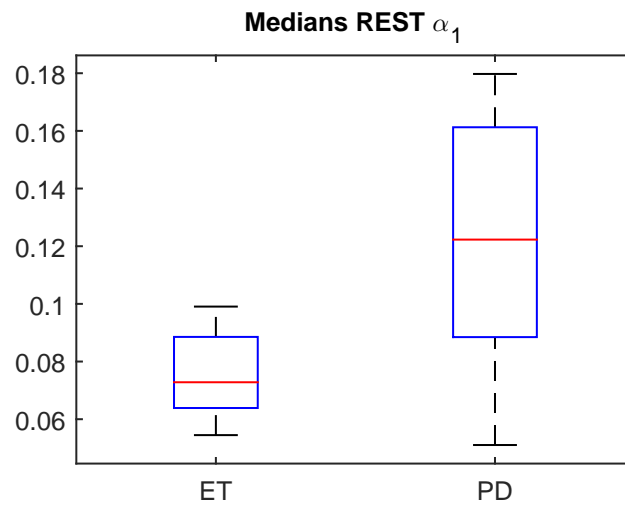
The medians are illustrated by the boxplots in Figure 4.3b. The ROC curve is shown in Figure 4.3c. The optimal cut-off point is 0.0890, which gives a true PD rate of 78% and a true ET rate of 79%. The AUC is equal to 0.83.

At  $\alpha_2$ , PD coherence exceeded ET at 12.2% of the electrode pairs (ET exceeded PD at only 0.4% of all pairs). The locations of the significant electrode pairs are shown in Figure 4.4a. Of all significant electrode pairs, 21% were found within the right hemisphere, 29% in the left and 50% between hemispheres.

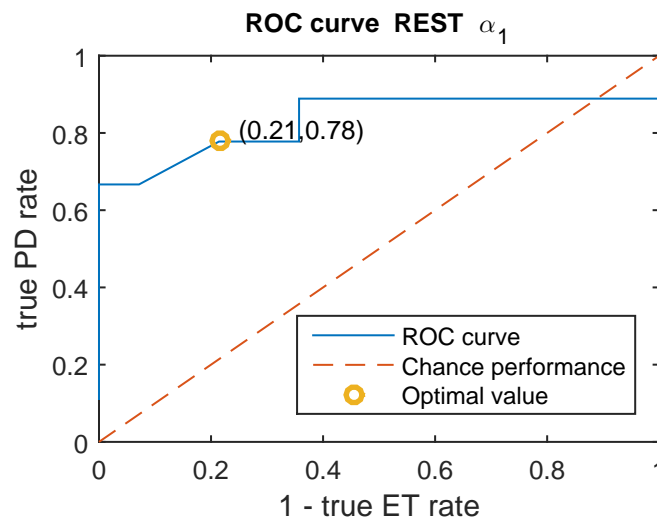
Boxplots of the medians are shown in Figure 4.4b. The ROC curve for  $\alpha_2$  is shown in Figure 4.4c. The optimal cut-off point is 0.0860, which gives a true PD rate of 63% and a true ET rate of 100%. The AUC is equal to 0.75.



(a) Significant electrode pairs: electrode pairs that showed group differences at  $P < 0.05$ . Left: electrode pairs where ET PLV exceeded PD PLV. Right: electrode pairs where PD PLV exceeded ET PLV.

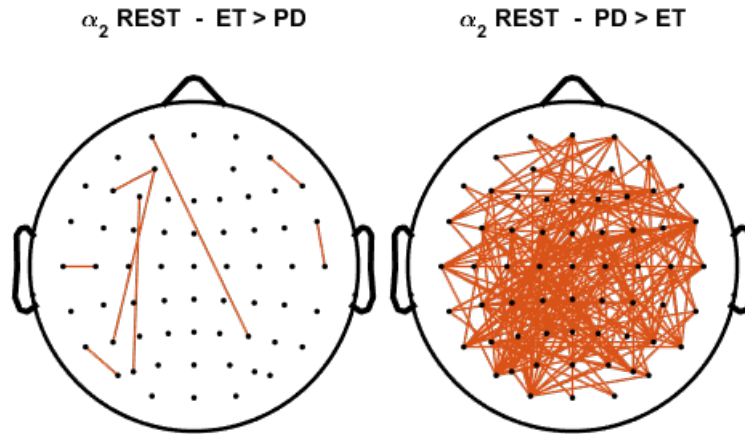


(b) Boxplot of the medians.

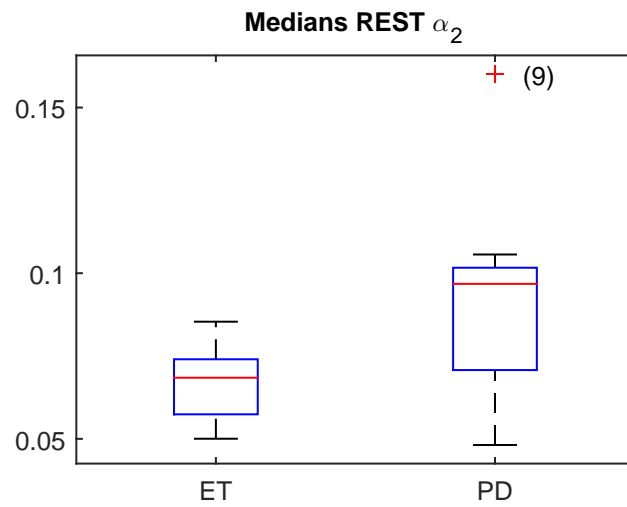


(c) ROC curve of the medians.

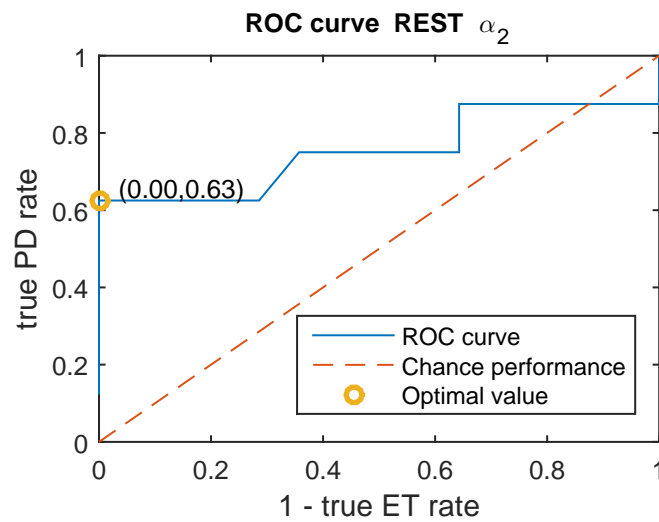
**Figure 4.3:** Results PLV analysis at the  $\alpha_1$  frequency band at the task REST.



(a) Significant electrode pairs: electrode pairs that showed group differences at  $P < 0.05$ . Left: electrode pairs where ET PLV exceeded PD PLV. Right: electrode pairs where PD PLV exceeded ET PLV.



(b) Boxplot of the medians. Outliers are marked with a plus sign (+).



(c) ROC curve of the medians.

**Figure 4.4:** Results PLV analysis at the  $\alpha_1$  frequency band at the task REST.

#### 4.4.2 RAO1

The PLV results at RAO1 are summarized in Figure 3.4. The PLV's shown are the mean and standard deviation of the medians of all subjects. The frequency bands marked with an asterisk (\*) are the significant frequency bands. Significant at RAO1 is the  $\alpha_1$  (7 - 10 Hz) frequency bands.

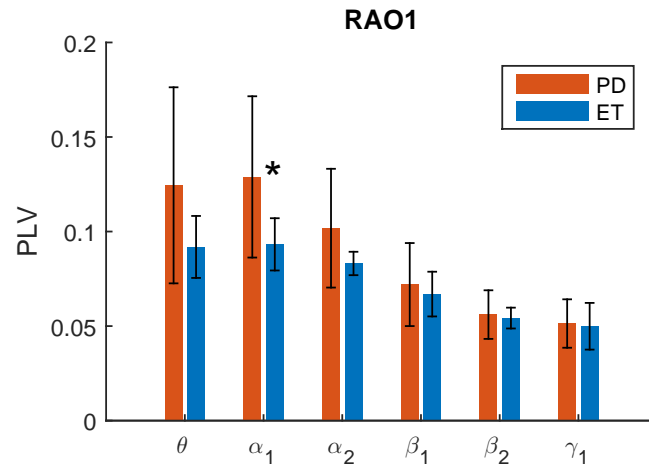
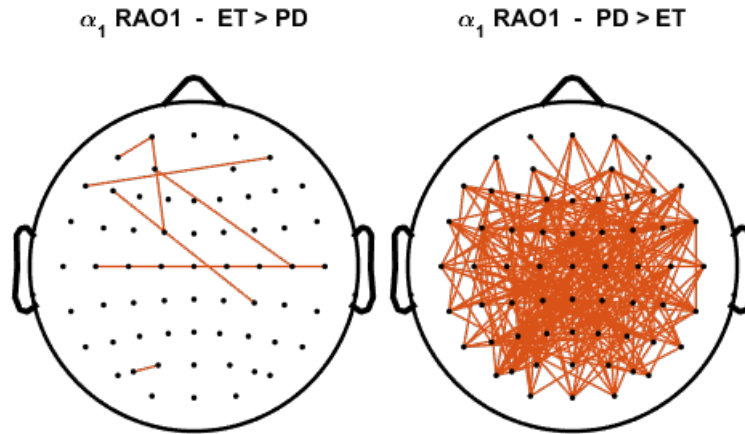


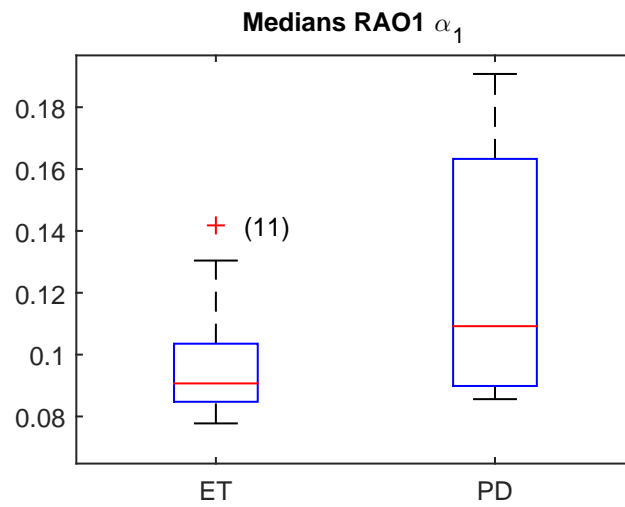
**Figure 4.5:** PLV results at the task RAO1. Shown are the mean (bars) and standard deviation (black lines) of the medians of all subjects. Significant frequency bands are marked with an asterisk (\*). The following outliers were removed:  $\theta$ : ET 15,  $\alpha_1$ : ET 11,  $\alpha_2$ : ET 4, 13, PD 9,  $\beta_2$ : ET 4,13, PD 5,  $\gamma_1$ : PD 5.

At the  $\alpha_1$  frequency band, PD PLV exceeded ET at 13.9% of all electrode pairs (ET exceeded PD at 0.4% of all pairs). The location of the significant electrode pairs are shown in Figure 4.6a. Of all significant electrode pairs, 34% were found within the right hemisphere, 31% in the left and 34% between hemispheres.

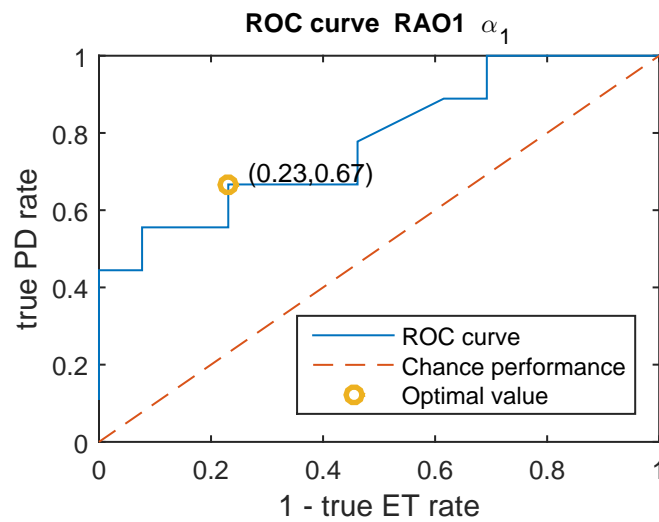
The medians are illustrated by the boxplots in Figure 4.6b. The ROC curve is shown in Figure 4.6c. The optimal cut-off point is 0.0930, which gives a true PD rate of 67% and a true ET rate of 77%. The AUC is equal to 0.78.



(a) Significant electrode pairs: electrode pairs that showed group differences at  $P < 0.05$ . Left: electrode pairs where ET PLV exceeded PD PLV. Right: electrode pairs where PD coherence exceeded ET coherence.



(b) Boxplot of the medians. Outliers are marked with a plus sign (+).



(c) ROC curve of the medians.

**Figure 4.6:** Results PLV analysis at the  $\alpha_1$  frequency band at the task RAO1.

### 4.4.3 RAO2

The PLV results at RAO1 are summarized in Figure 3.4. The PLV's shown are the mean and standard deviation of the medians of all subjects. The frequency bands marked with an asterisk (\*) are the significant frequency bands. Significant at RAO2 are the  $\alpha_1$  (7 - 10 Hz), the  $\beta_2$  (20 - 30 Hz) and the  $\gamma_1$  (30 - 45 Hz) frequency bands (significant at RAO1 was only the  $\alpha_1$  band).

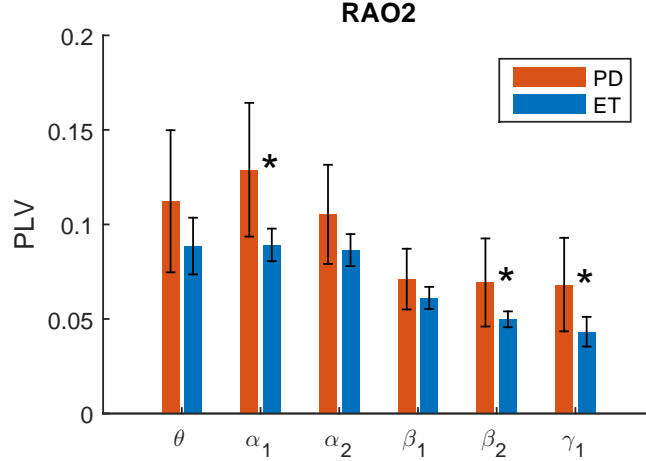


**Figure 4.7:** PLV results at the task RAO2. Shown are the mean (bars) and standard deviation (black lines) of the medians of all subjects. Significant frequency bands are marked with an asterisk (\*). The following outliers were removed:  $\theta$ : ET 3, 15,  $\alpha_1$ : ET 11, 13,  $\alpha_2$ : ET 13, PD 9,  $\beta_1$ : ET 13, PD 6,  $\beta_2$ : ET 3, 13,  $\gamma_1$ : ET 13.

At the  $\alpha_1$  frequency band, PD PLV exceeded ET at 15.5% of all electrode pairs (ET exceeded PD at 0.5% of all pairs). The location of the significant electrode pairs are shown in Figure 4.8a. Of all significant electrode pairs, 22% were found within the right hemisphere, 32% in the left and 45% between hemispheres.

The medians are illustrated by the boxplots in Figure 4.8b. The ROC curve is shown in Figure 4.8c. The optimal cut-off point is 0.1030, which gives a true PD rate of 89% and a true ET rate of 100% (67% and 77% at RAO1).

The AUC is equal to 0.89 (0.78 at RAO1).

At the  $\beta_2$  frequency band, PD PLV exceeded ET at 9.7% of all electrode pairs (ET exceeded PD at 1.4% of all pairs). The location of the significant electrode pairs are shown in Figure 4.9a. Of all significant electrode pairs, 25% were found within the right hemisphere, 23% in the left and 51% between hemispheres.

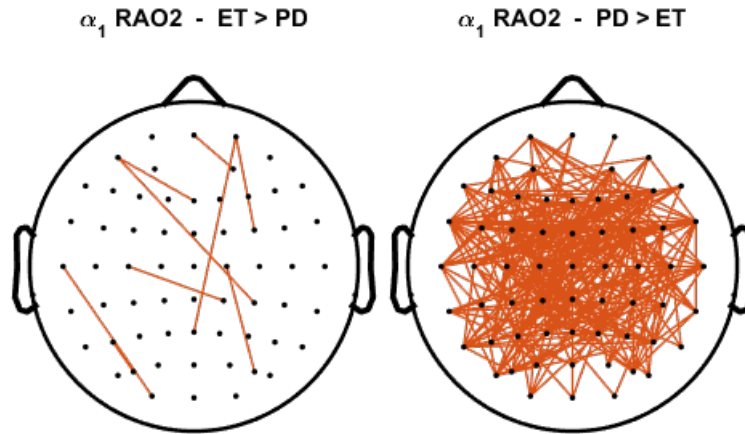
The boxplots in Figure 4.9b show the medians. The ROC curve is shown in Figure 4.9c. The optimal cut-off point is 0.0570, which gives a true PD rate of 56% and a true ET rate of 100%.

The AUC is equal to 0.75..

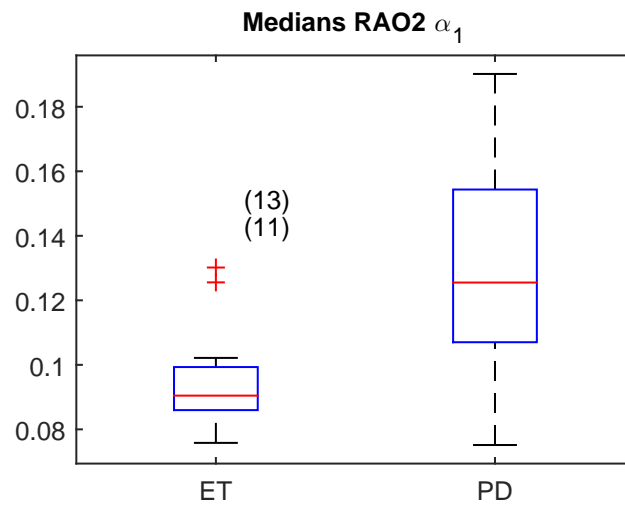
At the  $\gamma_1$  frequency band, PD PLV exceeded ET at 9.7% of all electrode pairs (ET exceeded PD at 1.0% of all pairs). The location of the significant electrode pairs are shown in Figure 4.10a. Of all significant electrode pairs, 26% were found within the right hemisphere, 27% in the left and 47% between hemispheres.

The medians are illustrated by the boxplots in Figure 4.10b. The ROC curve is shown in Figure 4.10c. The optimal cut-off point is 0.0490, which gives a true PD rate of 78% and a true ET rate of 85%.

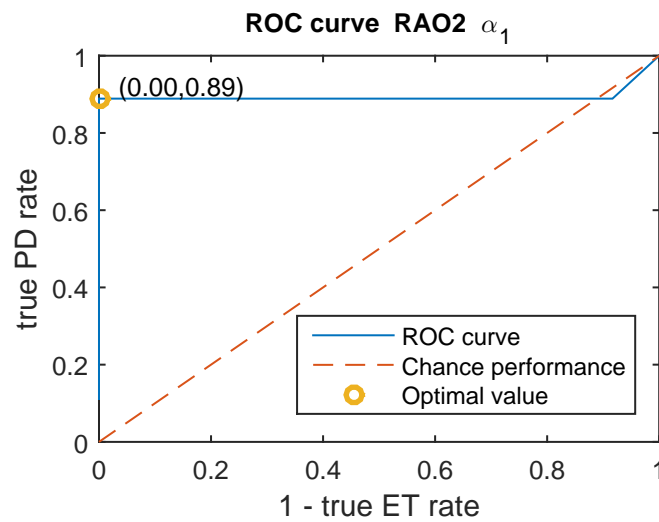
The AUC is equal to 0.88.



(a) Significant electrode pairs: electrode pairs that showed group differences at  $P < 0.05$ . Left: electrode pairs where ET PLV exceeded PD PLV. Right: electrode pairs where PD PLV exceeded ET PLV.

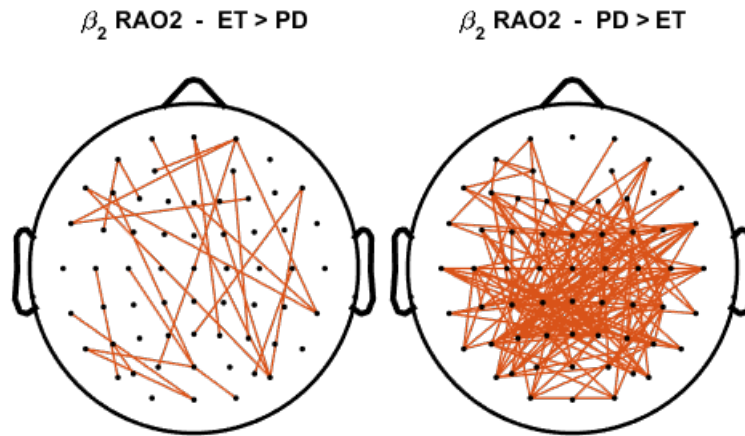


(b) Boxplot of the medians. Outliers are marked with a plus sign (+).

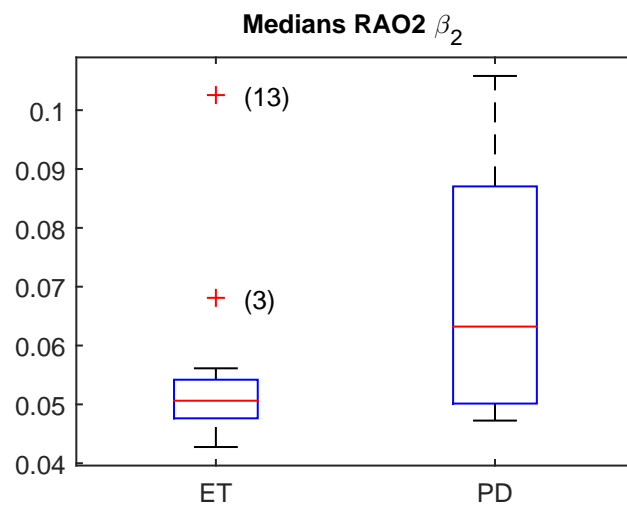


(c) ROC curve of the medians.

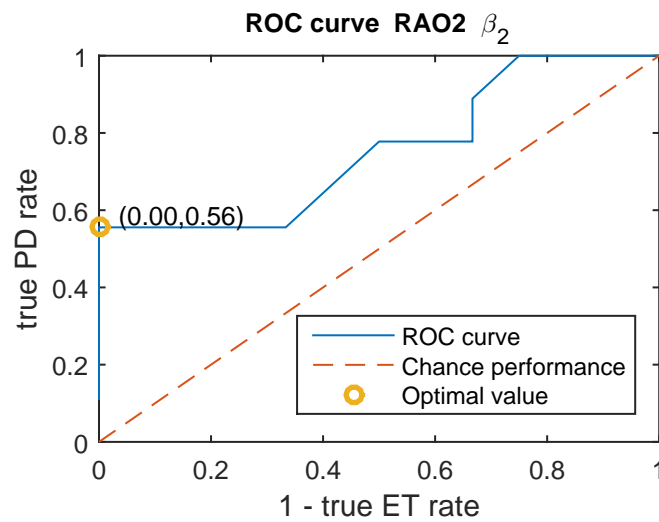
**Figure 4.8:** Results PLV analysis at the  $\alpha_1$  frequency band at the task RAO2.



(a) Significant electrode pairs: electrode pairs that showed group differences at  $P < 0.05$ . Left: electrode pairs where ET PLV exceeded PD PLV. Right: electrode pairs where PD PLV exceeded ET PLV.

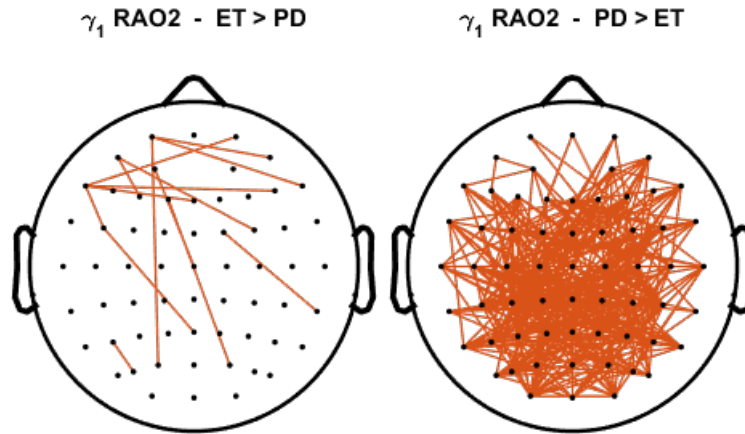


(b) Boxplot of the medians. Outliers are marked with a plus sign (+).

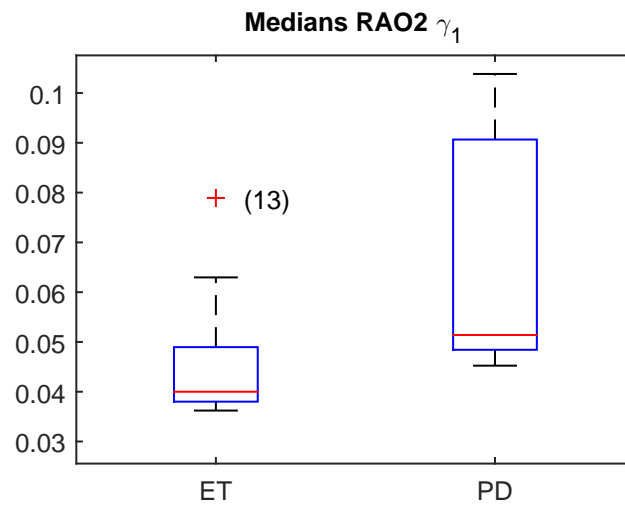


(c) ROC curve of the medians.

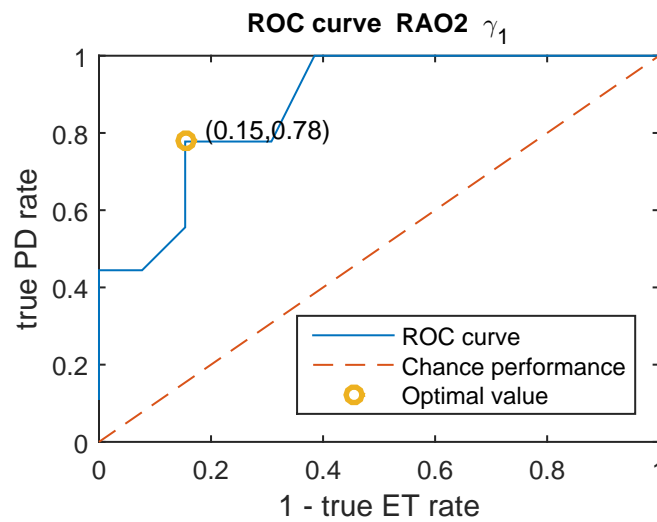
**Figure 4.9:** Results PLV analysis at the  $\beta_2$  frequency band at the task RAO2.



(a) Significant electrode pairs: electrode pairs that showed group differences at  $P < 0.05$ . Left: electrode pairs where ET PLV exceeded PD PLV. Right: electrode pairs where PD PLV exceeded ET PLV.



(b) Boxplot of the medians. Outliers are marked with a plus sign (+).



(c) ROC curve of the medians.

**Figure 4.10:** Results PLV analysis at the  $\gamma_1$  frequency band at the task RAO2.

#### 4.4.4 BAO1

The PLV results at RAO1 are summarized in Figure 3.4. The PLV's shown are the mean and standard deviation of the medians of all subjects. The frequency bands marked with an asterisk (\*) are the significant frequency bands. Significant at BAO1 is the  $\alpha_1$  (7 - 10 Hz) frequency band.

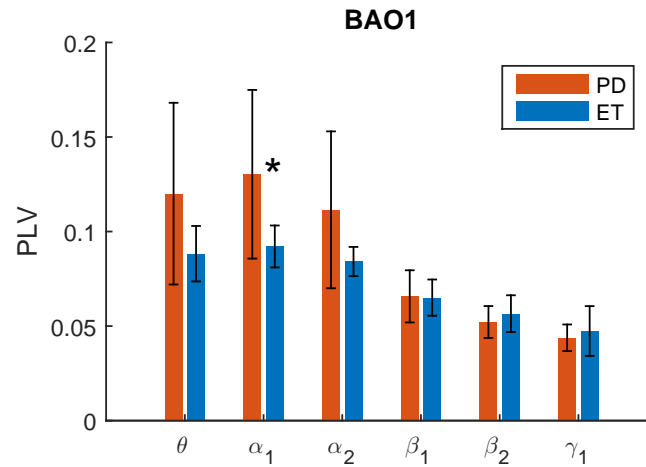
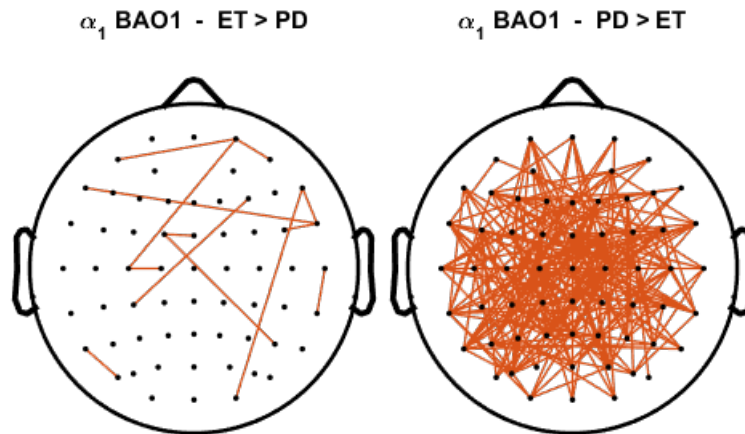


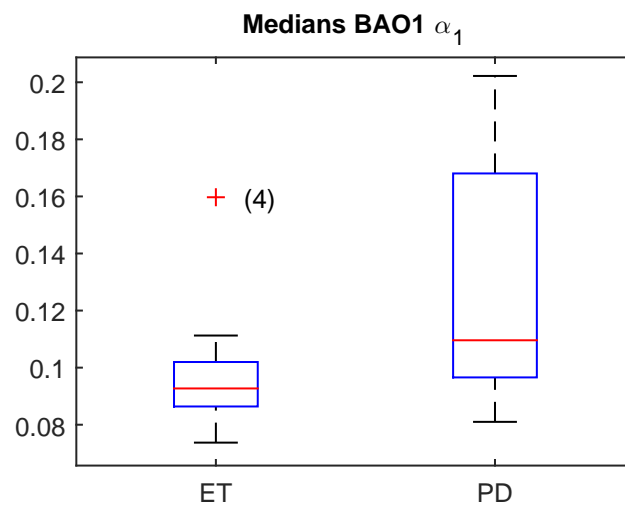
**Figure 4.11:** PLV results at the task BAO1. Shown are the mean (bars) and standard deviation (black lines) of the medians of all subjects. Significant frequency bands are marked with an asterisk (\*). The following outliers were removed:  $\theta$ : ET 3, 15,  $\alpha_1$ : ET 4,  $\alpha_2$ : ET 4,  $\beta_1$ : ET 4, PD 5,  $\beta_2$ : ET 4, PD 5,  $\gamma_1$ : PD 5.

At the  $\alpha_1$  frequency band, PD PLV exceeded ET at 12.3% of all electrode pairs, while ET exceeded PD at 0.7 % of all pairs. The location of the significant electrode pairs are shown in Figure 4.12a. Of all significant electrode pairs, 27% were found within the right hemisphere, 37% in the left and 37% between hemispheres.

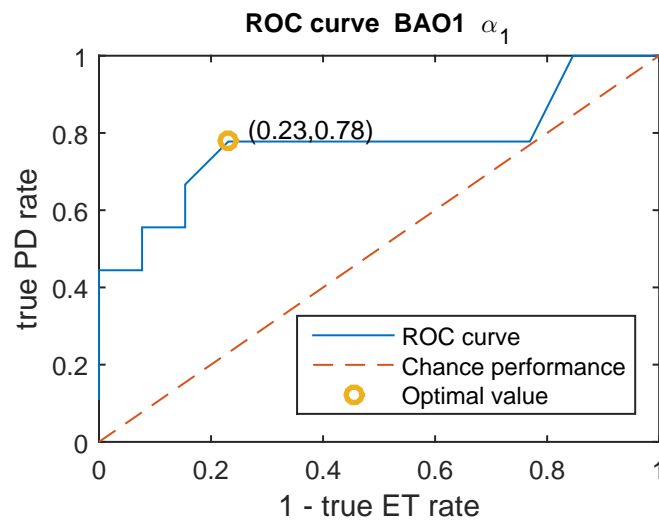
Boxplots of the medians are shown in Figure 4.12b. The ROC curve is shown in Figure 4.12c. The optimal cut-off point is 0.1000, which gives a true PD rate of 78% and a true ET rate of 77%. The AUC is equal to 0.77.



(a) Significant electrode pairs: electrode pairs that showed group differences at  $P < 0.05$ . Left: electrode pairs where ET coherence exceeded PD coherence. Right: electrode pairs where PD coherence exceeded ET coherence.



(b) Boxplot of the medians. Outliers are marked with a plus sign (+).



(c) ROC curve of the medians.

**Figure 4.12:** Results PLV analysis at the  $\alpha_1$  frequency band at the task BAO1.

#### 4.4.5 BAO2

The PLV results at BAO2 are summarized in Figure 3.4. The PLV's shown are the mean and standard deviation of the medians of all subjects. The frequency bands marked with an asterisk (\*) are the significant frequency bands. Significant at BAO2 are the  $\theta$  (4 - 7 Hz),  $\alpha_1$  (7 - 10 Hz) and  $\alpha_2$  (10 - 13 Hz) frequency bands (significant at BAO1 was only the  $\alpha_1$  band).

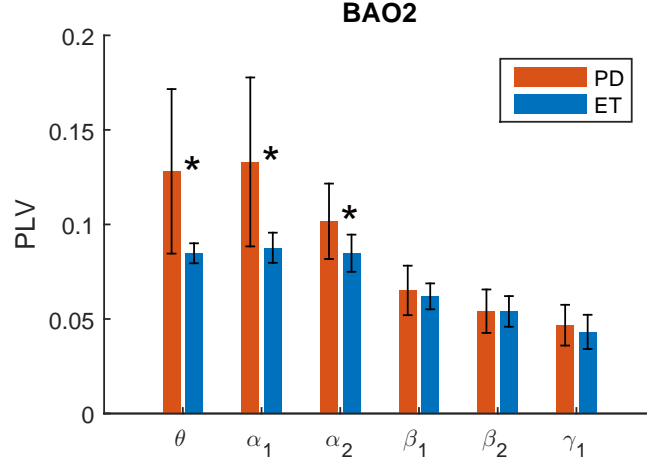


**Figure 4.13:** PLV results at the task BAO2. Shown are the mean (bars) and standard deviation (black lines) of the medians of all subjects. Significant frequency bands are marked with an asterisk (\*). The following outliers were removed:  $\theta$ : ET 3, 4, 15,  $\alpha_1$ : ET 4,  $\alpha_2$ : ET 4, PD 9,  $\beta_1$ : ET 4, 6, PD 5,  $\beta_2$ : ET 4, PD 5,  $\gamma_1$ : ET 4, PD 5.

At the  $\theta$  frequency band, PD PLV exceeded ET at 13.1% of all electrode pairs (ET exceeded PD at 0.4% of all pairs). The location of the significant electrode pairs are shown in Figure 4.14a. Of all significant electrode pairs, 23% were found within the right hemisphere, 34% in the left and 42% between hemispheres.

The medians are illustrated by the boxplots in Figure 4.14b. The ROC curve is shown in Figure 4.14c. The optimal cut-off point is 0.0910, which gives a true PD rate of 78% and a true ET rate of 100%. The AUC is equal to 0.82.

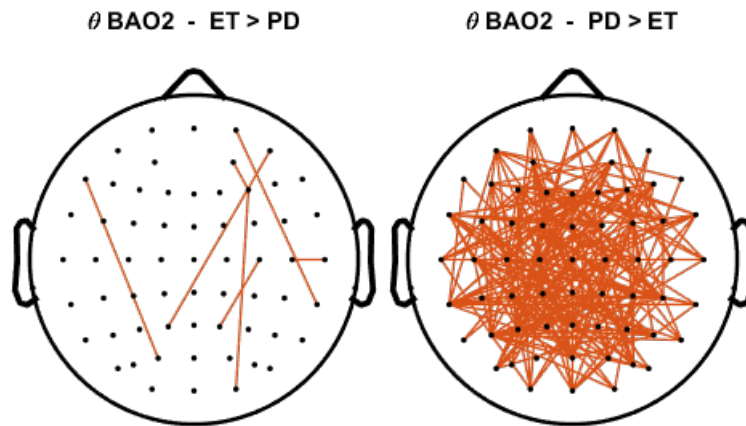
At the  $\alpha_1$  frequency band, PD PLV exceeded ET at 20.4% of all electrode pairs, while ET exceeded PD at only 0.3 % of all pairs. The location of the significant electrode pairs are shown in Figure 4.15a. Of all significant electrode pairs, 26% were found within the right hemisphere, 37% in the left and 37% between hemispheres.

The boxplots in Figure 4.15b show the medians. The ROC curve is shown in Figure 4.15c. The optimal cut-off point is 0.1010, which gives a true PD rate of 78% and a true ET rate of 92% (78% and 77% at BAO1).

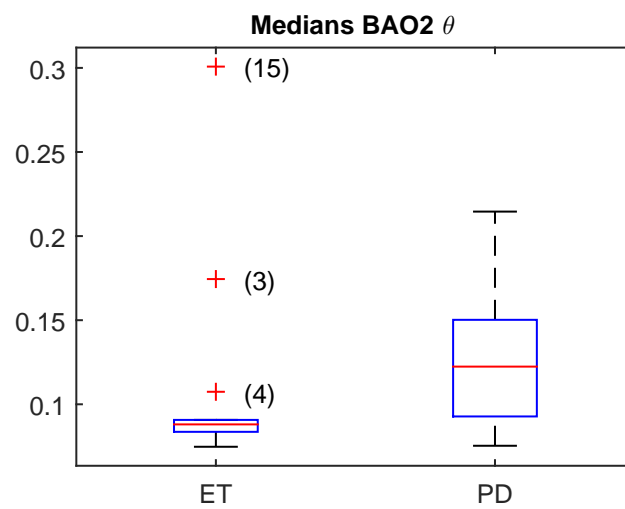
The AUC is equal to 0.87 (0.77 at BAO1).

At the  $\alpha_2$  frequency band, PD PLV exceeded ET at 9.5% of all electrode pairs, while ET exceeded PD at 0.9 % of all pairs. The location of the significant electrode pairs are shown in Figure 4.16a. Of all significant electrode pairs, 20% were found within the right hemisphere, 36% in the left and 45% between hemispheres.

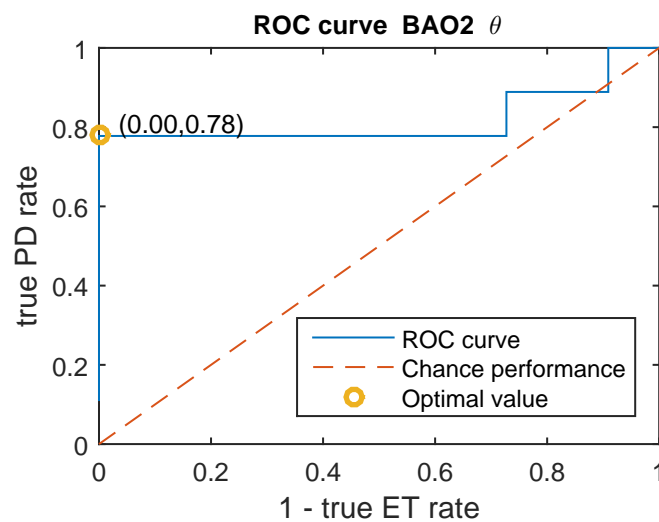
The medians are illustrated by the boxplots in Figure 4.16b. The ROC curve is shown in Figure 4.16c. The optimal cut-off point is 0.0880, which gives a true PD rate of 88% and a true ET rate of 70%. The AUC is equal to 0.78.



(a) Significant electrode pairs: electrode pairs that showed group differences at  $P < 0.05$ . Left: electrode pairs where ET PLV exceeded PD PLV. Right: electrode pairs where PD PLV exceeded ET PLV.

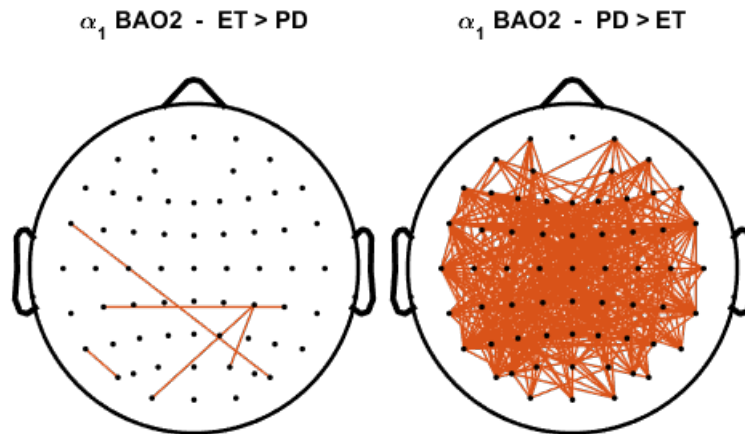


(b) Boxplot of the medians. Outliers are marked with a plus sign (+).

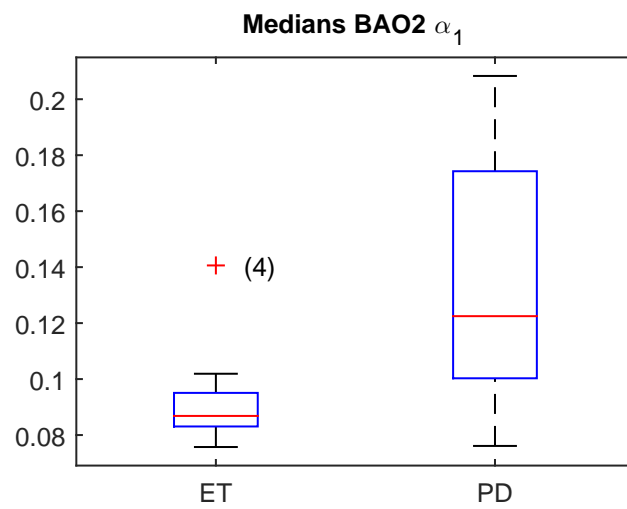


(c) ROC curve of the medians.

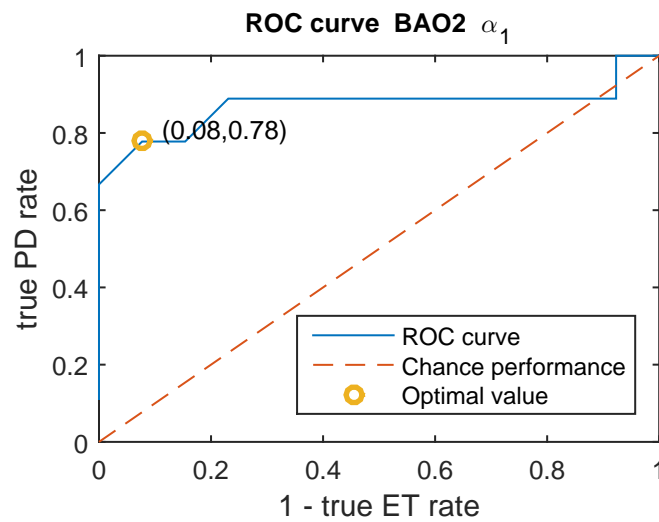
**Figure 4.14:** Results PLV analysis at the  $\theta$  frequency band at the task BAO2.



(a) Significant electrode pairs: electrode pairs that showed group differences at  $P < 0.05$ . Left: electrode pairs where ET PLV exceeded PD PLV. Right: electrode pairs where PD PLV exceeded ET PLV.

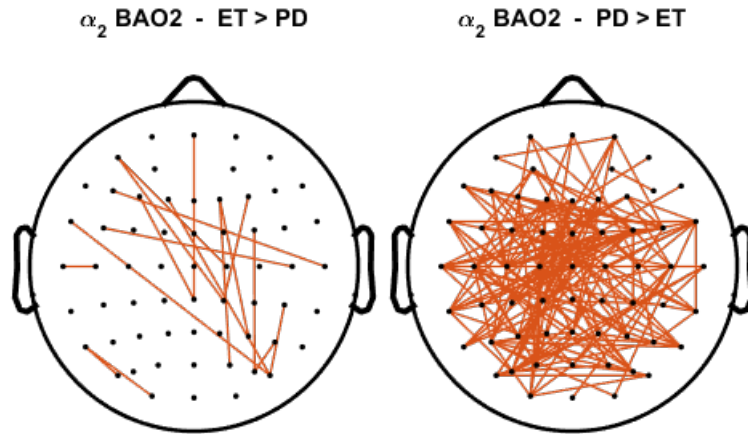


(b) Boxplot of the medians. Outliers are marked with a plus sign (+).

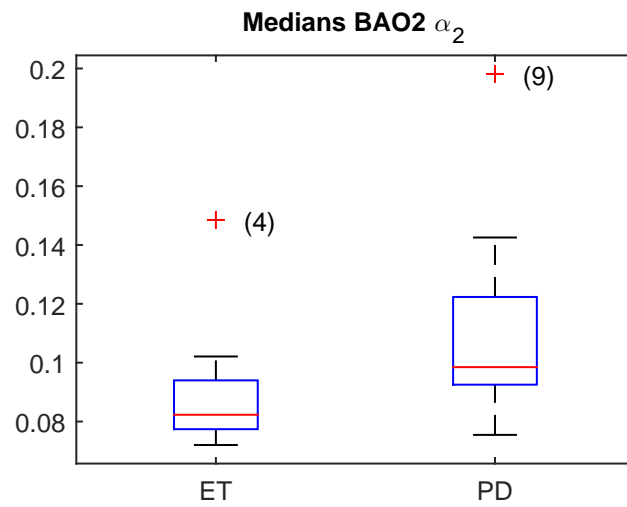


(c) ROC curve of the medians.

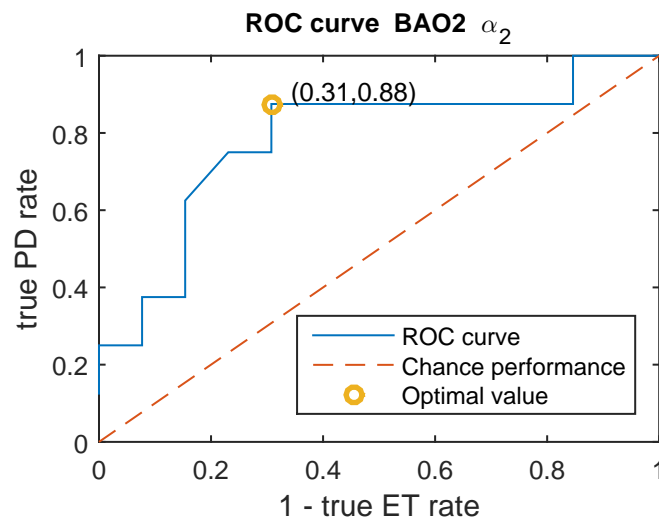
**Figure 4.15:** Results PLV analysis at the  $\alpha_1$  frequency band at the task BAO2.



(a) Significant electrode pairs: electrode pairs that showed group differences at  $P < 0.05$ . Left: electrode pairs where ET PLV exceeded PD PLV. Right: electrode pairs where PD PLV exceeded ET PLV.



(b) Boxplot of the medians. Outliers are marked with a plus sign (+).



(c) ROC curve of the medians.

**Figure 4.16:** Results PLV analysis at the  $\alpha_2$  frequency band at the task BAO2.

#### 4.4.6 Overview

An overview of the results of the PLV analysis is shown in Table 4.1. This table shows for every frequency band - task combination the AUC. For completeness, AUC values are also shown for the frequency bands that are not discussed in the previous sections.

**Table 4.1:** Summary coherence ROC analysis.

	(a) AUC values.						(b) AUC color legend.		
	AUC						AUC legend		
	$\theta$	$\alpha_1$	$\alpha_2$	$\beta_1$	$\beta_2$	$\gamma_1$	Value	Accuracy	Color
REST	0.60	0.82	0.75	0.57	0.57	0.55	0.50 - 0.75	Bad	
RAO1	0.68	0.78	0.73	0.52	0.51	0.57	0.75 - 0.80	Fair	
RAO2	0.69	0.89	0.71	0.70	0.75	0.88	0.80 - 0.90	Good	
BAO1	0.71	0.77	0.74	0.53	0.65	0.55	0.90 - 1.00	Excellent	
BAO2	0.82	0.87	0.78	0.55	0.61	0.60			

## 4.5 Discussion

The previous section shows the results of the PLV analysis. The plots of the locations of the significant electrode pairs do not show that the significant electrode pairs are located in a specific region. There is a slight asymmetry. At all tasks except RAO1 and the high frequency bands at RAO2, the percentage of significant electrode pairs within the left hemisphere is clearly larger than the percentage of significant electrode pairs within the right hemisphere. Because all patients in the group PD are right handed and have most tremor on the right side, more significant electrode pairs in the left hemisphere could indicate more abnormal behaviour in the hemisphere that controls the right side (as already mentioned in Section 3.5).

At almost all task-frequency band combinations, outliers were detected and removed before the ROC curve was determined. Because classification of the outliers depends on the set thresholds, it is important to note that all significant frequency bands were also significant ( $AUC > 0.75$ ) without outlier removal, except for the combinations BAO1 -  $\alpha_1$ , RAO2 -  $\beta_2$ , BAO2 -  $\theta$ . Furthermore, outliers were mostly the same patients. At the  $\theta$  frequency band, 5 of the 9 outliers were ET patient 15. At the other frequency bands, 12 of the 22 ET outliers were ET patient 4 and 7 were patient 13. For the PD group, 9 of the 14 outliers were PD patient 5 (ET patients 15 and 4 and PD patient 5 were also frequent outliers at the coherence analysis).

As with coherence, there is a difference between the first and second time the RAO and BAO tasks were performed. At RAO1, only  $\alpha_1$  had AUC higher than 0.75. At RAO2,  $\alpha_1$ ,  $\beta_2$  and  $\gamma_1$  had an  $AUC > 0.75$ . At BAO1, AUC values were above 0.75 at the  $\alpha_1$  band. At BAO2,  $\alpha_1$  band clearly had a higher AUC and the  $\theta$  and  $\alpha_2$  bands were also significant.

As already mentioned in the the discussion of the coherence analysis, it could be the case that abnormal brain activity increases when patients get tired or has to make more effort to perform the task. This could be further investigated by including another repetition (RAO3, BAO3) and determine the AUC values. Another option could be to increase the duration of BAO1 and RAO1 and to evaluate PLV in time (see also Chapter 6).

Based on the AUC values, the best frequency band-task combinations to distinguish between PD and ET are  $\alpha_1$  - (REST, RAO2, BAO2) and  $\gamma_1$  - RAO2.

## Chapter 5

# Global Field Synchronization

Global Field Synchronization (GFS) quantifies the instantaneous synchrony of multiple signals in one number. Instantaneous or zero-phase synchronization is different from the synchronization found with the PLV (Chapter 4). For GFS to be high, signals have to have the *same phase* at a given frequency, while for PLV to be high, signals must have a constant *phase difference*. Instantaneous synchronization can occur even between distant neuronal assemblies (Fischer et al., 2006; Gollo et al., 2010; Uhlhaas et al., 2009).

This chapter describes how GFS is determined (Section 5.1) and how it is applied to the EEG signals (Section 5.2). In Section 5.3 the statistical method for determining significant group differences is treated and Section 5.4 shows the results. The discussion of the results can be found in Section 5.5. The discussion of the used methods is given in Chapter 6.

### 5.1 Mathematical method

Global Field Synchronization (GFS) quantifies the synchrony of multiple signals  $x_1(t), x_2(t), \dots, x_n(t)$ . Computing the Fourier transforms  $\hat{x}_i(f)$  of the signals  $x_i$  results for each frequency  $f_0$  in a set of  $n$  complex numbers,  $\mathbf{c} = \{\hat{x}_1(f_0), \hat{x}_2(f_0), \dots, \hat{x}_n(f_0)\}$ . Every complex number  $\hat{x}_j(f_0) = a_j + ib_j$  could be represented as a two-dimensional vector in the complex plane (see Figure 5.1).

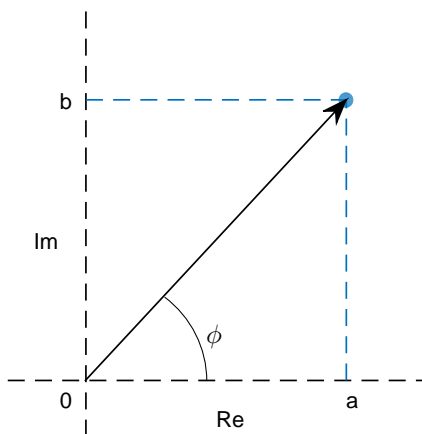


Figure 5.1: Vector in the complex plane.

The direction of this vector represents the phase  $\phi$ . If all signals would be in perfect phase or counter-phase, all vectors would point in the same or opposite direction and the endpoints of the vectors would lie on a straight line. Without any common phase, the endpoints would be scattered. So the better the endpoints of these vectors can be approximated by a single line, the more the total set of signals at the given frequency  $f_0$  is dominated by a single phase (Koenig et al., 2001).

To determine how much the endpoints of the vectors  $\hat{x}_i = a_j + ib_j$  in  $\mathbf{c}$  approach a single line, Principal Component Analysis (PCA) is used. PCA finds the principal components of the dataset  $X \in \mathbb{R}^{n \times m}$ . In a two-dimensional case, there are two principal components. The first principal component explains the highest amount of variance. The second principal component is orthogonal to the first and captures

the variance in the data that is not captured by the first principal component. Figure 5.2 shows three datasets with their corresponding principal components.

The principal components are the eigenvectors of the covariance matrix of the dataset. For the two-dimensional case where  $X = [X_1, X_2] \in \mathbb{R}^{n \times 2}$ , the covariance matrix  $\Sigma$  is defined as

$$\Sigma = \begin{bmatrix} \text{cov}(X_1, X_1) & \text{cov}(X_1, X_2) \\ \text{cov}(X_1, X_2) & \text{cov}(X_2, X_2) \end{bmatrix}, \quad (5.1)$$

where

$$\text{cov}(X_i, X_i) = \text{var}(X_i) = \frac{1}{n-1} \sum_{j=1}^n (X_i(j) - \bar{X}_i)^2, \quad i = 1, 2$$

and

$$\text{cov}(X_1, X_2) = \text{cov}(X_2, X_1) = \frac{1}{n-1} \sum_{j=1}^n (X_1(j) - \bar{X}_1)(X_2(j) - \bar{X}_2).$$

Here  $\bar{X}_i$  is the mean of column  $X_i$ .

For the connectivity analysis, the dataset is  $X = [R, I]$ , where  $R = [a_1, a_2, \dots, a_n]^T$  is the vector with the real parts of the  $\hat{x}_i$  and  $I = [b_1, b_2, \dots, b_n]^T$  is the vector with the imaginary parts of the  $\hat{x}_i$ . PCA results in two eigenvalues  $\lambda_i, i = 1, 2$  of the covariance matrix  $\Sigma$  per frequency  $f$ . The eigenvalue tells how much variation in the dataset is explained by its corresponding principal component (eigenvector). So the more the first eigenvalue exceeds the second eigenvalue, the more the data varies in only one direction, i.e. the more the endpoints of the vectors approximate a straight line (see also Figure 5.2). GFS is a measure to determine how much the first eigenvalue exceeds the second eigenvalue:

$$\text{GFS}(f) = \frac{|\lambda_1 - \lambda_2|}{\lambda_1 + \lambda_2}. \quad (5.2)$$

GFS ranges between 0 and 1, with 1 meaning that all points lie on a straight line and therefore all signals have a common phase.

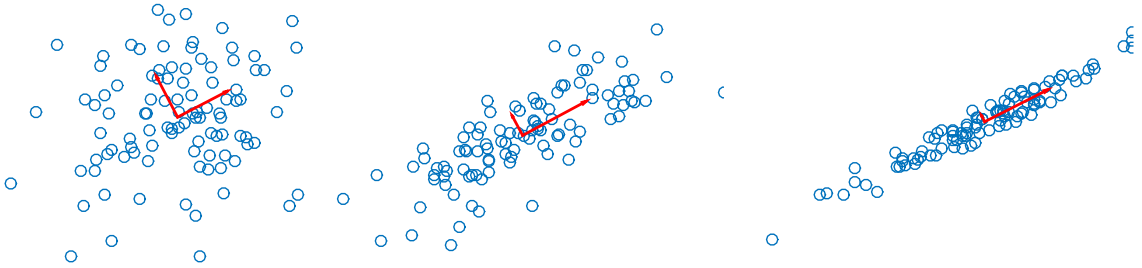


**Figure 5.2:** Three datasets with their principal components (red arrows). The principal components (eigenvectors of unit length) are scaled by the square root of the corresponding eigenvalue.

## 5.2 EEG analysis

The EEG signals of the 62 electrodes were divided into epochs of 2 seconds with 50% overlap. For every epoch, Fourier transforms were determined which resulted for every frequency  $f$  (in steps of 0.5 Hz) in a complex number  $\hat{x}_j(f) = a_j + ib_j$ ,  $j = 1, \dots, 62$ . For the dataset  $[R, I]$ , with  $R = [x_1, x_2, \dots, x_{62}]$  and  $I = [y_1, y_2, \dots, y_{62}]$ , the covariance matrix was computed (see Equation (5.1)). With the two eigenvalues of that covariance matrix, GFS was determined using Equation (5.2). Afterwards, GFS values were averaged over all epochs and averaged over the frequency bands given in Table 2.2. This resulted in 30 GFS values per subject: one for every frequency band, for every task.

## 5.3 Statistics

For each frequency band-task combination, differences between PD and ET were tested using the Wilcoxon rank sum test. The null hypothesis was rejected with  $P < 0.05$ .

Before the Wilcoxon rank sum test was performed, outliers were removed. Let  $G = \{g_1, \dots, g_n\}$  be the set of GFS values of a specific group, where  $n$  is the number of subjects in the group. A value  $g_i$  was removed if

$$g_i > Q_3 + 1.5 \cdot IQR \quad \text{or} \quad g_i < Q_1 - 1.5 \cdot IQR.$$

Here,  $Q_1$  and  $Q_3$  are the first and third quartile of  $G$  and the interquartile range (IQR) is defined as the distance between  $Q_1$  and  $Q_3$ .

A test was developed to discriminate between the two groups. The diagnostic test had the following form: if the GFS value of a patient is less than cut-off point  $c$ , the patient gets the diagnosis ET. If the GFS value is greater than  $c$ , the patients gets the diagnosis PD.

We used Receiver Operating Characteristic (ROC) curves to determine the optimal cut-off point  $c$  (see Infobox 2 on page 14) and we used AUC values to compare the different tests. Sensitivity and specificity are defined as the probability that the test results in ‘PD’ when the patient actually has PD (true PD rate) and as the probability that the test will result in ‘ET’ when a patient actually has ET (true ET rate). Because both are equally important, we chose the optimal cut-off point to be the point that corresponds to the point on the ROC curve that has minimal distance to the ideal point (0% 1-specificity, 100% sensitivity).

## 5.4 Results

In this section, the results of the GFS analysis are given. The results are shown separately for each task. Only those frequency bands are discussed where the null hypothesis of the Wilcoxon rank sum test is rejected with  $P < 0.05$ . These bands will be called *significant frequency bands*.

### 5.4.1 REST

The GFS results at REST are summarized in Figure 5.3. The frequency bands marked with an asterisk (\*) are the significant frequency bands. Significant at REST is the  $\alpha_1$  (7 - 10 Hz) frequency band.

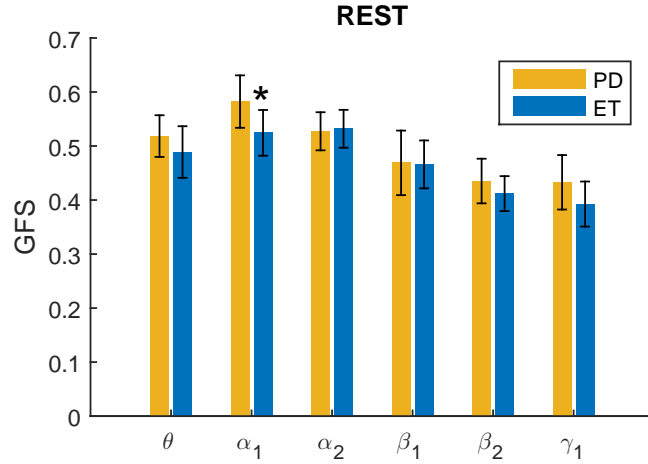


**Figure 5.3:** GFS results at the task REST. Shown are the mean GFS values (bars) and the standard deviation (black lines). Significant frequency bands are marked with an asterisk (\*). The following outliers were removed:  $\alpha_2$ : ET 15, 5, PD 2.

The boxplots of the GFS values at  $\alpha_1$  are shown in Figure 5.4a. The ROC curve is shown in Figure 5.4b. The optimal cut-off point is 0.5670, which gives a true PD rate of 78% and a true ET rate of 93%. The AUC is equal to 0.84.

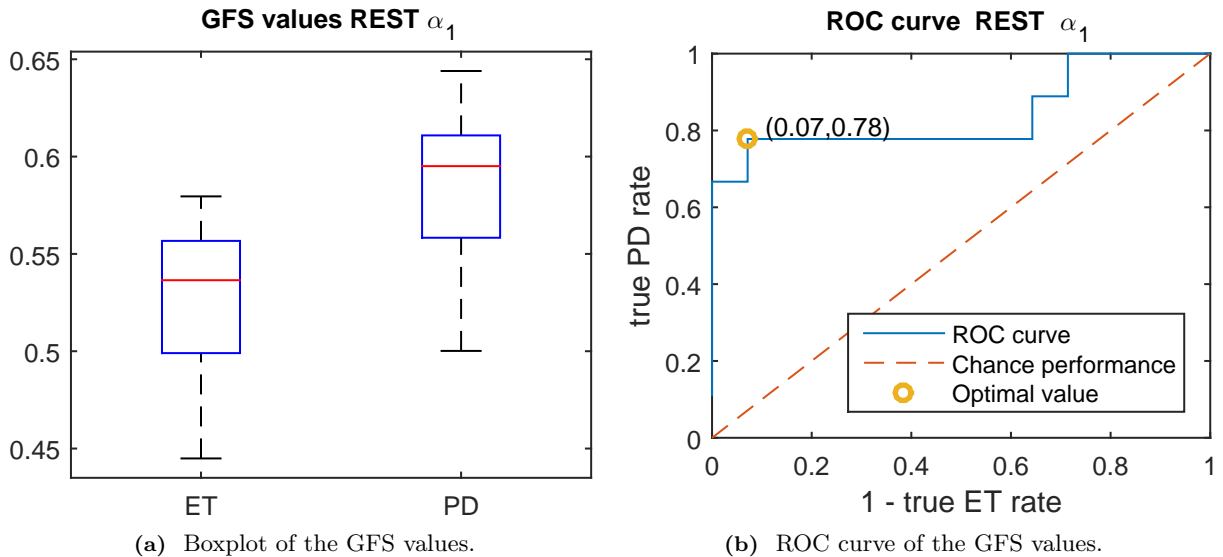


**Figure 5.4:** Results GFS analysis at the  $\alpha_1$  frequency band at the task REST.

### 5.4.2 RAO1

The coherence results at RAO1 are summarized in Figure 5.5. No frequency bands were significant at this task. Wilcoxon rank sum test performed on the GFS values at the  $\alpha_1$  frequency band resulted in  $P = 0.0507$ , slightly bigger than  $P = 0.05$  and hence the null hypothesis of the Wilcoxon rank sum test is not rejected. The AUC is however bigger than 0.75.

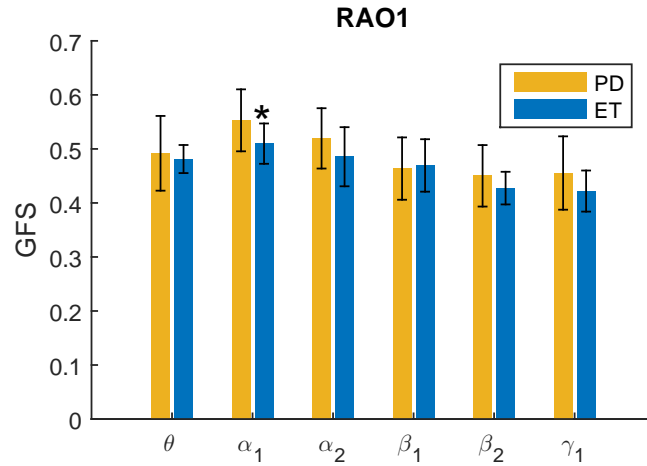


**Figure 5.5:** GFS results at the task RAO1. Shown are the mean GFS values (bars) and the standard deviation (black lines). The following outliers were removed:  $\theta$ : ET 5,  $\alpha_1$ : ET 15, 5,  $\beta_2$ : ET 4,  $\gamma_1$ : ET 4.

### 5.4.3 RAO2

The coherence results at RAO2 are summarized in Figure 5.6. The frequency bands marked with an asterisk (\*) are the significant frequency bands. Significant at RAO2 is the  $\alpha_1$  (7 - 10 Hz) frequency band (no frequency band was significant at RAO1).

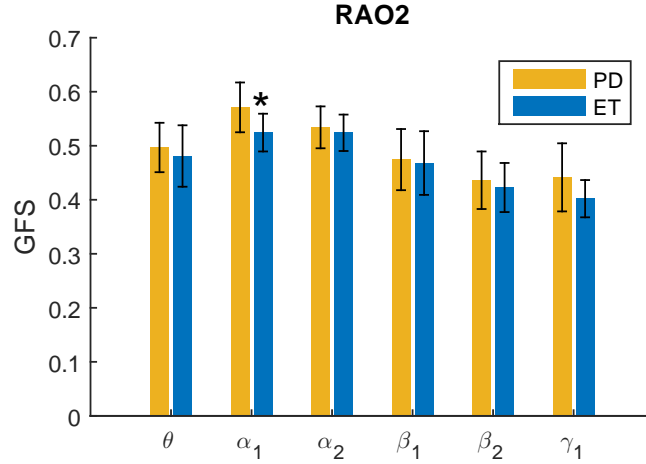
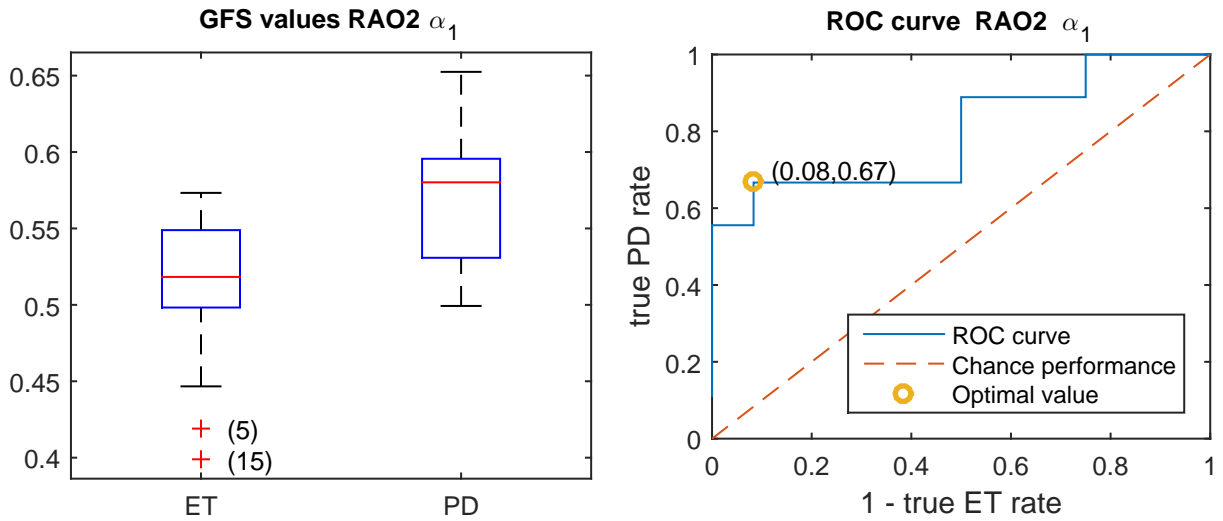


**Figure 5.6:** GFS results at the task RAO2. Shown are the mean GFS values (bars) and the standard deviation (black lines). Significant frequency bands are marked with an asterisk (\*). The following outliers were removed:  $\alpha_1$ : ET 5, 15,  $\alpha_2$ : ET 5, 15,  $\beta_2$ : ET 4,  $\gamma_1$ : ET 4.

The boxplots of the GFS values at  $\alpha_1$  are shown in Figure 5.7a. The ROC curve is shown in Figure 5.7b. The optimal cut-off point is 0.5600, which gives a true PD rate of 67% and a true ET rate of 92%. The AUC is equal to 0.80 (0.76 at RAO1).



(a) Boxplot of the GFS values. Outliers are marked with a plus sign (+).

(b) ROC curve of the GFS values.

**Figure 5.7:** Results GFS analysis at the  $\alpha_1$  frequency band at the task RAO2.

### 5.4.4 BAO1

The coherence results at BAO1 are summarized in Figure 5.8. The frequency bands marked with an asterisk (\*) are the significant frequency bands. Significant at BAO1 is the  $\alpha_1$  (7 - 10 Hz) frequency band.

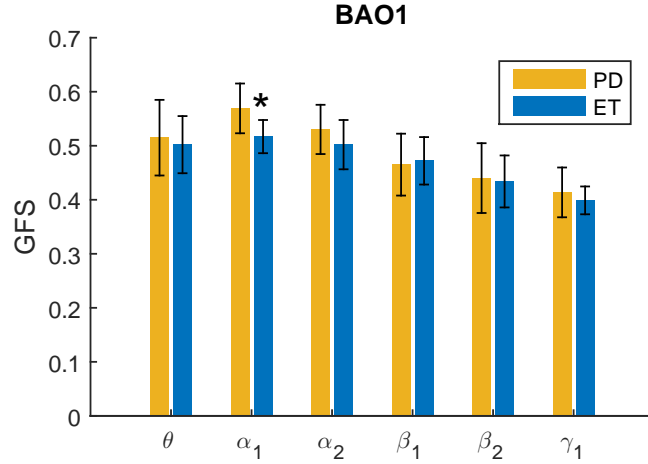


**Figure 5.8:** GFS results at the task BAO1. Shown are the mean GFS values (bars) and the standard deviation (black lines). Significant frequency bands are marked with an asterisk (\*). The following outliers were removed:  $\alpha_1$ : ET 15,  $\gamma_1$ : ET 3, 4, PD 5.

The boxplots of the GFS values at  $\alpha_1$  are shown in Figure 5.9a. The ROC curve is shown in Figure 5.9b. The optimal cut-off point is 0.5540, which gives a true PD rate of 78% and a true ET rate of 100%. The AUC is equal to 0.84.

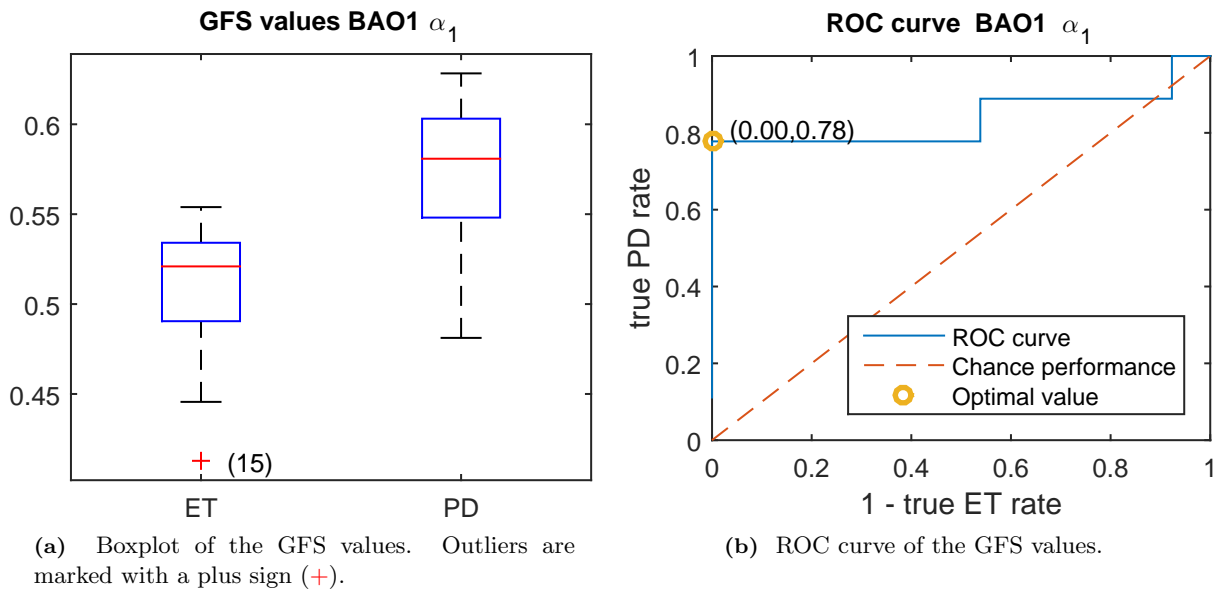


**Figure 5.9:** Results GFS analysis at the  $\alpha_1$  frequency band at the task BAO1.

### 5.4.5 BAO2

The coherence results at BAO2 are summarized in Figure 5.10. The frequency bands marked with an asterisk (\*) are the significant frequency bands. Significant at BAO2 is the  $\alpha_1$  (7 - 10 Hz) frequency band (this band was also significant at BAO1).

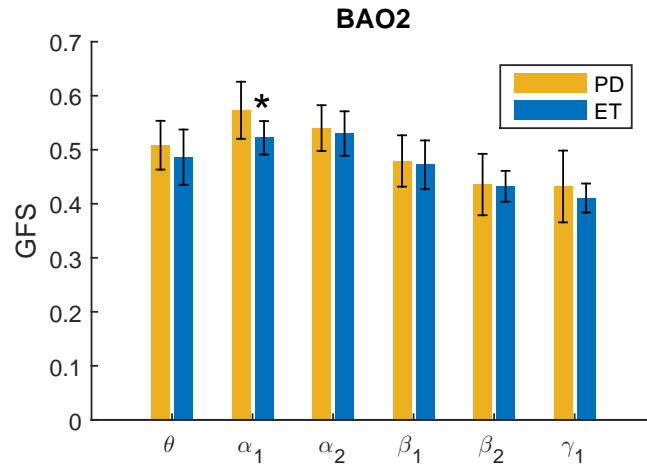
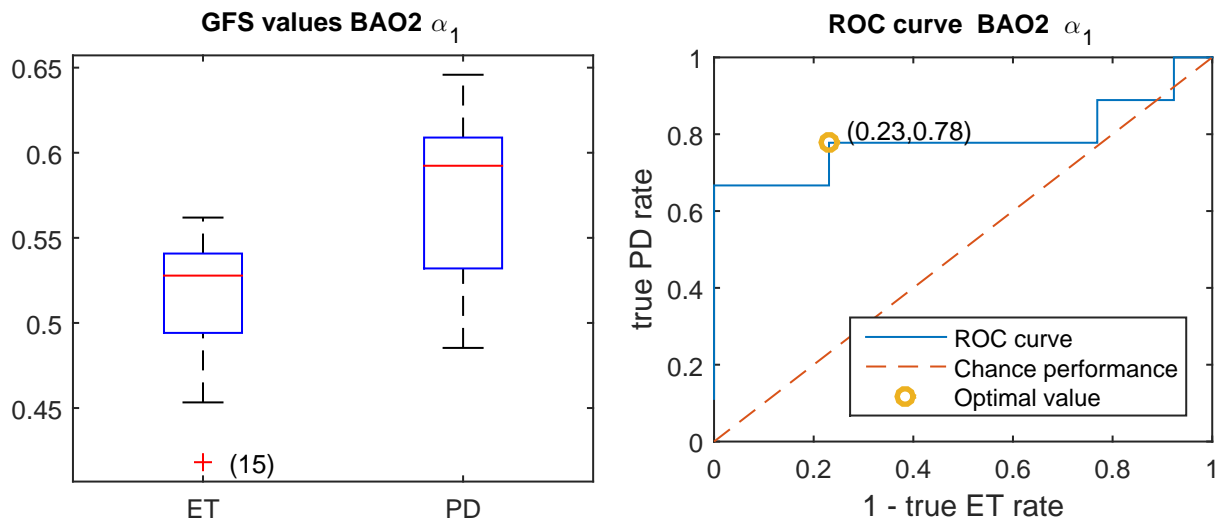


**Figure 5.10:** GFS results at the task BAO2. Shown are the mean GFS values (bars) and the standard deviation (black lines). Significant frequency bands are marked with an asterisk (\*). The following outliers were removed:  $\alpha_1$ : ET 15,  $\alpha_2$ : ET 15,  $\beta_2$ : ET 4,  $\gamma_1$ : ET 4.

The boxplots of the GFS values at  $\alpha_1$  are shown in Figure 5.7a. The ROC curve is shown in Figure 5.7b. The optimal cut-off point is 0.5410, which gives a true PD rate of 78% and a true ET rate of 77% (78% and 100% at BAO1).

The AUC is equal to 0.79 (0.84 at BAO2).



(a) Boxplot of the GFS values. Outliers are marked with a plus sign (+).

(b) ROC curve of the GFS values.

**Figure 5.11:** Results GFS analysis at the  $\alpha_1$  frequency band at the task BAO2.

### 5.4.6 Overview

An overview of the results of the GFS analysis is shown in Table 5.1. This table shows for every frequency band - task combination the AUC. For completeness, AUC values of the non-significant frequency bands are also included.

**Table 5.1:** Summary GFS analysis.

	(a) AUC values.						(b) AUC color legend.		
	AUC						AUC legend		
	$\theta$	$\alpha_1$	$\alpha_2$	$\beta_1$	$\beta_2$	$\gamma_1$	Value	Accuracy	Color
REST	0.69	0.84	0.52	0.55	0.68	0.73	0.50 - 0.75	Bad	
RAO1	0.52	0.76	0.68	0.52	0.66	0.71	0.75 - 0.80	Fair	
RAO2	0.54	0.80	0.56	0.52	0.62	0.74	0.80 - 0.90	Good	
BAO1	0.54	0.84	0.71	0.55	0.53	0.65	0.90 - 1.00	Excellent	
BAO2	0.63	0.78	0.58	0.58	0.50	0.61			

## 5.5 Discussion

The results show that GFS differences can be found in the  $\alpha_1$  frequency band at every task. These frequency bands were also significant without outlier removal. At the lower frequency ranges, all outliers were ET patient 15 and 5. At  $\beta_2$  and  $\gamma_1$ , patient ET 4 was the outlier 7 out of 8 times. Interesting is the fact that ET outliers are small compared to the other values, while outliers at the coherence and PLV analysis were higher than the other values.

Differences are found between RAO1 - RAO2 and BAO1 - BAO2. The AUC at the  $\alpha_1$  band at RAO2 is higher than at RAO1. This effect was also present at the coherence and PLV analysis and we argued that this could be due to the fact that abnormal brain behavior increases when patients become tired or have to make more effort to perform the task. At BAO2, however, the AUC value decreased at  $\alpha_1$  compared to BAO1, which would contradict the hypothesis.

Based on the AUC values, the best frequency band-task combinations to distinguish ET from PD are (REST, RAO2 , BAO1) -  $\alpha_1$ .

## Chapter 6

# Discussion

We chose to investigate functional connectivity using magnitude squared coherence, the phase locking value and global field synchronization. There are some things to consider when interpreting the results. Firstly, both coherence and PLV are bivariate measures, which means that it can only show the relationship of two signals at a time. It therefore does not distinguish between direct and indirect interrelations. If one source drives two responses, coherence might find correlation between the two responses, even if the responses do not influence each other. This problem does not occur when using multivariate measures, for example partial directed coherence (Pereda et al., 2005).

A common problem that all three measures suffer from is that of volume conduction. Volume conduction implies that the electrical activity of one source can be detected on multiple electrodes. The volume conduction effects may lead to the detection of spurious coupling between electrodes that are not caused by brain interaction.

Spurious coupling can also be detected because of reference effects. The local method that we used reduces these reference effects as already mentioned in Chapter 2. Different outcomes would result from using a common average reference or the average of the signals from the electrodes placed on the ears. GFS synchronization is independent of the chosen reference, as long as the same reference is used for all electrodes.

The most important difference between coherence and PLV is the fact that coherence depends, unlike PLV, on the power changes of the signal. Power might influence coherence measurements and coherence can therefore reflect changes in power of one source or genuine changes in coherence between two sources. An example of this dependence is given in Example 6 in Appendix A.

The results of our coherence analysis strongly agrees with our PLV analysis and we therefore tend to conclude that increased coherence values among PD patients is not a result of power changes. If it was, however, it would still be a good feature to distinguish PD from ET, which was the main goal of this research.

Another difference is that coherence assumes stationarity of the signals, while PLV does not. Based on the results, our assumption of stationarity when using coherence does not seem wrong, because the results of the coherence analysis agrees with those of the PLV analysis. The assumption of stationarity was already plausible because EEG signals were already separated for the different tasks. During one task, little difference in brain activity was expected. This does, however, not mean that there could not be further research into the connectivity over time. The differences in connectivity between the repetitions of BAO and RAO could indicate that abnormal brain activity in PD and/or ET patients changes over time. In the work of Zhan et al. (2006), continuous wavelet transform (CWT) and short-time Fourier transform (STFT) are used to evaluate the correlation between non-stationary processes.

Although PLV does not assume stationarity of the signals, PLV could also be used as a time-dependent measure. To this end, a sliding window could be used to determine the phase locking over multiple time windows (see, for example, the work of Mormann et al. (2000)). The fact that the EEG recordings were split for the different tasks was the main reason for not using time-dependent PLV in this research.

Because of the dependence on power and the stationarity assumption, PLV might be a better measure to detect brain connectivity, although this is not clearly reflected in our results.

GFS measures a whole different kind of synchronization, namely instantaneous synchronization. It does

not measure interrelations with a phase-delay. The results show higher connectivity in the  $\alpha_1$  band for the PD group, which was also found with the two other measures. The best way might be to use GFS together with coherence or PLV, to capture two different kinds of synchronization.

Independent of the connectivity measure is the limited spatial sampling of EEG recordings. Measurements are taken at the scalp, so the EEG signal is the sum of the electric field produced by a large population of neurons. Strong electrical activity can be picked up by several neighboring electrodes and EEG is therefore not useful for pinpointing the exact source of the activity. So when we were not able to detect connectivity at specific regions from the plots of significant electrode pairs, we have to take into account that EEG might not be the best technique to detect such regions. However, this was not the main objective of our study.

Eye blink artifacts were removed using ICA and removing two IC's that had the highest correlation with the EOG signals. The reason for using this automatic approach was the large amount of data to be inspected. At about 10% of the data, visual inspection showed that eye blink artifacts were not fully removed. At the other data sets, the peaks that represent eye blink artifacts were no longer present but to not undo the profit of an automatic approach, EEG signals were not visually inspected in detail. Hence, minor eye movement artifacts could still be present. Further research could be done in other methods to remove eye blink artifacts. In the work of [Joyce et al. \(2004\)](#) multiple criteria are used to determine if an IC has to be removed. Correlation with the EOG signals is used, but instead of removing the IC's with the highest correlation, all IC's with high correlation with the EOG signals are marked as candidates to be removed. If the marked IC's also have high power in the low frequency bands, these IC's are removed. The challenge then lies in setting the thresholds for 'high correlation' and 'high power', which makes this method less straightforward.

No artifacts were removed other than eye blink artifacts. Common artifacts other than eye blinks are muscle artifacts. A commonly used method to remove these artifacts is a low-pass filter. However, the frequency spectra of muscle artifacts overlap with that of the brain signals. A low-pass filter hence does not remove all muscle activity and can also remove important brain activity.

We investigated the use of ICA to remove muscle artifacts. IC's with muscle artifacts can be detected by its characteristics: more power at the higher frequencies and higher amplitude. However, removing these IC's automatically implied choosing thresholds for 'more power' and 'higher amplitude'. Due to volume conduction, muscle artifacts can also have low amplitudes and power at low frequencies. Hence, choosing thresholds is not straightforward. Moreover, it has been reported that ICA is not able to fully separate brain activity from muscle activity. ([Shackman et al., 2009](#); [De Clercq et al., 2006](#)). Hence, removing a muscle artifact component could result in removing brain activity.

Because we use 1891 electrode pairs and multiple subjects, we believe that the results found are not solely the results of artifacts. Artifact removal is however recommended in further research. Interesting could be the work of [De Clercq et al. \(2006\)](#), where canonical correlation analysis (CCA) is used. CCA is another blind source separation technique which assumes mutually uncorrelated sources which are maximally autocorrelated. Muscle artifacts are detected using the fact that muscle activity has a relative low autocorrelation in comparison with brain activity. The method outperformed both the low-pass filter and an ICA-based technique.

In this study, we used the EEG signal measured during the whole tasks. Results possibly differ if only those EEG segments were included when tremor was present.

Although PD is often associated with abnormal oscillations in the beta frequency band, our results do not show an increase of connectivity for the PD group in the beta band (only a small elevation in PLV's at the task RAO2). It is, however, also mentioned that there is an increase of functional connectivity in the low alpha range in untreated PD patients with a disease duration less than 2 years (*de novo* patients). Increased functional connectivity in the low alpha range is a feature of PD from the earliest clinical stages onward ([Stoffers et al., 2008](#)). [Berendse and Stam \(2007\)](#) conclude that increased beta synchronization is not a feature of early-stage PD. Our study included 9 PD patients, 2 of whom having a disease duration of only three years and 1 of only one year. Patients were also off tremor medication. However, to investigate the effect of disease duration, significantly more patients should be included in

the investigation.

In our study only 14 ET and 9 PD were included. Although the statistical test takes these small sizes into account, larger sample sizes are strongly recommended. A large sample size is more representative of the population and it would limit the influence of outliers. Furthermore, as mentioned above, a larger sample size would make it possible to include more variables like disease duration, age and gender.

Nevertheless, the results show that there are differences in connectivity between PD and ET and that these differences could be useful in clinical practice. All three methods could be used to determine if a patient gets diagnosed as PD or ET.

## Chapter 7

# Conclusions and recommendations

The aim of this research was to find differences in connectivity between patients with PD and ET. We used coherence, PLV and GFS and we found differences with all connectivity measures. To see whether these results could be used in clinical practice, we used three different test values: coherence median, PLV median and GFS value. We constructed tests with the following form: if the test value of a patient is less than cut-off point  $c$ , the patient gets the diagnosis ET. If the test value is greater than  $c$ , the patients gets the diagnosis PD.

Results of the coherence analysis strongly agreed with the results of the PLV analysis and the best frequency band-task combinations to distinguish between PD and ET are (REST, RAO2, BAO2) -  $\alpha_1$  and RAO2 -  $\gamma_1$ . GFS measures a different kind of synchronization and the results differed from the other results, but also showed increased synchronization for the PD patients at the  $\alpha_1$  frequency band. The best tasks to use for GFS at this frequency band are REST, RAO2 and BAO1.

All connectivity measures were able to distinguish between the two diseases, and although results differed, no measure was clearly better than the other. The best way might be to use a combination of GFS and coherence or PLV.

Further research into this topic is needed. The most important recommendation would be to increase the number of patients included in the analysis. In our study, only 9 PD patients and 15 ET patients were included, of which one was excluded from the analysis beforehand due to too much eye movement. Including more patients would increase the reliability of the results and would allow for division of the groups based on for example age or disease duration.

Further research should be done into the removal of artifacts. We removed eye blink artifacts but other methods could be explored. No other artifacts were removed, which could have caused some of the outliers.

Another recommendation would be to include an extra repetition of the BAO and RAO tasks. This could give some more insight in the hypothesis that if patients get tired or have to make more effort to perform the task, abnormal behavior in the brain becomes more pronounced. Another option would be to increase the length of tasks BAO1 and RAO1 and used time dependent connectivity measures.

Lastly, the effect of tremor could be further investigated. In this study, we used EEG signals measured during the whole time a task was performed. Results might be different when only those EEG segments where included when tremor was present.

# Appendix A

## Examples

In this appendix, examples are given that have been referred to throughout the thesis. More context can be found at the page were the reference was made.

**Example 1** (Eye blink artifacts, page 9). Figure A.2a shows a set of EEG signals together with the EOG signals. The eye blink artifacts are clear. Figure A.2b shows the independent components that are the output of the RobustICA algorithm. It can be seen that IC 1 and IC 2 resemble the EOG signals and have to be set to zero. However, an automatic approach is used, instead of visual inspection, to detect the unwanted components.

We make use of the normalized cross correlation, which can be estimated for two signals  $x$  and  $y$  as

$$cc_{xy}(k) = \frac{\sum_{n=-\infty}^{\infty} x_{n+k}y_n}{\|x\| \|y\|}$$

We choose to remove two IC's: the IC that has the highest absolute cross correlation with  $EOG_H$  and the one that has the highest absolute correlation with  $EOG_V$ , where the cross correlation is evaluated at  $k = 0$ . Figure A.1 shows the absolute cross correlation of the two EOG signals with all IC's. IC 1 and IC 2 have the highest correlation with the EOG signals. We conclude the same as by visual inspection: IC1 and IC2 have to be set to zero.

A clean EEG signal without the eye movement artifacts is shown in Figure A.3. ■

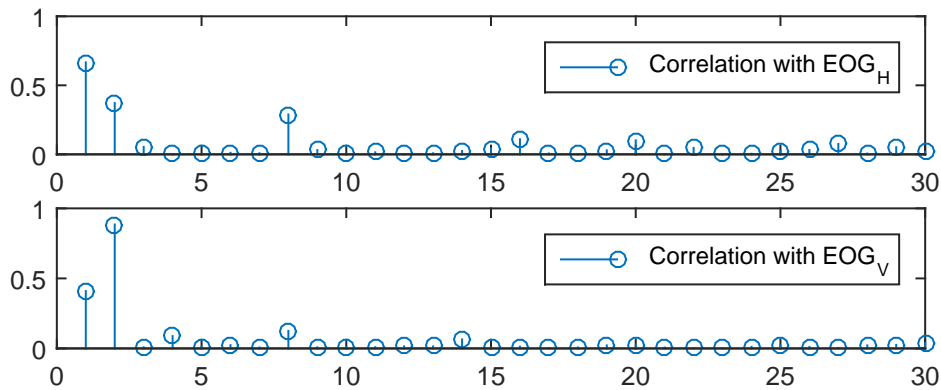
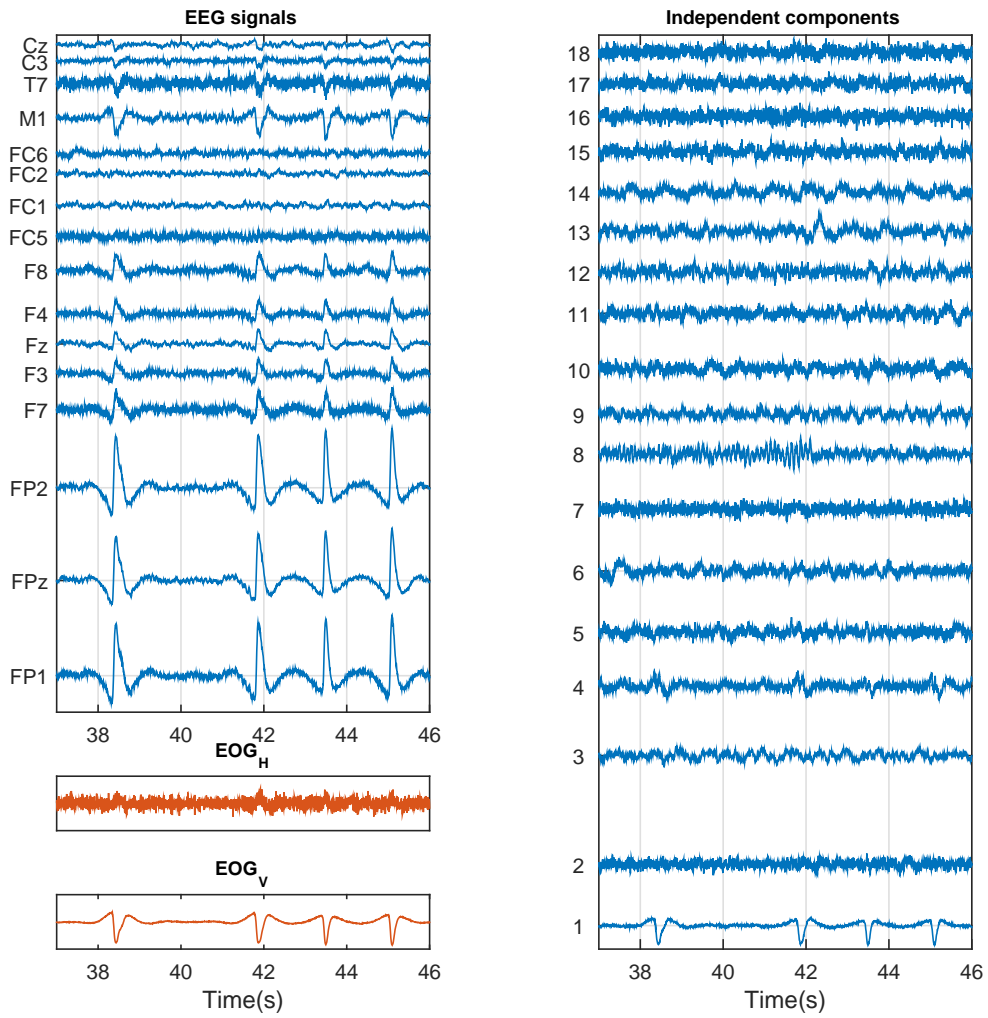


**Figure A.1:** Absolute normalized cross correlation of EOG signals and IC's.



(a) EEG signals.

(b) Independent components.

**Figure A.2:** Input (a) and output (b) of the ICA-algorithm.

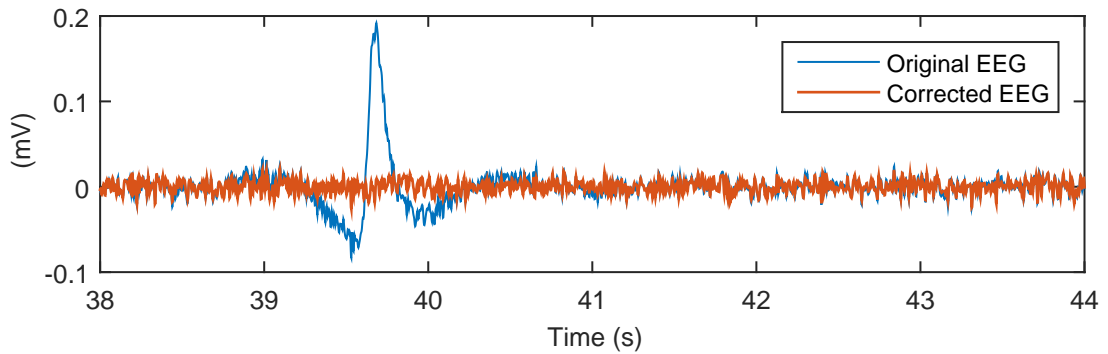


**Figure A.3:** Original EEG-signal (blue) and corrected EEG-signal (orange) with eye blink artifacts removed.

**Example 2** (Coherence statistics, page 13). Let us look at the coherence values for both ET and PD in the  $\alpha_1$  frequency band at the task REST. We take the two electrodes F8 and FC1. The coherence values are shown in Table A.1.

**Table A.1:** Coherence values for ET and PD.

ET		PD	
1	0.0104	1	0.0086
2	0.0258	2	0.0202
4	0.0062	3	0.0087
5	0.0115	4	0.0333
6	0.0082	5	0.0631
7	0.0053	6	0.0589
8	0.0057	7	0.0140
9	0.0280	8	0.0973
10	0.0173	9	0.0371
11	0.0137		
12	0.0133		
13	0.0190		
14	0.0044		
15	0.0041		
16	0.0086		

For ET, the following can be determined:

$$Q_1 = 0.0059$$

$$Q_3 = 0.0164$$

$$IQR = 0.0105$$

We therefore say that an ET coherence value ( $ET_i$ ) is an outlier if

$$ET_i > Q_3 + 1.5 \cdot IQR = 0.0321 \quad \text{or} \quad ET_i < Q_1 - 1.5 \cdot IQR = -0.0099.$$

Using these values, we see that the ET group does not contain any outliers.

The same can be done for the PD group, which results in the conclusion that no outliers are present in that group. The coherence values are illustrated by the boxplot in Figure A.4.

Now that the outliers are investigated, the statistical test can be performed. Performing the Wilcoxon rank sum test with the Matlab command `ranksum` results in

$$p = 0.0073.$$

This means that we reject the null hypothesis that the two samples come from the same population because  $p < 0.05$ . We now say that  $\{F8, FC1\}$  is a significant electrode pair because there is a statistical difference between ET and PD (in the range  $\alpha_1$  at the task REST). ■

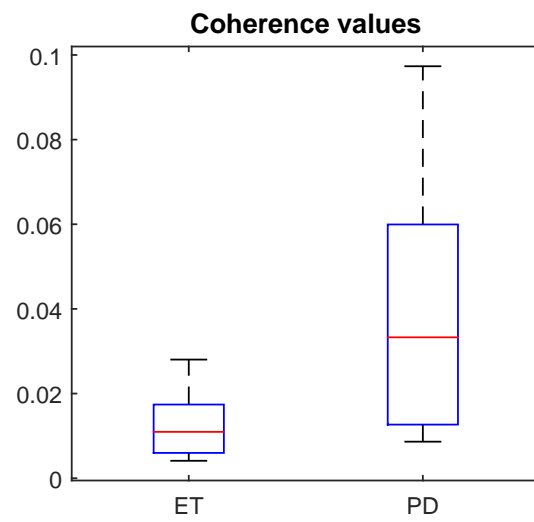


**Figure A.4:** Boxplot of the coherence values at the  $\alpha_1$  range at REST.

**Example 3** (High phase locking value, page 34). Consider the two signals  $x(t)$  and  $y(t)$  defined as

$$x(t) = \left( \frac{1}{t+1} (\sin(2\pi 10t + \pi/3) + e_x(t)) \right)$$

$$y(t) = 0.5(t+1)(\sin(2\pi 10t) + e_y(t)),$$

where  $e$  denotes white noise with standard deviation  $\sigma_e = 0.1$  and  $t \in \mathbb{Z}$ . See Figure A.5 (left, top). The phase difference  $\phi_{xy}(t)$  of  $x(t)$  and  $y(t)$  is close to constant (see Figure A.5 (left, bottom)). For every  $t$ , the phase difference is projected onto the unit circle by the projection

$$\phi_{xy}(t) \rightarrow e^{i\phi_{xy}(t)}.$$

A relative small portion of the unit circle is occupied and the average  $\langle e^{i\phi_{xy}(t)} \rangle$  is located close to the unit circle (see Figure A.5 (right)). Therefore, the PLV is high:

$$\text{PLV} = 0.99$$

■

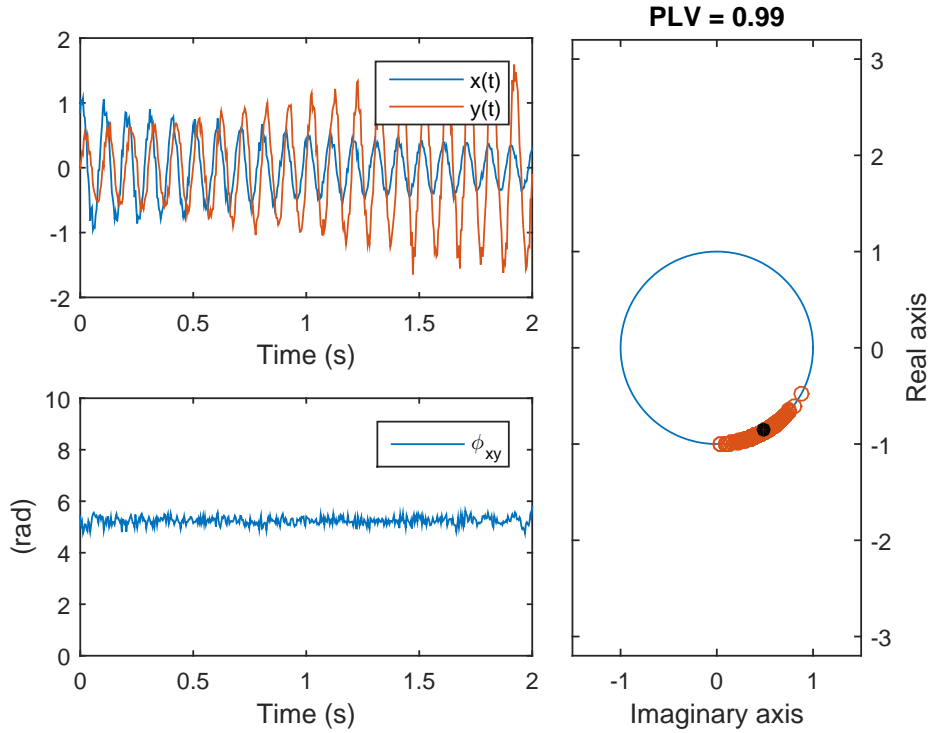


**Figure A.5:** Two signals  $x(t)$  and  $y(t)$  (left, top).  $x$  and  $y$  both consist of 500 samples. The phase difference  $\phi_{xy}(t)$  is close to constant (left, bottom). The right panel shows the projection of the phase difference onto the unit circle (orange circles). The average  $\langle e^{i\phi_{xy}(t)} \rangle$  (black dot) is located close to the unit circle. Therefore, the PLV is close to 1.

**Example 4** (Low phase locking value, page 34). What happens with the PLV if two signals are uncorrelated? Consider two signals  $h(t)$  and  $g(t)$  that are both realizations of white noise, i.e.

$$\begin{aligned} g(t) &= e_g(t) \\ h(t) &= e_h(t), \end{aligned}$$

with  $\sigma_g = \sigma_h = 1$  and  $t \in \mathbb{Z}$ . The two signals are shown in Figure A.6 (left, top).

The phase difference  $\phi_{gh}(t)$  is shown in the left panel of Figure A.6. The figure shows that  $\phi_{gh}(t)$  is far from constant and takes approximately all values in the range 0 to  $2\pi$ . The right panel of Figure A.6 shows that the projection  $e^{i\phi_{gh}(t)}$  occupies the whole unit circle and that the average is close to the center of the unit circle. This results in a PLV close to 0:

$$\text{PLV} = 0.08.$$

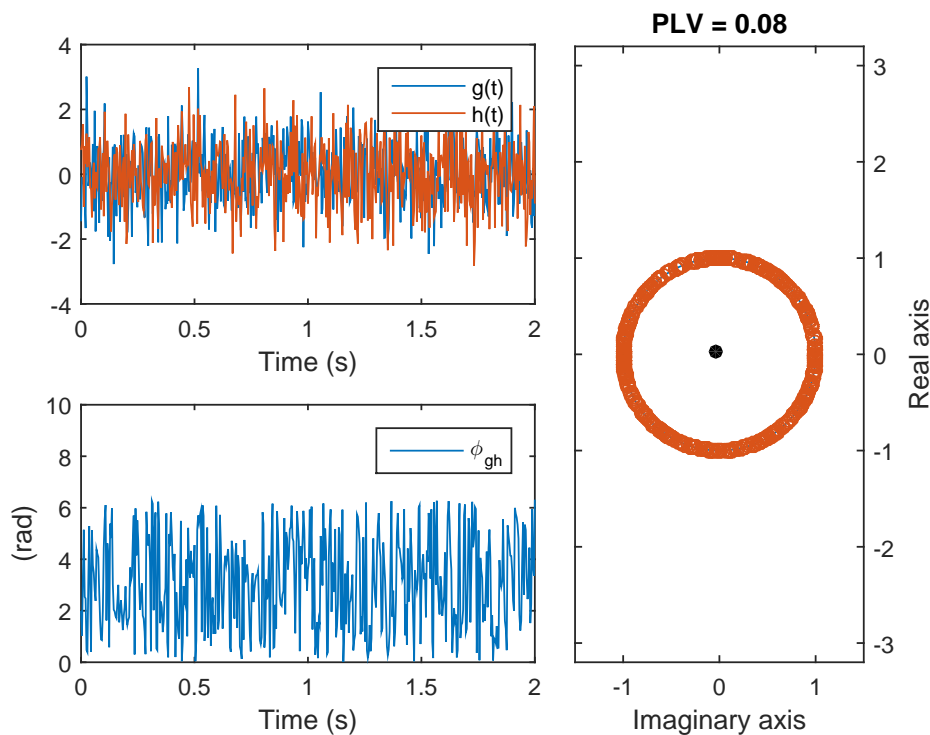


**Figure A.6:** Two realizations of white noise,  $g(t)$  and  $h(t)$  (left, top). Both  $g$  and  $h$  consist of 500 samples. The phase difference  $\phi_{gh}(t)$  is far from constant (left, bottom). The right panel shows that  $e^{i\phi_{gh}(t)}$  occupies the whole unit circle (orange circles) and that the average (black dot) is close to the center of the unit circle. Therefore, the PLV is close to 0.

**Example 5** (PLV statistics, page 35). Let us look at the PLV's for both ET and PD in the  $\alpha_1$  frequency band at the task REST. We take the two electrodes C3 and CP6. The coherence values are shown in Table A.2.

**Table A.2:** PLV's for ET and PD.

ET		PD	
1	0.1642	1	0.0381
2	0.0906	2	0.1177
4	0.0238	3	0.0236
5	0.0357	4	0.0693
6	0.0443	5	0.0541
7	0.0805	6	0.0752
8	0.0688	7	0.0180
9	0.0221	8	0.0931
10	0.0871	9	0.0487
11	0.0536		
12	0.0121		
13	0.0528		
14	0.0481		
15	0.0833		
16	0.0477		

For ET, the following can be determined:

$$\begin{aligned}
 Q_1 &= 0.0379 \\
 Q_3 &= 0.0826 \\
 IQR &= 0.0447
 \end{aligned}$$

We say that an ET PLV ( $ET_i$ ) is an outlier if

$$ET_i > Q_3 + 1.5 \cdot IQR = 0.1496 \quad \text{or} \quad ET_i < Q_1 - 1.5 \cdot IQR = -0.0291.$$

From the values in Table A.2 can be seen that  $ET_1$  is an outliers. The same can be done for the PD group, which results in the conclusion that no outliers are present in that group. The PLV's are illustrated by the boxplot in Figure A.7.

After the outliers are removed, the Wilcoxon ranksum test can be performed with the Matlab command `ranksum`. This results in

$$p = 0.6366.$$

Because we reject the null hypothesis if  $p < 0.05$ , the null hypothesis is not rejected and we conclude that  $\{C3, CP6\}$  is *not* a significant electrode pair (in the range  $\alpha_1$  at the task REST). ■

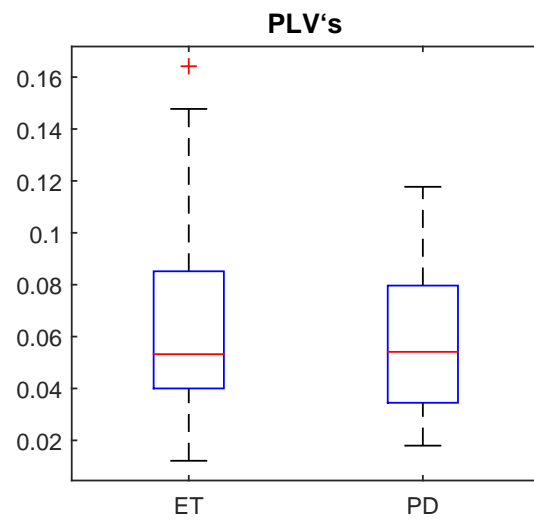


**Figure A.7:** Boxplot of the PLV's at the  $\alpha_1$  range at REST.

**Example 6** (Coherence depends on amplitude, page 62). Consider the two signals  $x(t)$  and  $y(t)$  defined as

$$\begin{aligned}x(t) &= \sin(2\pi 10t) + e_x(t) \\y(t) &= \sin(2\pi 10t + \pi/3) + e_y(t),\end{aligned}$$

where  $e$  denotes white noise with standard deviation  $\sigma_e = 0.1$  and  $t \in \mathbb{Z}$ . The signals are displayed in Figure A.8. Both coherence at 10 Hz ( $\gamma_{xy}(10)$ ) and PLV ( $P_{xy}$ ) are high:

$$\begin{aligned}\gamma_{xy}(10) &= 0.9999 \\P_{xy} &= 0.9896.\end{aligned}$$

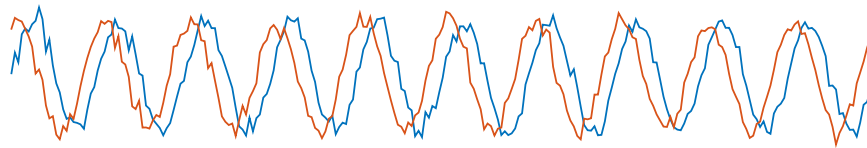


**Figure A.8:** Two signals  $x(t)$  (blue) and  $y(t)$  (orange).

Now suppose that the amplitude of  $x(t)$  decreases while that of  $y(t)$  increases, see Figure A.9. The new signals are defined as

$$\begin{aligned}\hat{x}(t) &= \left(\frac{1}{t+1}\right)x(t) \\ \hat{y}(t) &= (0.5(t+1))y(t),\end{aligned}$$

Coherence at 10 Hz is greatly affected, while the PLV is almost the same:

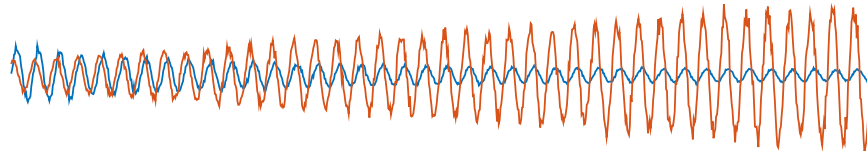


**Figure A.9:** Two signals  $\hat{x}(t)$  (blue) and  $\hat{y}(t)$  (orange).

$$\begin{aligned}\gamma_{\hat{x}\hat{y}}(10) &= 0.3830 \\P_{\hat{x}\hat{y}} &= 0.9854.\end{aligned}$$

The PLV is practically independent of the changes in amplitude, while coherence is clearly not. ■

# Bibliography

- Berendse, H. W. and Stam, C. J. Stage-dependent patterns of disturbed neural synchrony in parkinson's disease. *Parkinsonism and Related Disorders*, 13:S440–S445, 2007.
- Beudel, M., Little, S., Pogosyan, A., Ashkan, K., Foltynie, T., Limousin, P., Zrinzo, L., Hariz, M., Bogdanovic, M., Cheeran, B., Green, A. L., Aziz, T., Thevathasan, W., and Brown, P. Tremor reduction by deep brain stimulation is associated with gamma power suppression in parkinson's disease. *Neuromodulation: Technology at the Neural Interface*, 18(5):349–354, 2015.
- Boashash, B. Estimating and interpreting the instantaneous frequency of a signal. I. fundamentals. *Proceedings of the IEEE*, 80(4):520–538, 1992.
- De Clercq, W., Vergult, A., Vanrumste, B., Van Paesschen, W., and Van Huffel, S. Canonical correlation analysis applied to remove muscle artifacts from the electroencephalogram. *IEEE Trans Biomed Eng.*, 53(12):2583–2587, 2006.
- Fischer, I., Vicente, R., Buld, J. M., Peil, M., Mirasso, M. C., C. R. ans Torrent, and Carca-Ojalvo, J. Zero-lag long-range synchronization via dynamical relaying. *Physica Review Letters*, 97(12):–, 2006.
- Gollo, L. L., Mirasso, C., and Villa, A. E. P. Dynamic control for synchronization of separated cortical areas through thalamic relay. *NeuroImage*, 52:947–955, 2010.
- Jain, S., Steven, L. E., and Elan, L. D. Common misdiagnosis of a common neurological disorder - how are we misdiagnosing essential tremor? *Arch Neurol*, 63(8):1100–1104, 2006.
- Joyce, C. A., F., Gorodnitsky I., and M., Kutas. Automatic removal of eye movement and blink artifacts from eeg data using blind component separation. *Psychophysiology*, 41:313–325, 2004.
- Koenig, T., Lehmann, D., Saito, N., Kuginuki, T., Kinoshita, T., and Koukkou, M. Decreased functional connectivity of eeg theta-frequency activity in first-episode, neuroleptic-naive patients with schizophrenia: preliminary results. *Schizophrenia Research*, 50:55–60, 2001.
- Koenig, T., Prichep, L., Dierks, T., Hubl, D., Wahlund, L. O., John, E. R., and Jelic, V. Decreased eeg synchronization in alzheimer's disease and mild cognitive impairment. *Neurobiology of aging*, 26: 165–171, 2005.
- Little, S. and Brown, P. The functional role of beta oscillations in parkinson's disease. *Parkinsonism & Related Disorders*, 20(1):S44–S48, 2014.
- Meara, J., Bhowmick, B. K., and Hobson, P. Accuracy of diagnosis in patients with presumed parkinson's disease. *Age and Aging*, 28:99–102, 1999.
- Mormann, F., Lehnertz, K., David, P., and Elger, C. E. Mean phase coherence as a measure for phase synchronization and its application to the eeg of epilepsy patients. *Physica D: Nonlinear Phenomena*, 44(3-4):358–369, 2000.
- Murias, M., Swanson, J.M., and Srinivasan, R. Functional connectivity of frontal cortex in healthy and ADHD children reflected in EEG coherence. *Cerebral Cortex*, 17(8):1788–1799, 2007a.
- Murias, M., Webb, S.J., Greenson, J., and Dawson, G. Resting state cortical connectivity reflected in EEG coherence in individuals with autism. *Biol Psychiatry*, 62(3):270–273, 2007b.

- Pereda, E., Quiroga, R. Q., and Bhattacharya, J. Nonlinear multivariate analysis of neurophysiological signals. *Progress in Neurobiology*, 77:1–37, 2005.
- Sakkalis, V. Review of advanced techniques for the estimation of brain connectivity measured with eeg/meg. *Computers in Biology and Medicine*, 41(12):1110–1117, 2011.
- Shackman, A. J., McMenamin, B. W., Slagter, H. A., Maxwell, J. S., Greischar, L. L., and Davidson, R. J. Electromyogenic artifacts and electroencephalographic inferences. *Brain Topogr*, 22:7–12, 2009.
- Stoffers, D., Bosboom, J. L. W., Deijen, J. B., Wolters, E. Ch., Stam, C. J., and Berendse, H. W. Increased cortico-cortical functional connectivity in early-stage parkinson’s disease: An MEG study. *NeuroImage*, 41(2):212–222, 2008.
- Teplan, M. Fundamentals of eeg measurement. *Measurement science review*, 2, 2002.
- Uhlhaas, P. J., Pipa, G., Lima, B., Melloni, L., Neuenschwander, S., Nikolic, D., and Singer, W. Neural synchrony in cortical networks: history, concept and current status. *Front Integr Neurosci.*, 3(17):–, 2009.
- Zarzoso, V. Robust independent component analysis by iterative maximization of the kurtosis contrast with algebraic optimal step size. *IEEE Transactions on neural networks*, 21(2):248–261, 2010.
- Zhan, Y., Halliday, D., P., Jiang, X., Liu, and J., Feng. Detecting time-dependent coherence between non-stationary electrophysiological signals - a combined statistical and time-frequency approach. *Journal of Neuroscience Methods*, 156(1 - 2):322–332, 2006.